Trabajo Fin de Máster

Determination of parameters describing the hydraulic behaviour of filter materials for stormwater filters using the HYDRUS software package.

Intensificación: *TRATAMIENTOS DE AGUAS*

Autor:
CARLOS MIR LLORENS

Director:
IGNACIO ANDRÉS DOMÉNECH

Codirector/es:
GÜNTER LANGERGRABER

BERNHARD PUCHER

Julio, *2017*

UNIVERSITAT POLITÈCNICA DE VALÈNCIA

máster en ingeniería hidráulica y medio ambiente
mihma

ACKNOWLEDGEMENTS

First of all I would like to thank Dr. Günter Langergraber for giving me the opportunity of living an Erasmus experience and the possibility of working on a research study. I would also like to thank Bernhard Pucher for his support, advice, and his availability for asking questions, and solving problems all along the way of this thesis.

I have to thank also the support and availability of Wolfgang Stach during the laboratory experiments, and Tadele Measho Haile for his help and advice during the time spent in the laboratory.

From my time in Vienna I also have to thank Ida Scalmani for helping me even before arriving to the city with the daily life problems and for showing me how to arrive to my work place for 6 months. I would not like to forget her great lunches and dinners.

This experience would not have been the same without having met Giulia Cristofari, who not only has demonstrated to be a great colleague when working at the laboratory, but also an amazing friend. Thank you for the hours of your life invested in measuring drops of water and the talks. I will never forget the blue cheese cream recipe.

Voldria agrair a Ignacio Andrés Doménech per haver-me facilitat encontrar un tutor en la UPV i per la seua disponibilitat per a resoldre dubtes quan aquest apareixien.

M'agradaria agrair als meus pares que, amb el seu esforç, haja pogut viure aquesta experiència enriquidora en molts aspectes. També a la meua germana car no és sempre fàcil suportar-me.

També agrair als meus amics el seu suport, en el que ha sigut l'any que menys ens hem vist: Desi, Jose, Rubén, Isabel, Sonia i Sandra.

Per últim i, en absolut menys important, voldria donar-li les gràcies al meu amor, Majo Escrivà i Escrivà per creure en mi més que jo mateixa, per els seus ànims i suport incondicionals des que la conec i per l'enorme paciència que ha hagut de tindre amb mi. Moltes gràcies pateta. Et teraestime.

RESUMEN

La ciudad de Viena se caracteriza por tener un gran número de zonas verdes en las que podemos encontrar una gran variedad de vegetación. El incremento de escenarios climáticos extremos como inundaciones, sequias, olas de calor y escasez de agua, conllevan la necesidad de buscar nuevas soluciones interdisciplinares en la gestión de espacios verdes urbanos. En este contexto, las zonas verdes han de ser capaces de retener y tratar el agua de lluvia, así como, proporcionar un medio adecuado para el desarrollo de los árboles. La ciudad de Viena, en colaboración con el instituto de ingeniería sanitaria de la universidad de BOKU, trabaja en el desarrollo de un nuevo material filtrante que cumpla estas necesidades. Este material no ha de favorecer únicamente un medio adecuado para el desarrollo de la vegetación, sino que ha de ser capaz de eliminar contaminantes de la escorrentía generada por el agua de lluvia que se infiltra a través del sustrato. En este proyecto, se determinaran para los materiales estudiados los parámetros hidráulicos necesarios para el modelo de van Genuchten-Mualem. Esta información es esencial para la futura planificación del rendimiento del material filtrante en el tratamiento del agua, así como, la modelación de la obstrucción de estos filtros debido a la deposición de partículas arrastradas por la escorrentía. El primer paso de este trabajo es realizar ensayos en el laboratorio para la obtención de la conductividad hidráulica saturada de acuerdo con la norma ÖNORM B2506-3 (2016) y medir el flujo de agua en condiciones no saturadas para distintos episodios de lluvia. Una vez realizadas estas mediciones, el resto de parámetros hidráulicos de los suelos se determinarán empleando la solución inversa del modelo de flujo de agua mediante la herramienta informática HYDRUS. Con estos parámetros puede configurarse un modelo de flujo basado en los tres episodios de lluvia aplicados y emplearse como base de futuros modelos.

ABSTRACT

The city of Vienna is characterized for having several green zones within its city limits including a wide variety of vegetation. With the increase of extreme events leading to floods, droughts, heat islands and also water shortage, the demand for interdisciplinary solutions within the urban space is needed. In this context the green zones shall be used for the retention and treatment of street runoff and also provide a good environment for growing trees. The city of Vienna in collaboration with the Institute of Sanitary Engineering at BOKU University develops new filter materials to providing the needed properties. These properties shall not only provide a plant friendly environment for the plant growth but also to be able to remove contaminants from the rainwater runoff that infiltrates through the substrate. Within this project, the soil hydraulic parameters of the developed filter materials shall be determined for the van Genuchten-Mualem soil hydraulic model. This data is essential for future planned modelling of the treatment performance of the filters using the different filter materials or clogging of the filter due to occurring particulate matter from the runoff. The first step of this work includes experiments to obtain the saturated hydraulic conductivity according to ÖNORM B2506-3 (2016) and measurements of the water flow in unsaturated conditions for different defined rain events. With this measured data, the unknown soil hydraulic parameters are determined by using the inverse solution of the water flow model within the HYDRUS software package. With these parameters a water flow model based on the three applied rain events can be setup and furthermore be used as basis for future modelling approaches.

RESUM

La ciutat de Viena es caracteritza per tindre un gran nombre de zones verdes en les quals es poden encontrar una gran varietat de vegetació. L'increment d'escenaris climàtics extrems com inundacions, sequeres, efectes illa de calor, i escassesa d'aigua, les quals comporten la necessitat de buscar noves solucions interdisciplinàries en la gestió d'espais verds urbans. En aquest context, les zones verdes han de ser capaces de retindré i tractar l'aigua de pluja, així com proporcionar un medi adequat per al desenvolupament d'arbres. La ciutat de Viena en col·laboració amb l'institut d'enginyeria sanitària de la universitat de BOKU, treballa en el desenvolupament d'un nou material filtrant que satisfaci aquestes necessitats. Aquest material no sols ha d'afavorir un medi adequat per al desenvolupament de la vegetació, sinó que també ha de ser capaç d'eliminar contaminants de l'escorrentia generada per l'aigua de pluja que s'infiltra a través del substrat. En aquest projecte, es determinaran per als materials estudiats els paràmetres hidràulics necessaris per al model de van Genuchten-Mualem. Aquesta informació és essencial per a la futura aplicació del rendiment del material filtrant en el tractament de l'aigua, així com la modelació de la obstrucció d'aquests filtres degut a la deposició de partícules arrossegades per l'escorrentia. El primer pas d'aquest treball és realitzar assajos en el laboratori per a l'obtenció de la conductivitat hidràulica saturada d'acord amb la norma ÖNORM B2506-3 (2016) i mesurar el flux d'aigua en condicions no saturades per a distints episodis de pluja. Una vegada realitzats aquests mesuraments, la resta de paràmetres hidràulics dels sòls es determinaran utilitzant la solució inversa del model de flux d'aigua mitjançant la ferramenta informàtica HYDRUS. Amb aquests paràmetres pot configurar-se un model de flux basat en els tres episodis de pluja aplicats i utilitzar-se com a base de futurs models.

TABLE OF CONTENTS

1.- INTRODUCTION 1

2.- OBJECTIVES 3

3.- FUNDAMENTALS 5

3.1.- URBAN STORM WATER RUNOFF 5

3.2.- WATER FLOW MODELLING 13

3.3.- HYDRUS® SOFTWARE PACKAGE 22

3.4.- LOCATION OF THE STUDY AREA 23

3.4.1.- Austria 23

3.4.2.- Climate 24

3.4.3.- Economy 25

3.4.4.- Environmental policies 26

3.4.5.- Vienna 27

3.5.- CASE OF STUDY 29

4.- MATERIALS AND METHODS 31

4.1.- EXPERIMENTAL STUDY 31

4.1.1.- General experimental setup 31

4.1.2.- Description of the filter materials 33

4.1.3.- Water flow measurements 33

4.1.4.- Saturated hydraulic conductivity 34

4.1.5.- Pore volume 35

4.2.- SIMULATION STUDY 36

4.2.1.- Adsorption of Zinc study: an application of the model 53

5.- RESULTS AND DISCUSSIONS 59

5.1.- EXPERIMENTAL STUDY 59

5.1.1.- Water flow measurements 59

5.1.2.- Saturated hydraulic conductivity 64

5.1.3.- Pore volume 71

5.2.- SIMULATION STUDY 72

5.2.1.- Solute transport _____ *79*

6.- SUMMARY AND CONCLUSIONS _____ **83**

7.- OUTLOOK _____ **85**

8.- REFERENCES _____ **87**

ANNEX 1 _____ **93**

ANNEX 2 _____ **107**

ANNEX 3 _____ **123**

LIST OF TABLES

TABLE 1. MONTHLY ACCUMULATED PRECIPITATIONS* MEASURED IN VIENNA BETWEEN 1993 AND 2015 EXPRESSED IN MM. _____ 28
TABLE 2. COMPOSITION OF THE FILTER MATERIALS STUDIED._____ 33
TABLE 3. DOMAIN TYPE AND UNITS INTRODUCED FOR THE CONSTRUCTION OF THE MODEL. _____ 37
TABLE 4. GEOMETRY DIMENSIONS ESTABLISHED FOR THE MODELLING WITH HYDRUS®. _____ 37
TABLE 5. TIME INFORMATION USED FOR THE SIMULATIONS WITH HYDRUS®. _____ 39
TABLE 6. RECTANGULAR DOMAIN DISCRETIZATION VALUES USED IN HYDRUS®. _____ 41
TABLE 7. INITIAL VALUES OF THE PARAMETERS FOR THE SIMULATIONS WITH HYDRUS®. _____ 42
TABLE 8. DATA TYPES FOR THE OBJECTIVE FUNCTION (INVERSE PROBLEM). _____ 50
TABLE 9. DEFINITION OF THE COLUMN X IN FIGURE 27 BASED ON DATA TYPE (INVERSE PROBLEM)._____ 51
TABLE 10. DEFINITION OF THE COLUMN Y IN FIGURE 27 BASED ON DATA TYPE (INVERSE PROBLEM)._____ 51
TABLE 11. SOLUTE TRANSPORT MODIFIED PARAMETERS IN HYDRUS®. _____ 55
TABLE 12. VALUES OF THE SOLUTE TRANSPORT PARAMETERS USED FOR THE SIMULATION IN HYDRUS®. ___ 57
TABLE 13. STATISTICAL PARAMETERS OF THE DAILY PRECIPITATION VALUES BETWEEN 1993 AND 2015. ___ 59
TABLE 14. VALUES ESTABLISHED FOR THE APPLICATION OF THE THREE LOADINGS FOR THE FLOW CURVES EXPERIMENT. _____ 59
TABLE 15. SATURATED HYDRAULIC CONDUCTIVITY OF THE FILTER MATERIALS STUDIED. _____ 70
TABLE 16. PORE VOLUME OF THE DRAINGARDEN MATERIALS. _____ 71
TABLE 17. PORE VOLUME OF THE SAVE MATERIALS. _____ 71
TABLE 18. CONVERSION OF UNITS FOR THE TIME VARIABLE BOUNDARY CONDITIONS. _____ 72
TABLE 19. TIME VARIABLE BOUNDARY CONDITIONS OF THE PLOT 3 1ST COLUMN. _____ 73
TABLE 20. INVERSE SOLUTION RESULTS WHEN FLUX DATA IS USED._____ 74
TABLE 21. INVERSE SOLUTION RESULTS WHEN CUMULATIVE VOLUME DATA IS USED. _____ 74
TABLE 22. TIME WHEN THE BREAKTHROUGH IS PRODUCED. _____ 81

LIST OF FIGURES

FIGURE 1. GREEN ROOF IMPLEMENTED IN BENAGUASIL, SPAIN. (PHOTO TAKEN BY IGNACIO ANDRÉS DOMÉNECH). _____ 7

FIGURE 2. PERMEABLE PAVEMENT IMPLEMENTED IN DUNFERMLINE, SCOTLAND. (PHOTO TAKEN BY IGNACIO ANDRÉS DOMÉNECH). _____ 8

FIGURE 3. PERMEABLE PAVEMENT IMPLEMENTED IN BENAGUASIL, SPAIN. (PHOTO TAKEN BY IGNACIO ANDRÉS DOMÉNECH). _____ 8

FIGURE 4. FILTER STRIPS. (PHOTO SOURCE: WWW.SUSDRAIN.ORG). _____ 9

FIGURE 5. INFILTRATION BASIN IMPLEMENTED IN ARDLER, SCOTLAND. (PHOTO TAKEN BY IGNACIO ANDRÉS DOMÉNECH). _____ 9

FIGURE 6. GREEN SWALE IMPLEMENTED IN ARDLER, SCOTLAND. (PHOTO TAKEN BY IGNACIO ANDRÉS DOMÉNECH). _____ 10

FIGURE 7. GREEN SWALE IMPLEMENTED IN XÀTIVA, SPAIN. (PHOTO TAKEN BY IGNACIO ANDRÉS DOMÉNECH). 10

FIGURE 8. DETENTION BASIN. (PHOTO SOURCE: WWW.SUSDRAIN.ORG). _____ 11

FIGURE 9. RETENTION PONDS. (PHOTO SOURCE: WWW.SUSDRAIN.ORG). _____ 11

FIGURE 10. WETLAND. (PHOTO SOURCE: WWW.SUSDRAIN.ORG). _____ 12

FIGURE 11. LOCATION OF AUSTRIA IN EUROPE. _____ 23

FIGURE 12. LOCATION OF VIENNA. _____ 27

FIGURE 13. GENERAL SETUP OF THE COLUMN. _____ 31

FIGURE 14. IMAGE OF A MEASUREMENT MADE DURING THE SATURATED HYDRAULIC CONDUCTIVITY EXPERIMENT. _____ 35

FIGURE 15. DOMAIN TYPE AND UNITS DIALOG WINDOW. _____ 36

FIGURE 16. MAIN PROCESSES AND ADD-ON MODULES DIALOG WINDOW. _____ 37

FIGURE 17. TIME INFORMATION DIALOG WINDOW. _____ 38

FIGURE 18. OUTPUT INFORMATION DIALOG WINDOW. _____ 39

FIGURE 19. ITERATION CRITERIA DIALOG WINDOW. _____ 40

FIGURE 20. RECTANGULAR DOMAIN DISCRETIZATION DIALOG WINDOW. _____ 40

FIGURE 21. SOIL HYDRAULIC MODEL DIALOG WINDOW. _____ 41

FIGURE 22. SOIL HYDRAULIC PARAMETERS DIALOG WINDOW. _____ 42

FIGURE 23. TIME VARIABLE BOUNDARY CONDITIONS DIALOG WINDOW. _____ 43

FIGURE 24. MATERIAL DISTRIBUTION IN HYDRUS®. _____ 44

FIGURE 25. WATER FLOW INITIAL CONDITIONS IN HYDRUS®. _____ 45

FIGURE 26. INVERSE SOLUTION DIALOG WINDOW. _____ 49

FIGURE 27. WATER FLOW PARAMETERS FOR INVERSE SOLUTION DIALOG WINDOW. _____ 49

FIGURE 28. DATA FOR INVERSE SOLUTION DIALOG WINDOW. _____ 50
FIGURE 29. SOLUTE TRANSPORT DIALOG WINDOW. _____ 55
FIGURE 30. SOIL TRANSPORT PARAMETERS DIALOG WINDOW. _____ 56
FIGURE 31. REACTION PARAMETERS FOR SOLUTE DIALOG WINDOW. _____ 57
FIGURE 32. FLUX GRAPHIC OF THE PLOT 24. _____ 60
FIGURE 33. FLUX GRAPHIC OF THE PLOT 30. _____ 61
FIGURE 34. FLUX GRAPHIC OF THE SALZ 2. _____ 61
FIGURE 35. CUMULATIVE VOLUME GRAPHIC OF THE PLOT 24. _____ 62
FIGURE 36. CUMULATIVE VOLUME GRAPHIC OF THE PLOT 30. _____ 62
FIGURE 37. COMPARISON OF THE PLOT 11 DIFFERENT COLUMNS IN THE 1 L LOADING. _____ 63
FIGURE 38. COMPARISON OF THE PLOT 11 DIFFERENT COLUMNS IN THE 1.5 L LOADING. _____ 63
FIGURE 39. COMPARISON OF THE PLOT 11 DIFFERENT COLUMNS IN THE 0.5 L LOADING. _____ 64
FIGURE 40. PLASTIC CONTAINER USED FOR CARRYING OUT THE SATURATED HYDRAULIC CONDUCTIVITY EXPERIMENT. _____ 65
FIGURE 41. MEASUREMENTS OF THE SATURATED HYDRAULIC CONDUCTIVITY EXPERIMENT FOR THE DRAINGARDEN MATERIALS. _____ 66
FIGURE 42. SATURATED HYDRAULIC CONDUCTIVITY EXPERIMENT OF THE SLOWER MATERIALS FINISHED IN ONE DAY. _____ 67
FIGURE 43. SATURATED HYDRAULIC CONDUCTIVITY EXPERIMENT FASTER MATERIALS FINISHED IN ONE DAY. _ 67
FIGURE 44. SATURATED HYDRAULIC CONDUCTIVITY EXPERIMENT PLOT 3. _____ 68
FIGURE 45. SATURATED HYDRAULIC CONDUCTIVITY EXPERIMENT PLOT 9. _____ 68
FIGURE 46. SATURATED HYDRAULIC CONDUCTIVITY EXPERIMENT PLOT 11. _____ 69
FIGURE 47. SATURATED HYDRAULIC CONDUCTIVITY EXPERIMENT SALZ 2. _____ 70
FIGURE 48. INVERSE SOLUTION CUMULATIVE VOLUME RESULTS OF PLOT 3 1ST COLUMN. _____ 75
FIGURE 49. INVERSE SOLUTION CUMULATIVE VOLUME OF PLOT 3 2ND COLUMN. _____ 76
FIGURE 50. INVERSE SOLUTION CUMULATIVE VOLUME OF PLOT 25. _____ 76
FIGURE 51. INVERSE SOLUTION CUMULATIVE VOLUME RESULTS OF PLOT 24. _____ 77
FIGURE 52. INVERSE SOLUTION FLUX RESULTS OF PLOT 3 1ST COLUMN. _____ 77
FIGURE 53. INVERSE SOLUTION FLUX RESULTS OF PLOT 9. _____ 78
FIGURE 54. INVERSE SOLUTION FLUX RESULTS OF PLOT 24. _____ 78
FIGURE 55. BREAKTHROUGH OF THE PLOT 3 1ST COLUMN. _____ 80
FIGURE 56. BREAKTHROUGH OF PLOT 24. _____ 80
FIGURE 57. BREAKTHROUGH OF PLOT 3 2ND COLUMN. _____ 81

FIGURE A1. FLUX GRAPHIC OF THE PLOT 3 1ST COLUMN. _____ 93

FIGURE A2. CUMULATIVE VOLUME GRAPHIC OF THE PLOT 3 1ST COLUMN. 93
FIGURE A3. FLUX GRAPHIC OF THE PLOT 3 2ND COLUMN. 94
FIGURE A4. CUMULATIVE VOLUME GRAPHIC OF THE PLOT 3 2ND COLUMN. 94
FIGURE A5. FLUX GRAPHIC OF THE PLOT 6. 94
FIGURE A6. CUMULATIVE VOLUME GRAPHIC OF THE PLOT 6. 95
FIGURE A7. FLUX GRAPHIC OF THE PLOT 9. 95
FIGURE A8. CUMULATIVE VOLUME GRAPHIC OF THE PLOT 9. 95
FIGURE A9. FLUX GRAPHIC OF THE PLOT 11 1ST COLUMN. 96
FIGURE A10. CUMULATIVE VOLUME OF THE PLOT 11 1ST COLUMN. 96
FIGURE A11. FLUX GRAPHIC OF THE PLOT 11 3RD COLUMN. 96
FIGURE A12. CUMULATIVE VOLUME GRAPHIC OF THE PLOT 11 3RD COLUMN. 97
FIGURE A13. FLUX GRAPHIC OF THE PLOT 11 4TH COLUMN. 97
FIGURE A14. CUMULATIVE VOLUME GRAPHIC OF THE PLOT 11 4TH COLUMN. 97
FIGURE A15. FLUX GRAPHIC OF THE PLOT 16. 98
FIGURE A16. CUMULATIVE VOLUME GRAPHIC OF THE PLOT 16. 98
FIGURE A17. FLUX GRAPHIC OF THE PLOT 19. 98
FIGURE A18. CUMULATIVE VOLUME GRAPHIC OF THE PLOT 19. 99
FIGURE A19. FLUX GRAPHIC OF THE PLOT 22. 99
FIGURE A20. CUMULATIVE VOLUME GRAPHIC OF THE PLOT 22. 99
FIGURE A21. FLUX GRAPHIC OF THE PLOT 24. 100
FIGURE A22. CUMULATIVE VOLUME GRAPHIC OF THE PLOT 24. 100
FIGURE A23. FLUX GRAPHIC OF THE PLOT 25. 100
FIGURE A24. CUMULATIVE VOLUME GRAPHIC OF THE PLOT 25. 101
FIGURE A25. FLUX GRAPHIC OF THE PLOT 30. 101
FIGURE A26. CUMULATIVE VOLUME GRAPHIC OF THE PLOT 30. 101
FIGURE A27. FLUX GRAPHIC OF THE SALZ 1. 102
FIGURE A28. CUMULATIVE VOLUME GRAPHIC OF THE SALZ 1. 102
FIGURE A29. FLUX GRAPHIC OF THE SALZ 2. 102
FIGURE A30. CUMULATIVE VOLUME GRAPHIC OF THE SALZ 2. 103
FIGURE A31. FLUX GRAPHIC OF THE PFLANZ KALK. 103
FIGURE A32. CUMULATIVE VOLUME GRAPHIC OF THE PFLANZ KALK. 103
FIGURE A33. FLUX GRAPHIC OF THE GRANULIT. 104
FIGURE A34. CUMULATIVE VOLUME GRAPHIC OF THE GRANULIT. 104
FIGURE A35. FLUX GRAPHIC OF THE PFLANZ KOMBI. 104
FIGURE A36. CUMULATIVE VOLUME GRAPHIC OF THE PFLANZ KOMBI. 105

FIGURE A37. FLUX GRAPHIC OF THE PFLANZ ZEOLITH. _____ 105
FIGURE A38. CUMULATIVE VOLUME GRAPHIC OF THE PFLANZ ZEOLITH. _____ 105
FIGURE A39. FLUX GRAPHIC OF THE MA 42. _____ 106
FIGURE A40. CUMULATIVE VOLUME GRAPHIC OF THE MA 42. _____ 106
FIGURE A41. INVERSE SOLUTION FLUX RESULTS OF PLOT 3 1ST COLUMN._____ 107
FIGURE A42. INVERSE SOLUTION CUMULATIVE VOLUME RESULTS OF PLOT 3 1ST COLUMN._____ 107
FIGURE A43. INVERSE SOLUTION FLUX RESULTS OF PLOT 3 2ND COLUMN. _____ 108
FIGURE A44. INVERSE SOLUTION CUMULATIVE VOLUME RESULTS OF PLOT 3 2ND COLUMN. _____ 108
FIGURE A45. INVERSE SOLUTION FLUX RESULTS OF PLOT 6. _____ 109
FIGURE A46. INVERSE SOLUTION CUMULATIVE VOLUME RESULTS OF PLOT 6._____ 109
FIGURE A47. INVERSE SOLUTION FLUX RESULTS OF PLOT 9. _____ 110
FIGURE A48. INVERSE SOLUTION CUMULATIVE VOLUME RESULTS OF PLOT 9._____ 110
FIGURE A49. INVERSE SOLUTION FLUX RESULTS OF PLOT 11 3RD COLUMN. _____ 111
FIGURE A50. INVERSE SOLUTION CUMULATIVE VOLUME RESULTS OF PLOT 11 3RD COLUMN. _____ 111
FIGURE A51. INVERSE SOLUTION FLUX RESULTS OF PLOT 11 4TH COLUMN. _____ 112
FIGURE A52. INVERSE SOLUTION CUMULATIVE VOLUME RESULTS OF PLOT 11 4TH COLUMN._____ 112
FIGURE A53. INVERSE SOLUTION FLUX RESULTS OF PLOT 16. _____ 113
FIGURE A54. INVERSE SOLUTION CUMULATIVE VOLUME RESULTS OF PLOT 16. _____ 113
FIGURE A55. INVERSE SOLUTION FLUX RESULTS OF PLOT 19. _____ 114
FIGURE A56. INVERSE SOLUTION CUMULATIVE VOLUME RESULTS OF PLOT 19. _____ 114
FIGURE A57. INVERSE SOLUTION FLUX RESULTS OF PLOT 22. _____ 115
FIGURE A58. INVERSE SOLUTION CUMULATIVE VOLUME RESULTS OF PLOT 22. _____ 115
FIGURE A59. INVERSE SOLUTION FLUX RESULTS OF PLOT 24. _____ 116
FIGURE A60. INVERSE SOLUTION CUMULATIVE VOLUME RESULTS OF PLOT 24. _____ 116
FIGURE A61. INVERSE SOLUTION FLUX RESULTS OF PLOT 25. _____ 117
FIGURE A62. INVERSE SOLUTION CUMULATIVE VOLUME RESULTS OF PLOT 25. _____ 117
FIGURE A63. INVERSE SOLUTION FLUX RESULTS OF PFLANZ KALK. _____ 118
FIGURE A64. INVERSE SOLUTION CUMULATIVE VOLUME RESULTS OF PFLANZ KALK. _____ 118
FIGURE A65. INVERSE SOLUTION FLUX RESULTS OF GRANULIT. _____ 119
FIGURE A66. INVERSE SOLUTION CUMULATIVE VOLUME RESULTS OF GRANULIT. _____ 119
FIGURE A67. INVERSE SOLUTION FLUX RESULTS OF PFLANZ KOMBI. _____ 120
FIGURE A68. INVERSE SOLUTION CUMULATIVE VOLUME RESULTS OF PFLANZ KOMBI. _____ 120
FIGURE A69. INVERSE SOLUTION FLUX RESULTS OF PFLANZ ZEOLITH. _____ 121
FIGURE A70. INVERSE SOLUTION CUMULATIVE VOLUME RESULTS OF PFLANZ ZEOLITH_____ 121
FIGURE A71. BREAKTHROUGH OF PLOT 3 1ST COLUMN. _____ 123

FIGURE A72. BREAKTHROUGH OF PLOT 3 2ND COLUMN. _____ 123
FIGURE A73. BREAKTHROUGH OF PLOT 6. _____ 124
FIGURE A74. BREAKTHROUGH OF PLOT 9. _____ 124
FIGURE A75. BREAKTHROUGH OF PLOT 11 3RD COLUMN. _____ 124
FIGURE A76. BREAKTHROUGH OF PLOT 11 4TH COLUMN. _____ 125
FIGURE A77. BREAKTHROUGH OF PLOT 16. _____ 125
FIGURE A78. BREAKTHROUGH OF PLOT 19. _____ 125
FIGURE A79. BREAKTHROUGH OF PLOT 22. _____ 126
FIGURE A80. BREAKTHROUGH OF PLOT 24. _____ 126
FIGURE A81. BREAKTHROUGH OF PLOT 25. _____ 126
FIGURE A82. BREAKTHROUGH OF PFLANZ KALK. _____ 127
FIGURE A83. BREAKTHROUGH OF GRANULIT. _____ 127
FIGURE A84. BREAKTHROUGH OF PFLANZ KOMBI. _____ 127
FIGURE A85. BREAKTHROUGH OF PFLANZ ZEOLITH. _____ 128

1.- INTRODUCTION

Over the last decades there has been an increase of extreme events leading to floods, droughts, heat islands, and also water shortage which is linked to climate change (Zoppou, 2001; Hunt and Watkiss, 2011). These effects have an impact on water availability. Being the most vital resource of the planet for human being, the investments for the study of this issue should be primordial.

Within the urban scale, the increase of impervious areas have a strong impact on the quantity and quality of stormwater runoff (Thurston, et al., 2003). Hence, it is an important challenge for urban stormwater management to find interdisciplinary solutions that not only achieve a retention of the runoff volume but also rise the removal capacity of pollutants transported by water.

An effective management of urban stormwater is also a shared responsibility, requiring the active involvement of many State Government agencies, local councils, the private sector and the community. This is such a complex and challenging issue as it not only requires a good knowledge of the problem but also a lot of work in order to find out the best way to solve it. Therefore, it is a long process which has to be carried out to search a method that considers all the variables and leads to a solution.

In this sense, sustainable urban drainage systems (SUDS) are gaining popularity as they represent a cost-effective, sustainable, and environmental friendly approach to stormwater management (Good, et al., 2012). Examples of SUDS are green roofs, permeable pavements, filter strips, soakaways, infiltration trenches, infiltration basins, detention basins, swales, bioretention systems including rain gardens and ponds and wetlands (Ballard, et al., 2015). With those approaches, stormwater runoff volumes are reduced and/or delayed, including the peak runoff values. Moreover, the groundwater recharge can be enhanced and so do the removal of contaminants through infiltration.

It is at this point that scientists develop and study new filter materials that provide the required properties. In order to analyse their behaviour when stormwater runoff is generated, the developed filter materials are studied so that their soil hydraulic parameters are no longer unknown. Having obtained these parameters of the substrates, either there are determined

on field or at the laboratory, it helps to have a better understanding of the response that they may have. Furthermore, the information can be used by software that contain the equations of the models that describe the unsaturated behaviour of the soils as basis for modelling approaches.

2.- OBJECTIVES

The main objective of this thesis is to determine the soil hydraulic parameters of different filter materials developed by the Institute of Sanitary Engineering at BOKU University (Vienna, Austria). This data is essential for modelling the water flow and treatment performance of those filter materials. This is from upmost importance in order to investigate the lifespan of filter materials used in the urban environment for the retention and treatment of runoff waters from different origins.

The work within this thesis is split in two parts:

- The first step of this work includes experiments to obtain the saturated hydraulic conductivity according to *ÖNORM B2506-3 (2016)* and measurements of the water flow in unsaturated conditions for different defined rain events.
- With the experimental data, the soil hydraulic parameters of the van Genuchten soil hydraulic model are determined by using the inverse solution of the water flow model within the HYDRUS® software package. With these parameters, a water flow model of the different filter materials is set up and used to estimate the zinc adsorption capacity applying the solute transport and adsorption model in HYDRUS®.

3.- FUNDAMENTALS

3.1.- Urban storm water runoff

Precipitation is any product of the condensation of atmospheric water vapour that falls from the atmosphere and reach the ground. This occurs when a portion of the atmosphere becomes saturated with water vapour, so that the water condenses and precipitates (NOAA, 2017). This phenomenon has a variable behaviour related to the spatial and the time occurrence which means that neither it rains the same way in two different areas at the same time, nor it rains the same way in a specific place at two different times.

Precipitation is the beginning of the hydrological cycle and is subject to evaporation and initial loss due to interception by vegetation. The excess rainfall is available for infiltration, overland flow and depression storage. Depression storages consist on small pores and depressions on the land surface, where the water can be stored temporarily. Infiltrated water may flow through the upper layer of the soil which is general the unsaturated zone of the soil, or deeper into the soil reaching the groundwater, or saturated zone (Zoppou, 2001).

Infiltration is a combination of physical processes by which rain enters the soil. The maximum rate at which water can infiltrate into a given soil when in given conditions is called infiltration capacity. This phenomenon divides rainfall into two parts, which thereafter pursue different courses through the hydrologic cycle. One part goes via overland flow and stream channels to the sea as surface runoff; the other goes initially into the soil and thence through ground-water again to the stream or else returned to the air by evaporative processes (Horton, 1933).

Runoff is flow from a drainage basin or watershed that appears in surface streams. The flow is made up partly of precipitation that falls directly on the stream, surface runoff that flows over the land surface and through channels, subsurface runoff that infiltrates the surface soils and moves laterally towards the stream, and groundwater runoff from a deep percolation through the soil horizons (NOAA, 2017).

More than half of the world's population is living in urban areas. In many countries, the land occupied by the urban population is less than 5% of the total area. This concentration of human activities increases the necessity of all type of resources, being water the most vital.

Water is essential for human existence and human settlement and it is employed extensively in urban areas for the disposal of wastes (Zoppou, 2001).

Urban development can have an important effect on the local hydrology and water environment (Lee and Heaney, 2003). This impact depends on the level of imperviousness. On the one hand, if it rains on a pervious area, infiltration leads to groundwater recharge and reduce stream base flow, permitting the aquatic habitat to have more water during drier periods (Thurston, et al., 2003). On the other hand, when it rains on an impervious area, almost all the rainfall becomes runoff (Zoppou, 2001). As a result of higher levels of imperviousness, higher runoff volume with higher peak flow, shorter travel time, and transporting a higher pollutant load will occur (Lee and Heaney, 2003).

An urban area is by definition an area of concentrated human activity. In these sense, the streets and roads that have been built up to achieve the required characteristics for people and transport vehicles, now represent a problem related to stormwater runoff. The problematic associated to excess stormwater runoff result in negative ecological effects on receiving water bodies and an increased risk of flooding frequency and magnitude (Thurston, et al., 2003; Krishna, et al., 2014).

Pollutants carried into surface waters by storm water runoff have been identified as significant sources of water quality problems (Krishna, et al., 2014). Due to the introduction of legislation, the interest in urban stormwater quality has also increased (Zoppou, 2001). This is the reason why several studies about its quality have been made. Storm water contains significant concentrations of nutrients, heavy metals suspended, colloidal, and volatile fractions of inorganic and organic particulates, and other anthropogenic compounds (Krishna, et al., 2014).

Heavy metal contamination, primarily Cu, Pb, and Zn, originate from wear-and-tear of vehicle parts including brake linings (Cu) and tyre fillers (Zn) as well as additives in oil and petrol. These contaminants accumulate on impermeable surfaces and are transported via stormwater networks, often untreated, to local and downstream aquatic ecosystems (Good, et al., 2012).

Seeking for the mitigation of stormwater runoff, different technologies have been used based on infiltration basins which are primarily designed to remove suspended solids and reduce flood risk. One of the most extended methods used for restoring the natural hydrological cycle

and maintaining the local hydrology are sustainable urban drainage systems (SUDS). SUDS are a sequence of water management practices and facilities designed to drain surface water in a manner that will provide a more sustainable approach than what has been the conventional practice of routing run-off through a pipe to a watercourse. The facilities mentioned are generally constructed arrangements which include permeable surfaces, filter strips, filter and infiltration trenches, swales, detention basins, bioretention systems (raingardens), and wetlands and ponds (SEPA, 2016).

Figure 1. Green roof implemented in Benaguasil, Spain. (Photo taken by Ignacio Andrés Doménech).

Pervious pavements are permeable surfaces which are suitable for low traffic volumes and speeds, and allow rainwater to infiltrate through the surface and into the underlying structural layers. The water can be temporarily stored before its use, infiltrated to the ground, or be controlled discharged downstream. This method in cooperation with their associated substructures, is an efficient way of managing surface water runoff close to its source by intercepting runoff, reducing the volume and frequency of runoff, and providing a medium treatment. Treatment processes that occur within its structure include filtration, adsorption, biodegradation and sedimentation (Ballard, et al., 2015).

Figure 2. Permeable pavement implemented in Dunfermline, Scotland. (Photo taken by Ignacio Andrés Doménech).

Figure 3. Permeable pavement implemented in Benaguasil, Spain. (Photo taken by Ignacio Andrés Doménech).

Filter strips are uniformly graded and gently sloping strips of grass or other dense vegetation that are designed to treat runoff from adjacent impermeable areas by promoting sedimentation, filtration and infiltration (Ballard, et al., 2015). The runoff is designed to flow at low velocities in order to permit adequate contact time for the removal to take place. They can also reduce runoff volumes and encourage groundwater recharge due to infiltration, an attenuate peak flows. The habitat value of filter strips increases with vegetative cover and diversity, and they can provide a habitat corridor for wildlife (NSWEPA, 1997). When low to moderate velocities occur, filter strips effectively diminish particulate pollutant levels, organic materials and heavy metals. Some removal of free soluble pollutants is accomplished when

pollutants infiltrate into the soil, where they can be taken up by rooted vegetation (Ballard, et al., 2015).

Figure 4. Filter strips. (Photo source: www.susdrain.org).

There are many different types of drainage components that can be used to facilitate infiltration. These include soakaways, infiltration trenches, infiltration blankets and infiltration basins. Infiltration can contribute to reduce peak runoff rates and volumes while discharging of surface water runoff to the ground and ultimately into groundwater. Pre-treatment is required so that the risk of sediment clogging is prevented (Ballard, et al., 2015).

Figure 5. Infiltration basin implemented in Ardler, Scotland. (Photo taken by Ignacio Andrés Doménech).

Swales are shallow, flat bottomed, vegetated open channels designed to convey, treat and often attenuate surface water runoff which function is to slow the water, facilitate

sedimentation and filtration through the root zone and soil matrix, and to carry out the evapotranspiration and infiltration into the underlying soil. They are often used to drain roads, paths or car parks, where it is convenient to collect distributed inflows of runoff. However, they are difficult to incorporate into dense urban areas where space is limited (Ballard, et al., 2015).

Figure 6. Green swale implemented in Ardler, Scotland. (Photo taken by Ignacio Andrés Doménech).

Figure 7. Green swale implemented in Xàtiva, Spain. (Photo taken by Ignacio Andrés Doménech).

Detention basins are landscaped depressions that are normally dry except during storm events. Its principal objective is the retention of particulates and also the attenuation of the peak flow. Detention basins can be vegetated depressions that can provide treatment when designed to manage regular flows. The water quality benefits of a vegetated detention basin increase as the detention time for an event becomes longer. Where designed appropriately,

some or all of the basin area can also be used as a recreational or other amenity facility. Detention basins are generally applicable to most types of development, and can be used in both residential and non-residential areas (Ballard, et al., 2015).

Figure 8. Detention basin. (Photo source: www.susdrain.org).

Bioretention systems (including raingardens) are shallow landscaped depressions that can reduce runoff rates and volumes, and also treat pollutants through the use of engineered soils and vegetation. Specified engineered soil mixes can be used as filter media to enhance bioretention, treatment performance, and designs can be implemented that include submerged anaerobic zones to promote nutrient removal. With a wide variety of development landscapes using different shapes, materials, planting and dimensions they are generally used for managing and treating runoff from frequent rainfall events (Ballard, et al., 2015).

Figure 9. Retention ponds. (Photo source: www.susdrain.org).

Ponds and wetlands are features with a permanent pool of water that provide both attenuation and treatment of surface water runoff. They support aquatic vegetation which enhance treatment processes and has amenity and biodiversity benefits. Vegetation facilitate the adhesion of contaminants to themselves, aerobic decomposition of pollutants and can also help stabilise settled sediment by preventing resuspension. The system is controlled fixing the rates of discharge which influences the effectiveness of the treatment with better results associated to longer retention time. Well-designed and maintained permanent water bodies can offer important aesthetic amenity and wildlife benefits to development sites that can add significant economic value, increasing property values an attracting business and tourism (Ballard, et al., 2015).

Figure 10. Wetland. (Photo source: www.susdrain.org).

Good, et al. (2012) conclude that raingardens are gaining popularity as a bioinfiltrative SUDS but there are large differences in their design criteria because of the limited guidelines available. Organic material, a key component in raingarden design, reduces the overall hydraulic throughput but supports vegetation growth and is believed to play an important role in contaminant removal. However, raingarden design recommendations are not based on performance data as there is a lack of information on the hydraulic responses and treatment performance of these systems. Furthermore, such data is required for understanding the long-term responses of bioinfiltrative treatment systems and for modelling efforts aiming to predict their mitigation behaviour.

In this sense, there are several cities all around the world that are studying raingardens as an environmental method for the management and treatment of stormwater runoff. In Denmark, large national research programs include the “Water in urban areas” project working on transformation of the city water infrastructure to climatically robust systems, and the 2BG “Black, Blue and Green” project committed to integrated infrastructure planning for sustainable urban water systems. The working papers include case studies on sustainable urban drainage design implemented in Denmark and the Netherlands (Fryd, et al., 2009). In the United Kingdom, the Construction Industry Research and Information Association (CIRIA) promotes sustainable drainage systems and also published a series of documents on design practices and applied projects (Ashley, et al., 2007). In Ireland, Dublin’s strategic drainage study involves several local authorities to perform an in-depth drainage assessment of integrated constructed wetlands. In Sweden, a large six-year research project entitled “Sustainable Urban Water Management” was initiated by the Swedish Foundation for Strategic Research Programme with its focus on protecting valuable water resources in urban areas (Hellström, et al., 2000; Malmqvist, 1999). In Australia (Langenbach, et al., 2008; Wong, 2006; Wong and Brown, 2009), one of the largest research activities on sustainable drainage solutions is the Cooperative Research Centre (CRC) for Water Sensitive Cities, which brings together over 70 inter-disciplinary partners to deliver sustainable water strategies facilitating transformation of the city into a more liveable and resilient environment (Zhou, 2014).

It is not different the case of Vienna which is collaborating with the Institute of Sanitary Engineering at BOKU University on the development of new filter materials that provide the needed properties. These properties shall not only provide a friendly environment for plant growth but also be able to remove contaminants from the rainwater runoff that infiltrates through the substrate.

3.2.- Water flow modelling

The knowledge of the soil hydraulic properties is essential for understanding the water flow and solute transport in the vadose zone. Those are the water retention curve θ(h) and the unsaturated conductivity curve K(θ) which relate the soil water content, θ, to its water pressure head, h, and its hydraulic conductivity, K. Although the determination of the water

retention curve is generally easy, that of the conductivity curve is difficult, expensive and time consuming (Touma, 2009).

The use of numerical models for simulating water flow and solute transport in the unsaturated zone became popular during the 60s, which has remained until present days. There was much effort put into the development of such models. Probably the single most important factor that limited the successful application of unsaturated flow theory to field problems was the lack of information regarding the parameters entering the governing transfer equations. Reliable estimates of the unsaturated hydraulic conductivity are especially difficult to obtain, partly because of its extensive variability in the field, and partly because measuring this parameter is time-consuming and expensive (van Genuchten, 1980).

In 1927 Kozeny introduced a model relating soil permeability to porosity. Kozeny's model was based on application of Poisseuille's law to flow through granular porous media lacking structure or consolidation. He idealized the soil porous system as a bundle of cylindrical capillaries with a single representative radius.

Based on Kozeny's approach the Richards' (1931) contribution was related to saturated and unsaturated porous media, which empirically assumes that the relative hydraulic conductivity K_r is a function of a dimensionless soil water content S_e, effective water content, or of the matric potential head h(L):

$$K_r = \frac{K}{K_s} = S_e^{\varphi} = K_r(h) \tag{1}$$

$$S_e = \frac{\theta - \theta_r}{\theta_s - \theta_r} \tag{2}$$

where K is the hydraulic conductivity, K_s its maximum value and θ is the soil water content, being θ_r, and θ_s, respectively, the residual and saturated water content. In relation to this approach, for the case of $K_r = S_e^{\varphi}$, Irmay (1954) determined theoretically the value of the constant φ = 3, although Averjanov (1950) had before proposed the value φ = 3.5, which was later taken as correct by Brooks and Corey (1964) and Boreli and Vachaud (1966).

HYDRUS® permits the use of the Brooks and Corey (1964) analytical model for the hydraulic properties. The soil water retention, θ(h), and hydraulic conductivity, K(h), functions are given by:

$$S_e = \begin{cases} |\alpha\, h|^{-n} & h < -\dfrac{1}{\alpha} \\ 1 & h \geq -\dfrac{1}{\alpha} \end{cases} \tag{3}$$

$$K = K_s\, S_e^{\frac{2}{n}+l+2} \tag{4}$$

in which α is the inverse of the air-entry value (or bubbling pressure), n is a pore-size distribution index, and l is a pore-connectivity parameter assumed to be 2 in the original study of Brooks and Corey (1964). The parameters α, n, and l in HYDRUS® are considered to be merely empirical coefficients affecting the shape of the hydraulic functions (Šimůnek, et al., 2012).

Considering two and/or three dimensional isothermal uniform Darcian flow of water in a variably saturated rigid porous medium and assuming that the air phase plays an insignificant role in the liquid flow process, the governing flow equation for these conditions is given by the following modified form of the Richard's equation:

$$\frac{\partial \theta}{\partial t} = \frac{\partial}{\partial x_i}\left[K\left(\frac{\partial h}{\partial x_j} + K_{iz}^{A}\right)\right] - S \tag{5}$$

where h is the pressure head, S is a sink term, x_i (i=1, 2) are the spatial coordinates, t is time, K_{ij}^{A} are the components of a dimensionless anisotropy tensor, K^{A}, and K is the unsaturated hydraulic conductivity function given by:

$$K(h, x, y, z) = K_s(x, y, z) * K_r(h, x, y, z) \tag{6}$$

where K_r is the relative hydraulic conductivity and Ks the saturated hydraulic conductivity. The anisotropy tensor K_{ij}^{A} equal in equation (5) is used to account for an anisotropic medium. The diagonal entries of K_{ij}^{A} equal to one and the off-diagonal entries zero for an isotropic medium. If (5) is applied to planar flow in vertical cross-section, x_1 = x is the horizontal coordinate and x_2 = z is the vertical coordinate, the latter taken to be positive upward. Einstein's summation

convention is used in (5). Hence, when an index appears twice in an algebraic term, this particular term must be summed over all possible values of the index (Šimůnek, et al., 2012).

The permeability of a porous material to water is a function of the geometry of the boundary between the solid component and the pore space. Expressions of the Kozeny type purporting to represent this function are based upon the particle size or specific surface of the solids, and whilst, for engineering practice, they have given satisfaction for unsaturated sands, they may fail badly in other cases. By developing a Kozeny type of expression for the particular structure of a bundle of capillarity tubes of assorted radii, Childs and Collis-George demonstrated the cause of the failure (Childs and Collis-George, 1950).

Such failure is avoided by relating permeability to pore-size distribution, which is the factor of prime concern and which may be measured directly by even simpler means than are used to determine particle-size distribution. The pore-size distribution is derived by an interpretation of the moisture characteristic of the material, i.e. of the curve of moisture content plotted against pressure deficiency. A simple statistical theory, based upon the calculation of the probability of occurrence of sequences of pairs of pores of all the possible sizes, and of the contribution to the permeability made by each such pair, leads to an expression of the permeability as the sum of a series of terms. By stopping the summation at a selected upper limit of pore size one may calculate the permeability at any chosen moisture content and plot it as a function of that content (Childs and Collis-George, 1950).

Burdine (1953) developed a three parameters model based on Childs and Collis Gorge (1950) with the relationship fixed between two of them, leading to a two-parameter model. The α parameter is related to the inverse air entry value, the n parameter is related to the pore-size distribution of the soil. The m parameter is assumed to be a function of n, eliminating m as a fitting parameter. This model provides a reasonably accurate representation of data for a variety of soils. The effect of one parameter can be distinguished from the effect of the other parameter. Due to having only two parameters, the disadvantage of this model is that it is less flexible than the later model described by van Genuchten (1980).

Since Burdine (1953) and others overestimated the unsaturated permeability at high suction values, the concept of tortuosity was introduced to compensate for the poor fit between measured data and the predicted values (Rahimi, et al., 2015). In Burdine's model the square

of the normalized water content was used to account for tortuosity, which makes the theory more accurate than the same equation without the correction factor (Fredlung, et al., 1994).

Several investigators used, for these reasons, models for calculating the unsaturated conductivity from the more easily measured soil-water retention curve. Very popular among these models was the Millington and Quirk (1961) method, various forms of which were applied with some success in a number of studies. Unfortunately, this method has the disadvantage of producing tubular results which, for example, when applied to nonhomogeneous soils in multidimensional unsaturated flow models, are quite tedious to use (van Genuchten, 1980).

The series parallel-models (Childs and Collis-George, 1950; Marshall, 1958; Millington and Quirk, 1959; Kunze, et al., 1968; Mualem, 1976; Assouline, 2001) accounted for the random distribution of pore-sizes in the direction of flow by introducing a “cutting-and rejoining” concept. While these models may underestimate the relative permeability at low moisture contents, they do appear more theoretical, and they are well-suited for practical use due to the fewer empirical factor required (Rahimi, et al., 2015).

Mualem (1976) derived a new model for predicting the hydraulic conductivity from the soil-water retention curve and the conductivity at saturation. This model predicts the unsaturated hydraulic conductivity curves by using the moisture content-capillary head curve and the measured value of the hydraulic conductivity at saturation. It is similar to the Childs and Collis-George (1950) model but uses a modified assumption concerning the hydraulic conductivity of the pore sequence in order to take into account the effect of the larger pore section. A computational method is derived for the determination of the residual water content and for the extrapolation of the water content-capillary head curve as measured in a limited range (Mualem Y. , 1976). He obtained the relationship between K_r and h:

$$K_r(S_e) = S_e^{\mathrm{l}} \left[\frac{\int_0^{S_c} \frac{1}{h(S_e)} dS_e}{\int_0^1 \frac{1}{h(S_e)} dS_e} \right]^2 \tag{7}$$

where l is a dimensionless empirical parameter. Based on the permeability of 45 soils, Mualem (1976) found that the optimal value of l was 0.5.

Mualem's derivation leaded to a simple integral formula for the unsaturated hydraulic conductivity which enabled van Genuchten (1980) to derive the following closed-form analytical expressions, for the soil-water retention curve. It was the purpose of van Genuchten to derive such expressions using an equation for the soil-water retention curve which was both continuous and had a continuous slope. The resulting conductivity models generally contain three independent parameters which may be obtained by matching the proposed soil-water retention curve to experimental data (van Genuchten, 1980). The expression of van Genuchten (1980) are given by:

$$\theta(h) = \begin{cases} \theta_r + \dfrac{\theta_s - \theta_r}{[1 + |\alpha h|^n]^m} & h < 0 \\ \theta_s & h \geq 0 \end{cases} \tag{8}$$

$$K(h) = K_s S_e^l \left[1 - \left(1 - S_e^{1/m}\right)^m\right]^2 \tag{9}$$

where m = 1-1/n, and n > 1.

Equations (8) and (9) contain six independent parameters: θ_r, θ_s, α, n, K_s, and l. The pore connectivity parameter l in the hydraulic conductivity function was estimated (Mualem, 1976) to be about 0.5 (Šimůnek, et al., 2012).

The soil hydraulic properties were defined also according to Kosugi (1996), who suggested the following lognormal distribution model for S_e (h):

$$S_e = \frac{\theta - \theta_r}{\theta_s - \theta_r} = \begin{cases} \dfrac{1}{2} erfc\left\{\dfrac{\ln(h/\alpha)}{\sqrt{2}\, n}\right\} & h < 0 \\ 1 & h \geq 0 \end{cases} \tag{10}$$

Application of the Mualem's pore-size distribution model (1976) now leads to the following hydraulic conductivity function:

$$K = \begin{cases} K_s S_e^{\frac{1}{2}} \left\{\dfrac{1}{2} erfc\left[\dfrac{\ln(h/\alpha)}{\sqrt{2}\, n} + \dfrac{n}{\sqrt{2}}\right]\right\}^2 & h < 0 \\ K_s & h \geq 0 \end{cases} \tag{11}$$

Note that in this text it has been used the symbols α instead of h_0 and n instead of σ as used in Kosugi (1996) (Šimůnek, et al., 2012).

Durner (1994) divided the porous medium into two (or more) overlapping regions and suggested to use for each of these regions a van Genuchten-Mualem type function (van Genuchten, 1980) of the soil hydraulic properties. Linear superposition of the functions for each particular region gives then the functions for the composite multimodal pore system (Durner, et al. 1999):

$$KS_e = w_1[1 + (\alpha_1 h)^{n_1}]^{m_1} + w_2[1 + (\alpha_2 h)^{n_2}]^{m_2} \tag{12}$$

Combining this retention model with Mualem's (1976) pore-size distribution model leads now to:

$$K(S_e) = K_s \frac{\left(w_1 S_{e_1} + w_2 S_{e_2}\right)^l \left(w_1 \alpha_1 \left[1 - \left(1 - S_{e_1}^{1/m_1}\right)^{m_1}\right] + w_2 \alpha_2 \left[1 - (1 - S_{e_2}^{1/m_2})^{m_2}\right]\right)^2}{(w_1 \alpha_1 + w_2 \alpha_2)^2} \tag{13}$$

where w_i are the weighting factors for the two overlapping regions, and α_i, n_i, m_i (= 1-1/n_i), and l are empirical parameters of the separate hydraulic functions (i = 1, 2) (Šimůnek, et al., 2012).

Vogel and Císlerová (1988) modified the equations of van Genuchten (1980) to add flexibility in the description of the hydraulic properties near saturation. The soil water retention, θ(h), and hydraulic conductivity, K(h), functions are given by:

$$\theta(h) = \begin{cases} \theta_a + \dfrac{\theta_m - \theta_a}{(1 + |\alpha h|^n)^m} & h < h_s \\ \theta_s & h \geq h_s \end{cases} \tag{14}$$

$$K(h) = \begin{cases} K_s K_r(h) & h \leq h_s \\ K_k + \dfrac{(h - h_k)(K_s - K_k)}{(h_s - h_k)} & h_k < h < h_s \\ K_s & h \geq h_s \end{cases} \tag{15}$$

respectively, where

$$K_r = \frac{K_k}{K_s} \left(\frac{S_e}{S_{ek}}\right)^{1/2} \left[\frac{F(\theta_r) - F(\theta)}{F(\theta_r) - F(\theta_k)}\right]^2 \tag{16}$$

$$F(\theta) = \left[1 - \left(\frac{\theta - \theta_a}{\theta_m - \theta_a}\right)^{1/m}\right]^m \tag{17}$$

$$S_{ek} = \frac{\theta_k - \theta_r}{\theta_s - \theta_r} \tag{18}$$

The equations above allow for a non-zero minimum capillary height, h_s, by replacing the parameter θ_s in van Genuchten's retention function by a fictitious (extrapolated) parameter θ_m slightly larger than θ_s. While this change from θ_s to θ_m has little or no effect on the retention curve, the effect on the shape and value of the hydraulic conductivity function can be considerable, especially for fine-textured soils when n is relatively small (e.g., $1 < n < 1.3$). To increase the flexibility of the analytical expressions, the parameter θ_r in the retention function was replaced by the fictitious (extrapolated) parameter $\theta_a \leq \theta_r$. The approach maintains the physical meaning of θ_r and θ_s as measurable quantities. Equation (16) assumes that the predicted hydraulic conductivity function is matched to a measured value of the hydraulic conductivity, $K_k = K(\theta_k)$, at some water content, θ_k, less than or equal to the saturated water content, i.e., $\theta_k \leq \theta_s$ and $K_k \leq K_s$ (Vogel and Cislerová, 1988; Luckner, et al., 1989). Inspection of (14) through (16) shows that the hydraulic characteristics contain 9 unknown parameters: θ_r, θ_s, θ_a, θ_m, α, n, K_s, K_k, and θ_r. When $\theta_a = \theta_r$, $\theta_m = \theta_k = \theta_s$, and $K_k = K_s$, the soil hydraulic functions of Vogel and Cislerová (1988) reduce to the original expressions of van Genuchten (1980) (Šimůnek, et al., 2012).

Relatively small changes in the shape of the soil water retention curve near saturation can significantly affect the results of numerical simulations of variably saturated flow, including the performance of the numerical scheme itself in terms of stability and rate of convergence. Vogel et al (2000) used a modified form of the van Genuchten-Mualem soil hydraulic functions to account for a very small, but non-zero minimum capillary height, h_s, in the soil water retention curve. The modified van Genuchten-Mualem model was contrasted with the original formulation by comparing simulation results for infiltration in homogeneous soils assuming both textured soils, even for h_s values as small as -1 cm. Incorporating a small minimum capillary height in the hydraulic properties leads to less non-linearity in the hydraulic conductivity function near saturation and, because of this, to more stable numerical solutions of the flow equation. This study indicates an urgent need for experimental studies that assess

the precise shape of the hydraulic conductivity curve near saturation, especially for relatively fine-textured soils. For example, a considerable improvement in the predicted conductivity function was found when a value of -2 cm for h_s was used in the modified model (Vogel, et al., 2000).

Another modified van Genuchten-Mualem formulation was studied in 2005 (Schaap and van Genuchten, 2006) when the studies suggested several shortcomings of these functions near saturation, notably the lack of second-order continuity of the soil water retention function to account for macroporosity. It was this modified van Genuchten-Mualem model that improved the description of the hydraulic conductivity near saturation. The modified model introduced a small but constant air-entry pressure (h_s) into the water retention curve. Analysis of the UNSODA soil hydraulic database revealed an optimal value of -4 cm for this parameter, more or less independent of the soil texture. The modified model used a pressure dependent piece-wise linear correction to ensure that deviations between measured and fitted conductivities between pressure heads of 0 and -40 cm were eliminated. A small correction was found necessary between -4 and -40 cm, and a much larger correction was needed between 0 and -4 cm. This model appeared well suited for large-scale vadose zone flow and transport simulation, including inverse modelling studies (Schaap and van Genuchten, 2006).

New models appeared few years ago in order to give an explanation to the distinct behaviour that water transport follows depending on the water content. In contrast to the commonly used models for characterizing hydraulic conductivity of porous media, which rely on pore bundle concepts that account for capillary flow only and neglect film flow, experimental evidence suggests that water transport over the entire range of matric head in wet media, which mostly occurs in water saturated capillaries, is quite different from that in dry media, which occurs in thin liquid films. As a result, water flow at medium to low water contents in unsaturated porous media can be significantly underestimated by those capillary bundle models.

In this sense, Peters and Durner (2008) presented a new model that combines a simple film flow function with the capillary flow model of Mualem. This new model can easily be coupled to any water retention function. Moreover, due to its mathematical simplicity, it can easily and efficiently be implemented in existing codes for the numerical solution of unsaturated flow problems. In the same way, Lebeau and Konrad (2010) proposed a new model for

predicting the hydraulic conductivity of porous media that accounts for both capillary and thin film flow processes. As with other predictive models, a mathematical relationship is established between hydraulic conductivity and the water retention function. The model is mathematically simple and can easily be integrated into existing numerical models of water transport in unsaturated soils.

Following the studies mentioned before, Iden, et al.(2015) conclude that the hydraulic conductivity curve exhibits a sharp drop close to water saturation if the pore-size distribution is wide. So far, this artefact has been ignored or removed by introducing an explicit air-entry value into the capillary saturation function. However, this correction leads to a retention function which is not continuously differentiable. They presented a new parameterization of the hydraulic properties which uses the original saturation function of van Genuchten and introduces a maximum pore radius only in the pore-bundle model. In contrast to other models using an explicit air-entry, the resulting conductivity function is smooth and increases monotonically close to saturation. The model concept can easily be applied to any combination of retention curve and pore-bundle model.

3.3.- HYDRUS® software package

The modelling part of this thesis is carried out by utilising the HYDRUS® software package for simulating the two and three dimensional movement of water, heat, and multiple solutes in variably-saturated porous media.

This program numerically solves the Richards equation for saturated-unsaturated water flow and the convection-dispersion equation for heat and solute transport. The flow equation incorporates a sink term to account for water uptake by plant roots. The heat transport equation considers transport due to conduction and convection with flowing water. The solute transport equation consider convective-dispersive transport in the liquid phase, as well as diffusion in the gaseous phase. The transport equations also include provisions for nonlinear nonequilibrium reaction between the solid and liquid phases, linear equilibrium reactions between the liquid and gaseous phases, zero-order production, and two first-order degradation reactions (Šimůnek, et al., 2012).

The program may be used to analyse water and solute movement in unsaturated, partially saturated, or fully saturated porous media. HYDRUS® can handle flow regions delineated by

irregular boundaries. The flow region itself may be composed of nonuniform soils having an arbitrary degree of local anisotropy. Flow and transport can occur in the vertical plane, the horizontal plane, a three-dimensional region exhibiting radial symmetry about the vertical axis, or fully three-dimensional domain. The water flow part of the model can deal with prescribed head and flux boundaries, boundaries controlled by different conditions, as well as simplified representation of nodal drains using results of electric analogous experiments. The two-dimensional part of this program also includes a Marquardt-Levenberg type parameter optimisation algorithm for inverse estimation of soil hydraulic and/or solute transport and reaction parameters from measured transient or steady-state flow and/or transport data for two dimensional problems (Šimůnek, et al., 2012).

3.4.- Location of the study area

3.4.1.- Austria

Vienna is the capital and largest city of Austria and one of its nine states. Austria is a federal republic and a landlocked country of over 8.7 million people in central Europe. It is bordered by eight countries: Czech Republic and Germany to the north, Hungary and Slovakia to the east, Slovenia and Italy to the south, and Switzerland and Liechtenstein to the west. Its territory covers 83879 km^2, and it is a largely mountainous country due to its location in the Alps. Of the total area of Austria, only about a quarter can be considered low lying, and only 32% of the country is below 500 m.

Figure 11. Location of Austria in Europe.

3.4.2.- Climate

Austria lies within a temperate climatic zone. Weather conditions vary only slightly across the country, in which four regions can be differentiated: the lowland regions in the north and east, where Vienna is settled, have more continental influenced conditions, with colder winters and hotter summers and with moderate precipitation throughout the year; the southeastern areas of Austria have longer and warmer, almost Mediterranean summers; and in the western part of the country there is an influence of the temperate Atlantic which means that this part is subject to less extreme weather conditions; winters are usually mild and summers rather warm. The west is also characterized by high precipitation.

The geographic features in the more mountainous regions of the country have given rise to yet another climate zone, the Alpine climate, which causes winters to be colder than at lower altitudes. Temperatures depend largely on altitude, with averages 5^{o}C lower for each additional 300 m of elevation. The diversity of topographical and climatic conditions results in a very versatile flora and fauna.

Precipitation is quite uniformly distributed over the entire year. However, the months May, September and the first half of October tend to be the driest and the months April and November tend to be the wettest periods. Again, altitude determines precipitation pattern; while high-level areas in the Alps may have high average rainfall in excess of 2000 mm per year, some regions in the flatlands of Austria have only 600 mm annually. From June through August, rain usually comes in the form of sometimes heavy thunderstorms that can bring heavy hail and snowfall in the mountainous regions of the Alps, even in summer.

With an average annual precipitation of around 1100 mm Austria is one of Europe's most water-wealthy countries. About 50% of the drinking water used is from groundwater resources. Water is the most important foodstuff; agriculture, industry, trade and commerce as well as households need water. Water is used to generate energy; it is important for tourism, spare-time activities and recreation. Rivers, brooks and lakes provide unique habitats for numerous animals and plants. Water has a climate-regulating effect. After having been used, the waste water is treated, purified and returned to the water cycle via its rivers. But water is also threatening: It is an unpredictable force of nature which may entail high water and floods.

The world is challenged to deal respectfully with this precious asset. It is obvious that the protection and sustainable utilization of the resource water for future generations must be a priority goal (Austria, Climate, 2011).

3.4.3.- Economy

As one of the most prosperous and stable EU Member States, Austria offers its investors ideal conditions. The Austrian economic system can be characterized as a free market economy with a strong social focus by also taking into account the weaker members of society.

Austria is a highly developed industrialized country with an important service sector. The most important industries are food and luxury commodities, mechanical engineering and steel construction, chemicals, and vehicle manufacturing.

In the field of agriculture, Austria is witnessing a strong trend towards organic farming. With an overall share of 11.9%, organic farms in Austria occupy a leading position among the EU Member States. In this organic branch of agriculture, 88.1% of enterprises are dedicated to livestock farming.

As regards raw materials and energy production, Austria can draw on an abundance of resources. It has natural resources of iron ore, non-ferrous metals, important minerals and earths. Austria has its own resources of petroleum and natural gas. The generation of hydroelectric power is constantly being expanded, which makes this country the leader in the field of hydroelectric power in the European Union.

Austria's industrial and commercial sectors are characterized by a high proportion of medium-sized companies. Austrian industry covers every branch of manufacturing, from basic goods to the labour-intensive production of highly processed products. Austria is world-famous for its arts and crafts, most notably fine hand-crafted items, customized jewellery, ceramics, and glassware. Tourism is an essential pillar of the Austrian economy. Austria is a mountainous country with one of the largest natural land reserves in central Europe.

In the global-political arena, Austria is increasingly becoming an international meeting point, which is illustrated by the large number of summits and conferences held in Austria. At the same time, the country's relevance as a vital transit country between the economic areas of

Europe is increasing, especially for European energy supplies, including petroleum, natural gas, and electricity (Austria, 2011).

3.4.4.- Environmental policies

Environmental protection has become an increasingly important item on the Austrian socioeconomic policy, being one of the leading countries in Europe in the field of environmental strategy. Due to the complex nature of the problems related to environmental pollution and the traditional distribution of public tasks among a number of regional authorities, measures headed for protecting the environment are not only taken by the federal authorities, but also by Province governments and municipalities, all of whom make considerable investments.

In the fields of waste management, chemicals or air pollution related to boiler installations, the standards in force in Austria are very stringent compared to the European. Moreover, ecological criteria have increasingly been taken into account in agriculture, which means the ratification of strict regulations for the use of pesticides and fertilisers.

As a result of the programs implemented, the water quality of its lakes was raised to excellent levels. Implementing the EU Water Framework Directive (EU, 2000), which undertakes a specific assessment of the ecological state of domestic bodies of water, Austria has amended its Water Act.

Likewise, Austria attaches vital importance to safeguarding and improving the protective function of forests which is indispensable to a mountainous country. To this end, a national concept for the rehabilitation of protective forests was elaborated, which is further complemented by the implementation of several measures. Moreover, the specific steps taken with respect to emissions of airborne pollutants also led to considerable reductions.

By adopting the Federal Constitutional Act for a Nonnuclear Austria, the country renounced the use of nuclear energy. In this spirit it is advocating the creation of a nonnuclear Central Europe. At the international level Austria strongly supports strengthening the International Atomic Energy Agency as a control instrument and advocates the increase of funds for nonnuclear energy research under the EURATOM program (Austria, 2011).

3.4.5.- Vienna

Vienna is by far the most populated city of the country with around 1.8 million inhabitants, and it is also its cultural, economic and political centre. Vienna is located in the northeast of Austria. The first settlement was established at the south part of the Danube River but nowadays the city spans both sides of the river. Elevation ranges from 151 m to 542 m, and with a total area of 414.65 km^2 is the largest city in Austria by area.

Figure 12. Location of Vienna.

As said before, due to its location, Vienna has a more continental conditions, with colder winters and hotter summers and with moderate precipitation throughout the year, being the mean of the annual cumulative precipitation in the period 1993-2015 of 675 mm per year. Raining in moderation and frequently makes it easier to maintain several green zones within the urban space, so that the friendly environmental strategies related to urban stormwater management can be carried out. It is in table 1 that the monthly cumulative precipitation during this period is shown.

Table 1. Monthly accumulated precipitations measured in Vienna between 1993 and 2015 expressed in mm.*

Year	Month												Total
	January	February	March	April	May	June	July	August	September	October	November	December	
1993	43.8	58.9	45.8	19.6	22.3	60.6	87.3	98.7	40.1	65.4	48.2	52.8	643.5
1994	30.8	7.9	48.3	102.9	58.2	44.2	76.3	76.3	22.2	42	67.1	41.2	617.4
1995	29.7	33.4	65.3	82	58.2	118.9	24.4	73.9	129	11.2	73.1	78.3	777.4
1996	48.6	41.5	30.9	111.4	84.6	71.9	27.5	66.3	137	50.7	22.1	25.8	718.3
1997	14.4	23.4	90.6	63.9	71.3	43.3	244.1	31.4	22.1	28.3	73.7	52.6	759.1
1998	28.9	3.5	65.2	30.7	42.6	61.8	136.3	37.8	120.4	93.7	35.2	33.3	689.4
1999	17.2	111.6	30.8	48	89.5	60.2	79.2	73.1	60.4	15.8	52.5	66.4	704.7
2000	43.7	35.1	80.4	11.1	50.4	22.4	65.3	54.1	46.2	53.7	33.3	41.8	537.5
2001	19.1	19.4	49.1	32	30	47.4	79.5	43	98.9	8.8	55.3	52.1	534.6
2002	13.4	34.2	66.1	57.3	46.6	70.8	51.7	207.1	41.3	92	69.2	63.8	813.5
2003	67.6	1	14.1	27.5	111.2	29.3	36.4	19.4	42.8	36.2	24.8	36.6	446.9
2004	71.7	89.2	90.4	26.1	54.4	121.7	46.4	26.1	39.6	38	47.8	14	665.4
2005	61.4	75.4	17.5	29.1	46.8	45	63.2	103.6	43.2	3.1	23.8	83.3	595.4
2006	46.9	35.2	76.9	70.2	73.7	65.1	37.3	207	16.6	14.9	31.8	17.5	693.1
2007	53.6	71.9	89.4	1.8	86.5	66	55.9	58.1	196.2	69.1	54.6	60.2	863.3
2008	39.9	9.4	63.4	59.6	56.2	115.4	95.5	43.9	60.1	28.1	58.1	39.7	669.3
2009	34.8	71.7	142	4.4	82.7	140.9	148.1	83.9	19.7	41.2	75.3	54.9	899.6
2010	61.7	18.4	16.6	89.7	163.9	118.1	86.6	119.9	64.1	21.9	34.6	40.9	836.4
2011	29.7	8.9	36.5	42.9	54.5	111.7	87.3	31	21.7	73.1	0	18.2	515.5
2012	90.8	26.2	27.3	26.7	37.5	68.2	130.8	39.9	44.9	43.5	20.4	52.3	608.5
2013	102.6	55	39.4	13	135.6	144.4	10.6	57.9	90.2	26.6	40.9	18.1	734.3
2014	8.3	20.5	12.3	66	188.9	32.6	91.3	109.7	108.9	37.3	34.4	42.6	752.8
2015	70.9	37.4	40.4	22.2	47.7	23.7	34.3	44.3	49.6	79.6	36.5	24.7	511.3

**Precipitation data obtained from https://www.zamg.ac.at/cms/de/klima/klimauebersichten/jahrbuch.*

3.5.- Case of study

Urban stormwater management involves various challenges that have to be solved in an interdisciplinary approach. The City of Vienna is being affected by the increase of urban areas as well as the rise of extreme climate events which lead to overload many of the wastewater sewerages and treatment systems. This is the reason why the city in collaboration with the Institute of Sanitary Engineering at BOKU University have started two projects that pursue the same goal.

Both projects, SAVE and Draingarden, are established in order to find suitable solutions for the stormwater problem. They are both green infrastructure initiatives which contribute to an improved urban life. Not only do they allow reducing the volume of rainwater runoff that needs to be managed but also treat the infiltrated water through the substrate. Robust plants create a good environment for the development of flora and fauna that remove slowly degradable substances from rainwater runoff. In contrast to other common systems these solutions are presented as very cost effective and less environmentally harmful.

SAVE (Straßen-Abwasserlösungen für Vegetation und Entwässerungssysteme) project is set for four years (May 2016 until April 2020). The characteristics of the SAVE materials are tested at laboratory and field scales. There are five pilot sites within Vienna city limits with different scopes of application chosen for the project in order to evaluate the designed filter materials and to monitor their performance. The chosen sites for swale infiltration are located in the 19th district (Kuchelauer Hafenstraße) and 22nd district (two pilot plants in the *Seestadt Aspern*, an urban development project: Edith-Piaf-Straße and Seestadtstraße). Tree filter systems will be tested at one site in the 22nd district (Attemsgasse) and one pilot plant is located in the 10th district (Himbergerstraße) (Beinlich, 2016).

Draingarden is an integrated urban rainwater management which helps to improve the microclimate and subsequently the climate balance is positively affected. Draingarden is a natural alternative to the technical filter solutions. There are substrates that provide better storage and percolation capacity due to their composition and structure. In contrast to lawn wells they are made of industrially-produced substrates.

The greatest goals to be achieved are the retention and storage of stormwater. The idea of these projects includes the availability of water in root zones for urban trees. Having in

consideration the pollutants, flushed away from urban street surface, innovative filter materials are needed to cope with the requirements for the retention and treatment capacities. The aim of the projects is to assist in water and soil pollution control, as well as tree growth. The objective of these projects is to investigate the applicability of above mentioned filter materials (Beinlich, 2016).

The Institute of Sanitary Engineering at BOKU University has developed some filter materials that have to be tested in order to know if the required properties are provided. It is also needed the construction of a model by using the HYDRUS® software package, and the information obtained with the laboratory experiments, to determine the unknown soil hydraulic parameters which are needed to set up a water flow model. This water flow model is a base for future studies, leading to solute transport modelling with which the adsorption of heavy metals within the filter materials structure can be studied. Furthermore, simulations using the wetland module can be done in future modelling approaches (Langergraber and Šimůnek, 2011).

In this thesis, different filter materials related to both projects are under investigation. The SAVE substrates were studied previously by Beinlich (2016) and the Draingarden materials are being analysed for the first time.

4.- MATERIALS AND METHODS

4.1.- Experimental study

4.1.1.- General experimental setup

To evaluate the behaviour of the developed filter materials, column experiments were carried out. The columns were setup according to the requirements of the Austrian Standard *ÖNORM B2506-3, 2016 "Soakaways for rainwater from roof gutters and reinforced surfaces – Part 3: Filter Materials – Requirements and Tests"* (ASI, 2016).

The column (Figure 13) used has a diameter of 10 cm and a total height of 80 cm. Besides the filter material a drainage and infiltration layer is used. The drainage layer is 25 cm in height and shall prevent the filter media from washing out. The infiltration layer over the filter material is to avoid the loss of particles that can be produced when the water is introduced into the column. Between each layer a mesh is inserted in order to prevent the filter material clogging the drainage layer, hence the experiment is evaluating the real behaviour of the soil. Before the column is filled, each filter material is fully mixed to provide a homogeneous distribution of the constituents.

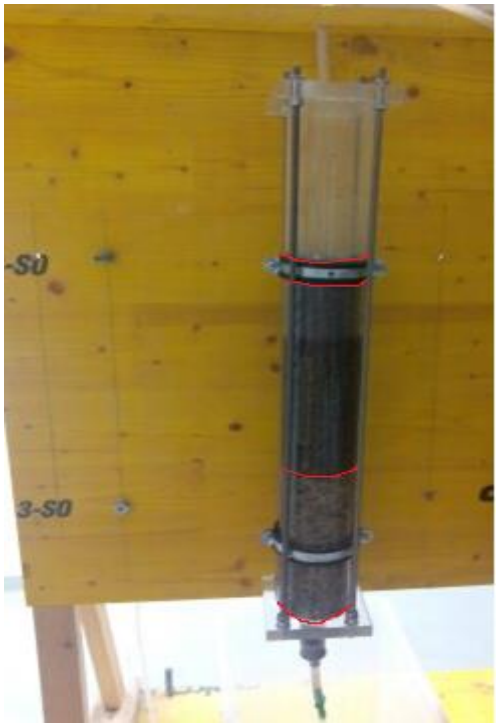

Figure 13. General setup of the column.

Furthermore, the columns were then saturated after their construction just to have them all the same operational system, so that the initial conditions during the experiments were the same for all the filter materials. This process was carried out by filling the columns from the bottom to be sure that all the pores were occupied by water. After full saturation of 15 minutes the column was drained again.

The same procedure was followed at the laboratory for determining the saturated hydraulic conductivity and the flow curves of the filter materials studied. The operation took at least three days to be finished depending on how many days were needed to determine the saturated hydraulic conductivity. First, the column was built up as described before. The next day, the experiments began determining the flow curves for three different loadings, which were applied one after the other. To put on the next loading, almost all the volume of the previous loading had to be picked up. The day after the saturated hydraulic conductivity experiment was started, however, it was not possible to finish it the same day for all the substrates, some of which took two or three days. The process finished emptying the column and cleaning the plastic cylinder in order to be ready for its construction with the next material.

The experiments at the laboratory were carried out using the following equipment:

- A plastic cylindrical column which lengths were: 10 cm diameter and 80 cm high.
- Two process pumps (Watson Marlow 520) with flow rates up to 2.4 L/min.
- A valve that let the water be stored inside the column.
- A plastic container that can contain more than 84 L.
- Beakers in order to collect the volumes of water that flows through the column.
- Measuring cylinders for measuring the volume of water collected by the beakers.
- A stopwatch to measure the time between measurements.
- Meshes for separating the different materials within the column built up.
- Drainage material 4-8 mm with which the columns were built up according to Austrian O-NÖRM.
- Filter materials that are being studied by the Institute of Sanitary Engineering at BOKU University.
- Water used for doing the experiments was treated with inverse osmosis.

4.1.2.- Description of the filter materials

In this thesis 17 different filter materials are studied, five materials from the SAVE project and twelve materials from the Draingarden project (table 2) they are described with all the information proportioned by the Institute of Sanitary Engineering at BOKU University.

Table 2. Composition of the filter materials studied.

Project	Material	Composition
DRAINGARDEN	Plot 3**	Dolomite
	Plot 6	Dolomite mud
	Plot 9	Recycled material + Perlite
	Plot 11**	Dolomite + Perlite
	Plot 16	Granulite + Perlite
	Plot 19	Recycled material
	Plot 22	Granulite
	Plot 24	Expanded clay
	Plot 25	Haldit
	Plot 30*	Schönbrunner mixture (not detailed information available)
	Salz 1*	Not detailed information available
	Salz 2*	Not detailed information available
SAVE	Pflanz Kalk	Compost + Leca + Limestone + Perlite + Zeolite
	Granulite	Compost + Granulite + Leca + Perlite
	Pflanz Kombi	Compost + Granulite + Leca + Perlite + Sand + Zeolite
	Pflanz Zeolite	Compost + Granulite + Leca + Zeolite
	MA 42*	Not detailed information available

**These materials have not been modelled with the HYDRUS® software package.*
***These materials have been modelled twice with the HYDRUS® software package.*

4.1.3.- Water flow measurements

Following the built up of the column, its saturation and drainage, the experiment for determining the flow curve of the filter materials started. This data is later used for the calibration of the water flow model. Three different rain events were applied to measure the response of each filter material. The volume of those loadings was chosen by the daily cumulative precipitations in Vienna and having into account the ratio of street runoff accumulation (15:1), which means that 15 m^2 of street runoff are drained to 1 m^2 of filter material (Beinlich, 2016). Measurements of the outflow were carried out at the beginning each and every 1 minute. The time step was increased after the peak was reached.

4.1.4.- Saturated hydraulic conductivity

This parameter is a measure of the soil's ability to transmit water depending on the hydraulic gradient and has a high variation in space and time. The flow conditions and transport processes can be estimated with the help of this parameter (Vienken and Dietrich, 2011).

The saturated hydraulic conductivity of the filter materials was determined according to Austrian Standard *ÖNORM B2506-3 (2016)*. Thereby saturated conditions with a constant head of 5 cm above the top filter layer are established and maintained by using a process pump (Watson Marlow 520) throughout the experiment. By filling the column from the bottom upwards it is allowed entrapped air to escape through the top, ensuring the system saturation and reducing the possibility for preferential flow paths to occur (Good, et al., 2012).

The measurements, which have to be distributed during the time while the experiment takes place, requires measuring the time that takes 1 L to go out of the system, and the overflow level's measurement right after. By applying the equation 20 for each measurement, different values of the saturated hydraulic conductivity will be calculated, the mean of which gives as a result the saturated hydraulic conductivity of the soil.

$$K_{sat} = \frac{Q * L}{A * (L + P)} \tag{20}$$

Where K_{sat} is the saturated hydraulic conductivity, Q is the flow (m^3/s), L is the depth of the substrate (m), A is the area of the column's cross section, and P is the water over substrate (m).

According to the normative followed to carry out this experiment, the laboratory column is flushed with a defined volume of water which is calculated by the next formula:

$$V = P * A * (A_s/A_{red}) \tag{21}$$

where P is the mean annual precipitation (estimation: 720 mm/year), A is the area of the column in m^2, and A_s/A_{red} is the ratio of filter area to drainage area (1:15).

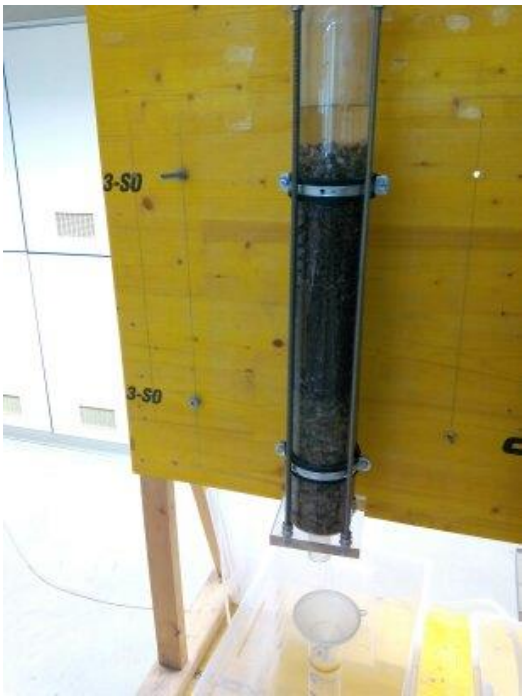

Figure 14. Image of a measurement made during the saturated hydraulic conductivity experiment.

In case of being not able to finish this experiment the day it was started, two procedures were followed:

a) the system was drained which meant that the next day the saturation of the column from bottom upwards was needed in order to proceed to the continuation of the experiment;
b) the system remained saturated until the experiment was restarted by putting a valve that prevented the water from being drained.

What happened in both cases will be explained in the results.

4.1.5.- Pore volume

Pore volume or total porosity is a measure of the empty spaces in a material, and is represented as a fraction of the volume of voids and the total volume of a sample, which values are between 0 and 1. The pore volume is connected to the grain size distribution of the material and is therefore important for the estimation of the hydraulic conditions.

This parameter is measured with an experimental approach, developed according to the Austrian Standard *ÖNORM B2606-1, 2009 "Surfaces for sports areas – Lawns"*. The experimental setup consists of two columns, which are connected with a tube. One of the columns is filled with the filter and the drainage materials, with the same layering as described

in the *ÖNORM 2506-3*. The other is filled with a known volume of water until the first one reaches an overflow of 5 cm. The material has time to be saturated for four hours. The water is added into the right column and measured (V_s), necessary to keep a constant level at both columns.

The total volume of the filter material layer (V_t) is calculated from the column dimensions. The pore volume (V_p) is calculated with the following formula:

$$V_p = \frac{V_s}{V_t} * 100 \tag{22}$$

4.2.- Simulation study

For modelling the water flow behaviour and determine the soil hydraulic parameters of the van Genuchten-Mualem soil hydraulic model HYDRUS® is used. A detailed description of the workflow is presented within this subchapter.

GENERAL MODEL SETUP

Defining the type of the domain and the units in which all the variables will be expressed is the first step for constructing the model.

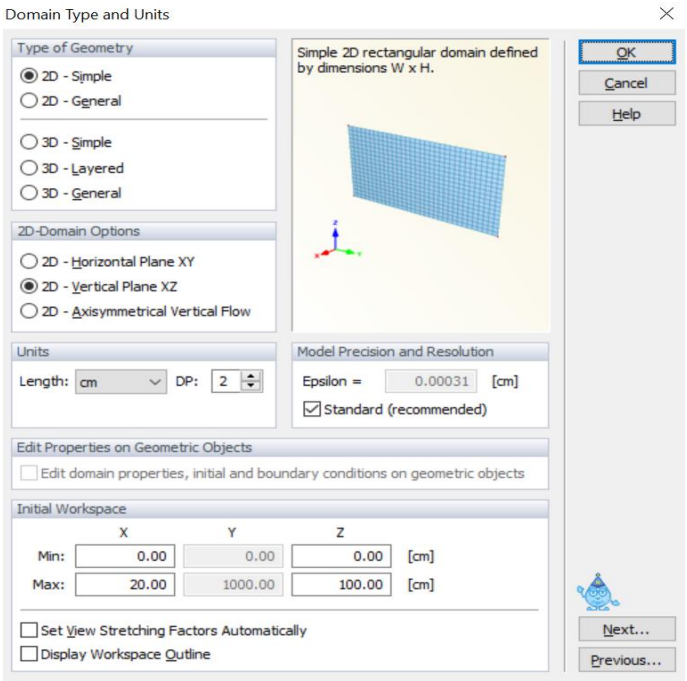

Figure 15. Domain type and units dialog window.

As shown in figure 15 the dimensions of the 2D domain, and the length units have to be defined (table 3).

Table 3. Domain type and units introduced for the construction of the model.

Domain type and units	
Type of geometry	2D-Simple
2D-Domain options	2D-Vertical plane XZ
Units: length	cm

It was decided to use a squared domain (2D) for the construction of the model instead of a round one (3D). When using the squared domain, it is necessary to take into account the areal differences within the results in order to be representing the real area of the column.

Table 4. Geometry dimensions established for the modelling with HYDRUS®.

Geometry		
X direction	10	cm
Z direction - All materials except plot 6	61	cm
Z direction - Plot 6	55	cm

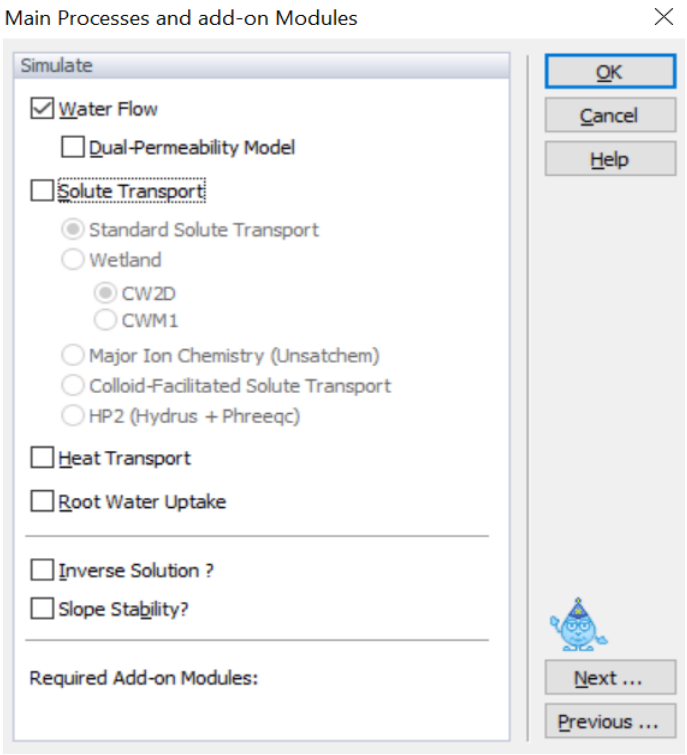

Figure 16. Main processes and add-on modules dialog window.

Figure 16 shows the main processes available in HYDRUS®, namely water flow, solute transport, heat transport and root water uptake. To determine unknown soil hydraulic or solute transport parameters the inverse solution is available.

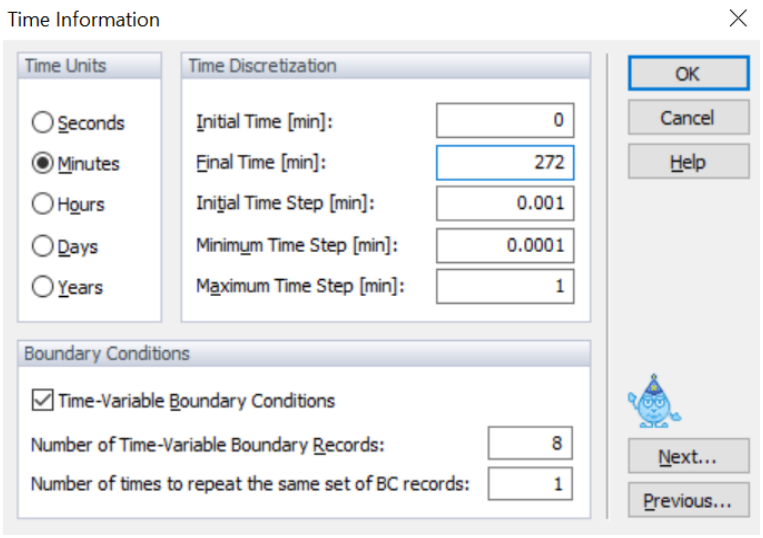

Figure 17. Time information dialog window.

In this window the time units are defined. They must be consistent throughout the project. It is also required to establish the initial time and the final time of the simulation: the initial time tends to be 0, except for more advanced applications when re-starting existing runs, and the final time is the time of the last measurement that will be introduced in the time variable boundary conditions dialog window (figure 23).

The initial time step relates to the numerical solution, which is a self-adjusting time marching scheme. This is the initial time step that the program adopts at the beginning of the solution and whenever boundary conditions change significantly. As the iterative numerical solution finds it more difficult to converge, the time step is automatically reduced. However, a limit is introduced on how small the time step is allowed to become. This limit is minimum time step. On the other hand, if the solution is converging fast, the time step is increased. The maximum time step is a limit on how large the time step can become (Rassam, et al., 2003).

The final time is settled as if the first loading (1 L) was introduced twice. This is done because of the inverse solution module, as it uses the first measurements for adjusting the calculations. Hence there were four loadings which were finally introduced into the program, the first loading (1 L) twice consecutively, the second loading (1.5 L) and the last loading (0.5 L).

Time variably boundary condition allows a user to include atmospheric data such as precipitation and evaporation, plant transpiration, and time variable boundary conditions such as pressure head and/or fluxes; the relevant data is input as a time-series. Once this option is selected, the box 'Number of Time-Variable Boundary Records' will be activated and prompt the user to enter an integer ≥ 1, depending on how many intervals are needed to define the number of loadings that need to be introduced (Rassam, et al., 2003). It is in table 5 that the values used for the modelling are shown.

Table 5. Time information used for the simulations with HYDRUS®.

Time information			
Time units	minutes		
Time discretization	Initial Time	0	min
	Final Time	Time needed to finish the flow curve experiment	min
	Initial time step	0.001	min
	Minimum time step	0.0001	min
	Maximum time step	1	min
Boundary conditions	Number of time variable boundary records	8	
	Number of times to repeat the same set of BC records	1	

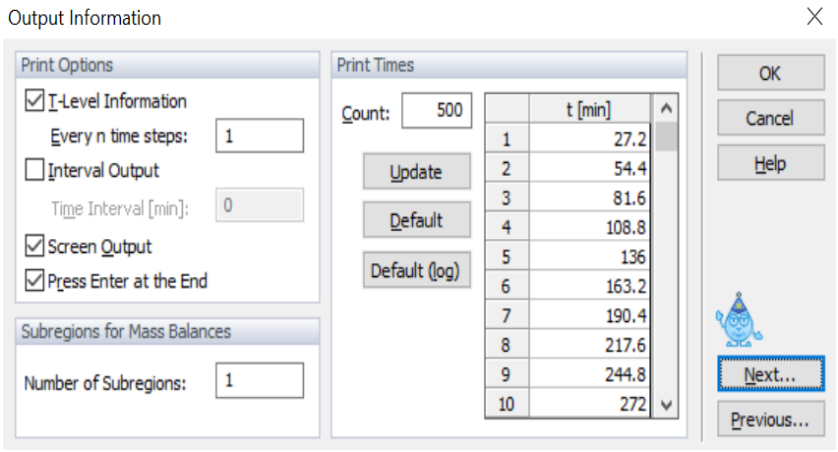

Figure 18. Output information dialog window.

Figure 18 shows the output information window defining print times of the results. If time level information is checked, then detailed results of fluxes, pressure heads, and other variables are printed at each time step. The number of time steps is settled with the count value, which shows in how many parts the time of the simulation is going to be divided. This division is proportionally done. Being checked the screen output option, the results are

dynamically shown on the computer screen during the simulation. This option is recommended to uncheck when inverse solution is used (Rassam, et al., 2003).

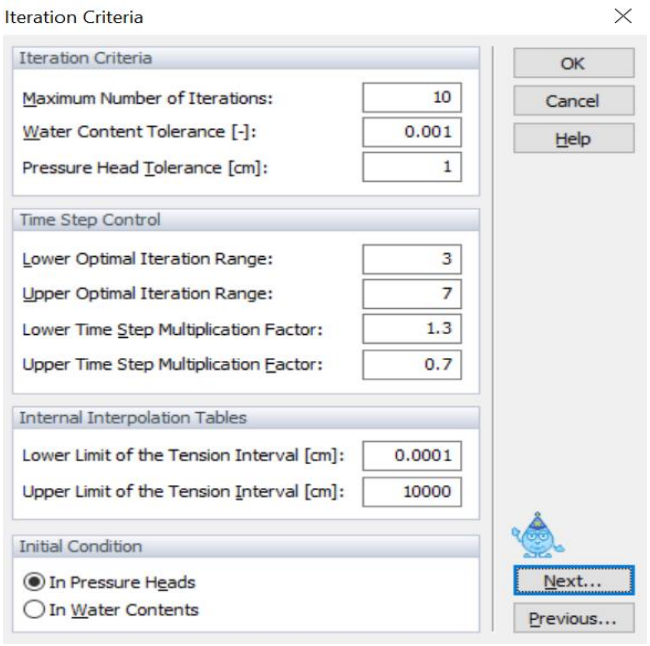

Figure 19. Iteration criteria dialog window.

Figure 19 shows the iteration criteria for the numerical simulation. It is recommended to work with the standard values.

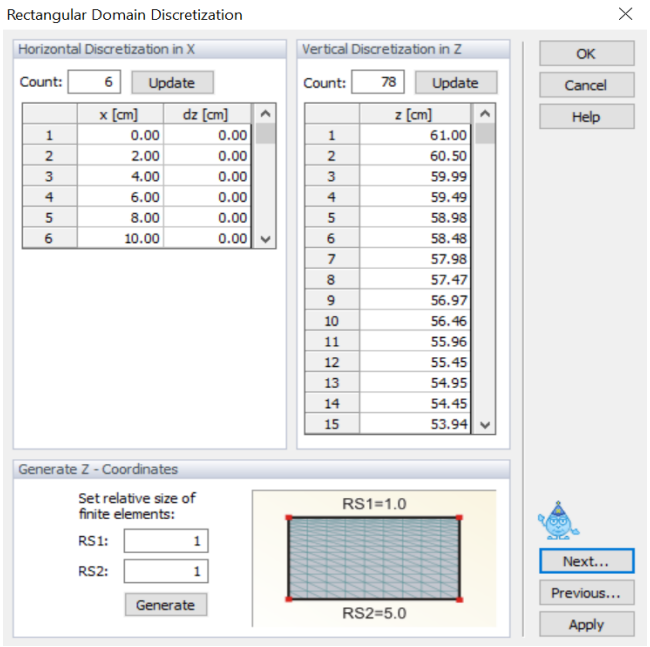

Figure 20. Rectangular domain discretization dialog window.

The rectangular domain discretization is the option that lets the user define a finite element mesh. The number of vertical and horizontal columns refers to the number of rows and columns that will be used to construct the mesh.

Table 6. Rectangular domain discretization values used in HYDRUS®.

Rectangular domain discretization		
Horizontal discretization in X direction		6
Vertical discretization in Z direction		78
Set relative size of finite elements	RS1	1
	RS2	1

When these values are introduced the mesh is defined by 468 nodes, 164 1D-elements (discretization of boundary and internal curves), and 770 2D elements.

WATER FLOW SIMULATION

HYDRUS® allows users to select three types of soil hydraulic models in order to describe the water flow: van Genuchten (1980), Brooks and Corey (1964), modified van Genuchten type equations (Vogel and Cislerova, 1988) and Kosugi (1995). Those models describe water retention parameters of the soil as well as the hydraulic conductivity function, often referred to also as the constitutive relationships. They relate water content and hydraulic conductivity to the pressure head. Dual-porosity and dual-permeability can also be used.

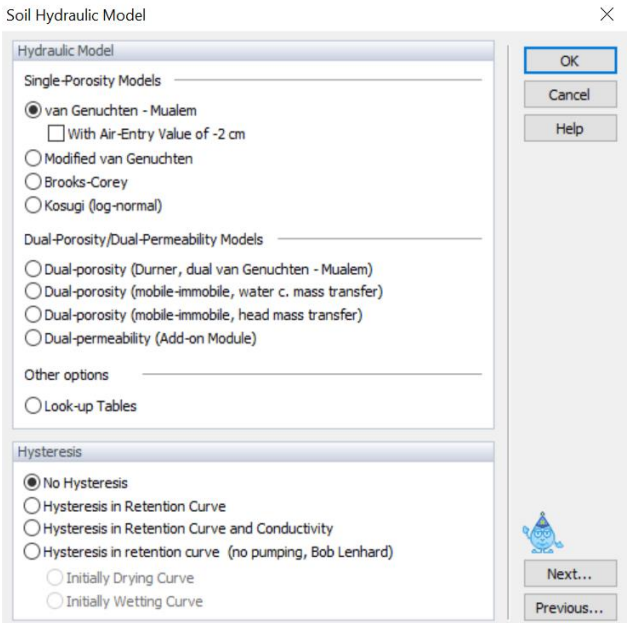

Figure 21. Soil Hydraulic Model dialog window.

For the simulation study the van Genuchten-Mualem hydraulic model without hysteresis is chosen as the number of parameters are simple to determine or estimate using HYDRUS®.

Hysteresis refers to the non-unique relationship between pressure head and water content in the soil water retention curve. A drying cycle requires more energy (a higher negative pressure head) to arrive at the same water content compared to a wetting cycle. That is, it is easier to wet the soil than to dry it to the same water content. It is possible to incorporate hysteresis with HYDRUS® only when using the van Genuchten-Mualem soil hydraulic model. This can be extended also to the conductivity function (Rassam, et al., 2003). This has not been taken into account for developing the model.

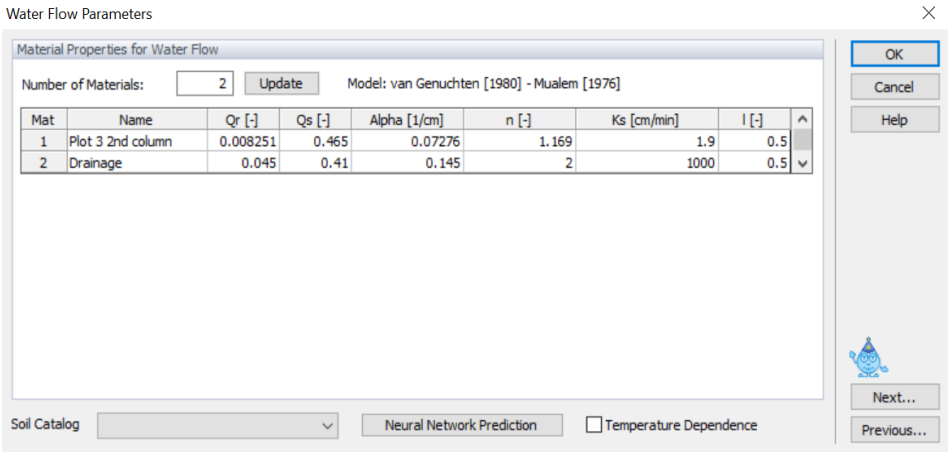

Figure 22. Soil hydraulic parameters dialog window.

Figure 22 shows the needed soil hydraulic parameters as well as the two materials, namely the filter material and the drainage material. A catalogue provides values for different soils. Initial parameters for all filter materials are listed in table 7.

Table 7. Initial values of the parameters for the simulations with HYDRUS®.

Initial values						
Material	**Q_r**	**Q_{sat}**	**α**	**n**	**K_{sat}**	**l**
Filter Materials	0.045	Determined	0.145	2.68	Determined	0.5
Drainage Material	0.045	0.41	0.145	2	1000	0.5

The pore volume parameter is important in this project since the saturated water content (θ_s) of the filter materials can be set equal to the total porosity. As pore volume is easy to be calculated, setting saturated water content equal to total porosity is challenged by several authors. This assumption can be done because of the size of the grains. When a gravel sized

porous media is being studied, this hypothesis can be done. However, when it is a finer-textured porous media, the saturated water content is supposed to be smaller than total porosity due to entrapped air or the presence of flow irregularities (Morvannou, et al., 2013).

The variable boundary conditions define the loading of the system (figure 23).

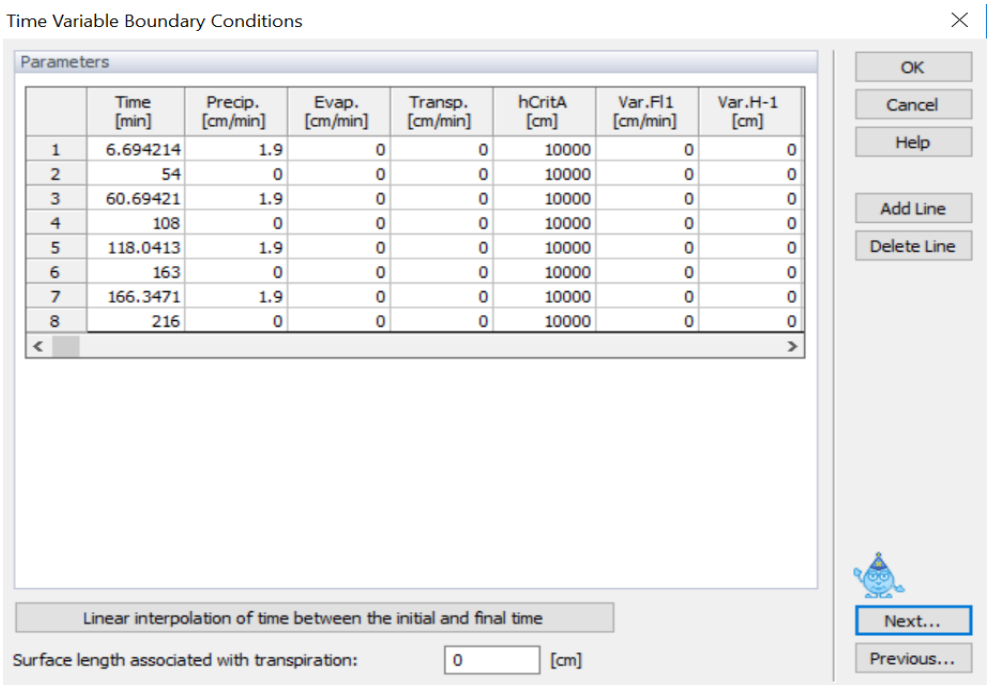

Figure 23. Time variable boundary conditions dialog window.

These conditions are dynamic (variable) through the simulation but static (constant) through a defined period of time. That is, the modeller discretizes the total simulation time into portions with different boundary values (Rassam, et al., 2003).

The program is not able to work with surface runoff. When surface runoff is generated, due to the higher value of precipitation than the infiltration capacity, HYDRUS® eliminates this volume of water from the system and continues the calculations. Therefore, this operation procedure restricts the precipitation that can be introduced without generating surface runoff. Thus, it was decided to limit the precipitation rate to the saturated hydraulic conductivity and calculate the time needed to introduce the volumes of the different loadings. It is also needed the previous conversion of the units from the international system to the units used by the program.

$$\frac{Loading\ (l)}{Area\ of\ the\ column\ (m^2)} * \frac{1\ (cm)}{10\ (mm)} = Loading\ (cm) \tag{23}$$

$$\frac{Loading\ (cm)}{K_{sat}(^{cm}/_{min})} = Time\ (\min) \tag{24}$$

As done at the laboratory, the application of the loadings are made one after the other. However, for introducing this information in HYDRUS® the first loading is repeated twice.

Before running the calculations for the water flow simulation there are three more steps to have in consideration: material distribution, initial conditions, and boundary conditions.

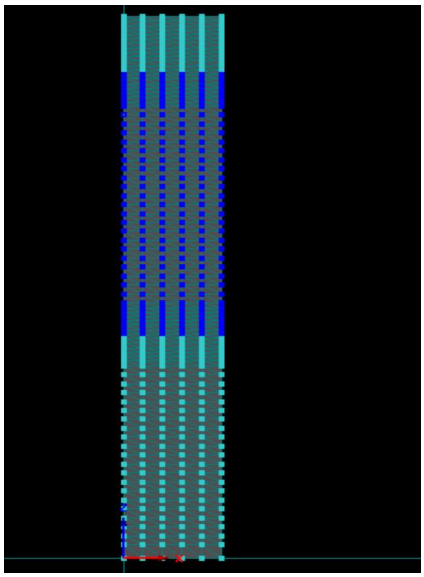

Figure 24. Material distribution in HYDRUS®.

The material distribution is the act of assigning one defined material to its proper location. This assignment is done by awarding the nodes, which have been created because of the mesh, the properties of the corresponding material. In figure 24figure 25, the result of this action can be seen.

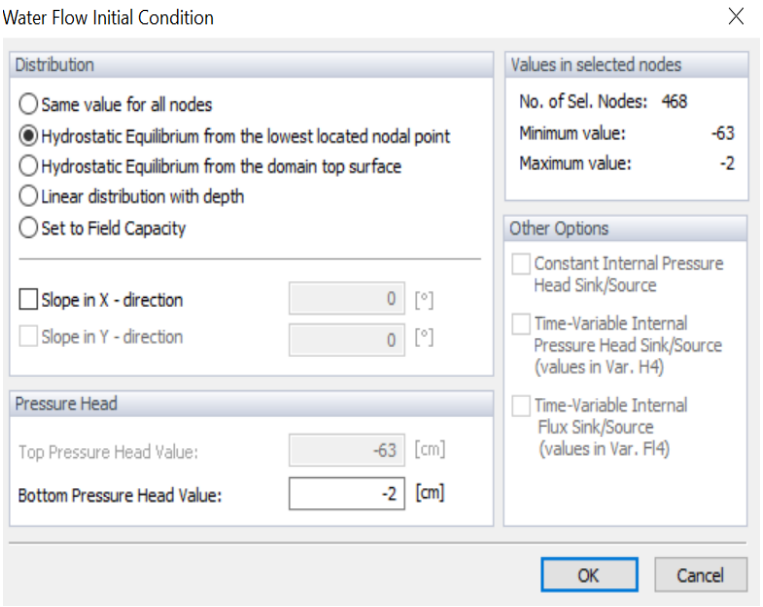

Figure 25. Water flow initial conditions in HYDRUS®.

As settled in the iteration criteria dialog window, the initial water flow conditions are defined in terms of pressure heads. They describe the state of the system prior to the simulation. The initial condition selected is a hydrostatic equilibrium from the lowest located nodal point. The bottom pressure head value was established as -2 cm which generates a small depression in the lowest part of the column. This depression forces the water to go out of the system which lets the calculations start without numerical problems.

Finally, it is necessary to establish boundary conditions at the top and the bottom sections. On the one hand, the top section is settled with an atmospheric boundary condition which allows the precipitation to happen. On the other hand, a constant pressure head equal to -2 cm is the boundary condition used for the lowest section. As explained before, the correct running of the calculations is ensured with this boundary condition.

Once this first simulation has finished, it is necessary to simulate it again in order to achieve pseudo-steady state, i.e. periodic behaviour of the system. In this second simulation, the results of the pressure head at the end of the first simulation are fixed as the new initial conditions.

INVERSE SOLUTION SIMULATION

Currently, many laboratory and field methods exist to determine the highly nonlinear soil hydraulic functions in the vadose zone, represented by soil water retention curve and

unsaturated hydraulic conductivity curves. Most methods require either static or steady-state flow conditions to satisfy the assumptions of the corresponding analytical solutions, which can make measurements time consuming. In contrast, the inverse modelling approach estimates soil hydraulic properties from transient experiments, giving much more flexibility in experimental boundary conditions than required for steady-state methods. As an additional advantage, inverse modelling allows the simultaneous estimation of both the soil water retention and unsaturated hydraulic conductivity function from a single transient experiment. In other ways, inverse modelling of transient water flow is not much different than methods applied to steady flow. In either case, inversion of the governing equation is required to estimate the unsaturated hydraulic conductivity function from experimental data. Whereas the steady-state methods invert Darcy's equation, transient methods invert Richards' equation. Inversion of Richards' equation requires repeated numerical simulation of the governing transient flow problem. Successful application of the inverse modelling technique improves both speed and accuracy, as there is no specific need to attain steady-state flow (Hopmans, et al., 2002).

By definition, inverse modelling is a general mathematical method to determine unknown causes on the basis of observation of their effects, as opposed to modelling of direct problems whose solution involves finding effects on the basis of a description of their causes. Inverse modelling is widely accepted in engineering and physical sciences for system characterization. The inverse modelling approach assumes a priori that the applied process model and the selected hydraulic relationships are an exact description of the soil's physical behaviour, and therefore assumes that the model error is negligible. This implies that deviations between simulation and observation are caused only by randomly distributed inaccuracies of measurements (Hopmans, et al., 2002).

The inverse method includes three interrelated functional parts:

- A controlled transient flow experiment for which boundary and initial conditions are prescribed and various flow variables are measured, such as pressure head, water content or flow curves.
- A numerical flow model simulating the transient flow regime of this experiment, using initial estimates of the parametric soil hydraulic functions.

- An optimization algorithm, which estimates the unknown parameters through minimization of the difference between observed and simulated flow variables (residuals) defined in an objective function (ϕ) through an iterative solution of the transient flow equation.

The quality of the final solution of the parameter estimation problem is dependent on each of these three individual components as well as their integration within a computational framework. The three components are interfaced through data files that include experimental, numerical flow model, and parameter optimization results. Parameters of the soil hydraulic functions are updated iteratively in the optimization routine, thereby continuously reducing the residuals until a predetermined convergence criterion has been achieved. As any other soil hydraulic characterization method, the magnitude of the residuals in the objective function will depend on the proper selection of the soil hydraulic model; that is, an inappropriate model will increase deviations between measurements and simulations (Hopmans, et al., 2002).

Soil hydraulic parameter estimation by inverse modelling is a relatively complex procedure that provides a quick method for soil hydraulic characterization, yielding parameters for both the soil water retention and unsaturated hydraulic conductivity function from a single experiment. Its successful application requires suitable experimental procedures as well as advanced numerical flow codes and optimization algorithms. However, since the method as a whole is not fully developed yet, both experimental and numerical modelling expertise is required for successful application of the methodology and correct interpretation of the results (Hopmans, et al., 2002).

When compared with other measurement methods, the inverse modelling approach renders a suite of benefits. First and foremost, it mandates the combination of experimentation with numerical modelling. Since the optimized hydraulic functions are mostly needed as input to numerical flow and transport models for prediction purposes, it is an added advantage that the hydraulic parameters are estimated using similar numerical models as used for predictive forward modelling. An additional benefit of the inverse procedure is their application to transient experiments, thereby providing relatively fast results. Finally, the parameter optimization procedure computes confidence intervals of the optimized parameters, although their interpretation can be misleading (Hopmans, et al., 2002).

Inverse problems for parameter estimation of soil hydraulic functions can be ill-posed because of inadequate experimental design, measurement errors, and model errors. Analysis of such flow problems must include a search for the optimum number of flow variables required in the objective function (Hopmans, et al., 2002).

Improvements in parameter estimation methods in combination with experimental requirements and optimization algorithms continue to appear in a steady stream of publications. Nevertheless, the general inverse method has demonstrated to be an excellent new tool that allows for soil hydraulic characterization using a wide spectrum of transient laboratory and field experiments. To date, the application of the inverse parameter estimation method in the vadose zone has been limited to the estimation of soil hydraulic properties. This is not surprising because hydraulic parameters are required in most flow and transport models and their direct measurements are time-consuming. We pose that inverse modelling can be used to estimate not only other soil properties as well, such as solute transport, heat flow, and gaseous transport parameters, but also plant root uptake. Summarizing, we conclude that parameter estimation by inverse modelling has tremendous potential in characterizing vadose flow and transport processes, while simultaneously presenting us with an additional tool to better understand their fundamental mechanisms (Hopmans, et al., 2002).

HYDRUS® implements a Marquardt-Levenberg nonlinear minimization method for inverse estimation of soil hydraulic and/or solute transport and reaction parameters from measured transient or steady-state flow and/or transport data. This method combines the Newton and steepest descent methods, and generates confidence intervals for the optimized parameters. The method was found to be very effective and has become a standard in nonlinear least-squares fitting among soil scientists and hydrologists.

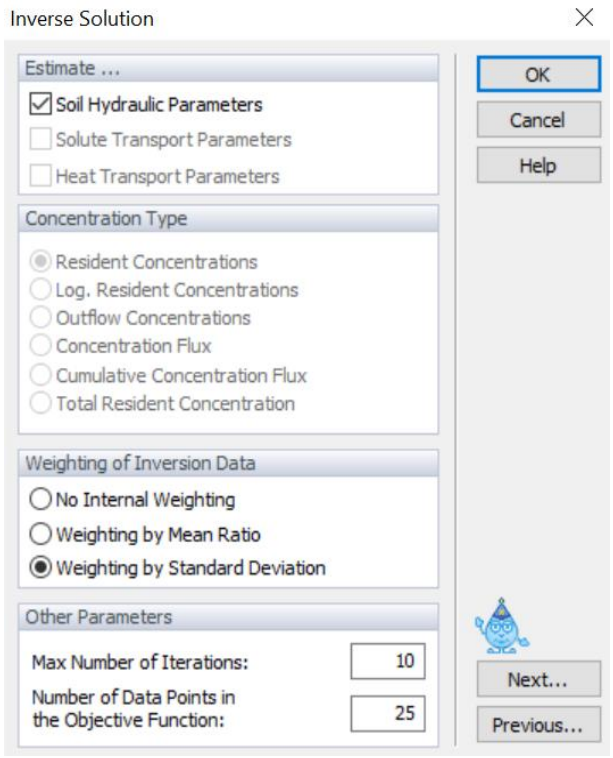

Figure 26. Inverse solution dialog window.

In the inverse solution window (figure 26), one selects the method of weighting of inversion data in the objective function. The maximum number of iterations is recommended to be 10, and the number of data points in the objective function is the number of measured data available to be introduced for its comparison with the calculated values.

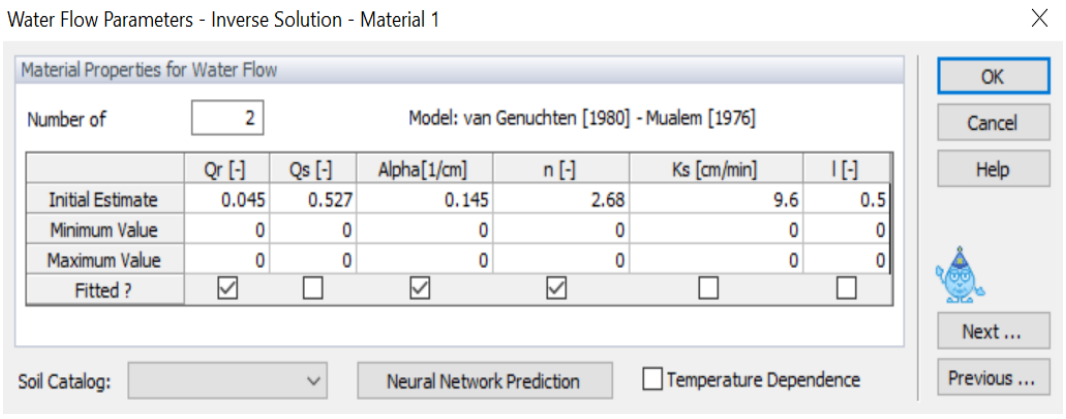

Figure 27. Water flow parameters for inverse solution dialog window.

In the dialog window shown in figure 27 the unknown soil hydraulic parameters have to be checked. Hence, the parameters that were calculated by the inverse solution are: the residual water content (Q_r), and the shape parameters (alpha and n).

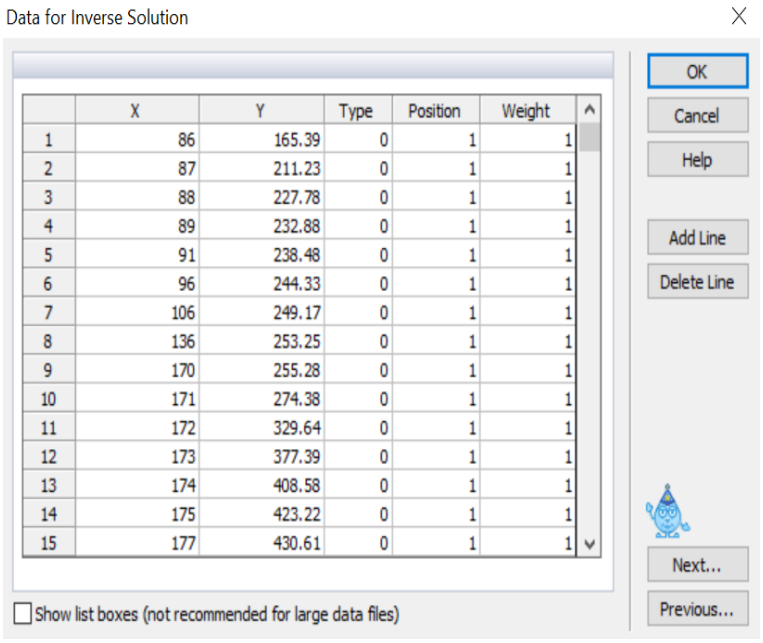

	X	Y	Type	Position	Weight
1	86	165.39	0	1	1
2	87	211.23	0	1	1
3	88	227.78	0	1	1
4	89	232.88	0	1	1
5	91	238.48	0	1	1
6	96	244.33	0	1	1
7	106	249.17	0	1	1
8	136	253.25	0	1	1
9	170	255.28	0	1	1
10	171	274.38	0	1	1
11	172	329.64	0	1	1
12	173	377.39	0	1	1
13	174	408.58	0	1	1
14	175	423.22	0	1	1
15	177	430.61	0	1	1

Figure 28. Data for inverse solution dialog window.

The last part of the inverse solution dialog windows is where the measured data that will be analysed during the parameter optimization process has to be introduced. Many different types of data can be used to define the objective function that will be minimized for this purpose. How the values in the X and Y columns are interpreted depends on the 'Type' and 'Position' values. Weight is the weight associated with a particular data point. The following information can be included into the objective function:

Table 8. Data types for the objective function (inverse problem).

Type	Data point
0	Cumulative boundary fluxes across a specified boundary
1	Pressure head measurements at selected observation point(s)
2	Water content measurements at selected observation point(s)
3	Boundary flux across a specified boundary
4	Concentration or temperature measurements at observation point(s)
5	h(θ) measurements; soil water retention data
6	K(h) measurements; hydraulic conductivity data point
7	Prior knowledge of parameter α
8	Prior knowledge of parameter n
9	Prior knowledge of parameter θ_r
10	Prior knowledge of parameter θ_S
11	Prior knowledge of parameter K_S

Two different simulations were carried out for the inverse modelling: one introducing the cumulative boundary fluxes across a specified boundary (Type 0) and the other introducing the boundary flux across a specified boundary (Type 3).

The cumulative volume data was processed before being introduced. This process consisted of increasing the last measure obtained in the experiments in order to make it coincide with the total amount of water introduced in the columns. All the rest were raised the same value so that the shape of the curves were preserved. The reason why it was done this way is that HYDRUS® does not consider that the water can be stored within the soil pores so all the water that is introduced as precipitation is flushed out of the column. This method was followed in order to avoid the differences between the real experiments and the software analysis.

Depending upon the value of parameter 'Type', the first column (X) contains the following information:

Table 9. Definition of the column X in figure 27 based on Data Type (inverse problem).

X	Type
Time	0, 1, 2, 3, 4
Pressure head	5, 6
Dummy variable	7, 8, 9, 10, 11

For both simulations, the information that has to be introduced in the X column is the time. Depending upon the value of the parameter 'Type', the second (Y) and forth (Position) columns contain the following information:

Table 10. Definition of the column Y in figure 27 based on Data Type (inverse problem).

Y	Type	Position
Cumulative boundary fluxes across a specified boundary	0	Code for specified boundary*
Pressure head	1	Observation node number
Water content	2	Observation node number
Averaged water content of the entire flow domain	2	0
Averaged water content of the subregion	2	Negative subregion number
Concentrations/temperatures	4	Observation node number
Concentrations for the second solute	4	Negative observation node number
Total amount of solute in the entire flow domain	4	0
Boundary flux across a specified boundary	3	Code for specified boundary*
Water content	5	Material number

Y	Type	Position
Hydraulic conductivity	6	Material number
Particular parameter	7-11	Material number

**1 – constant pressure head or flux boundary; 2 – seepage face; 3 – variable pressure head or flux boundary; 4 – atmospheric boundary; 5 – drain; 6 – free or deep drainage boundary; 7, 8, and 9 – variable pressure head or flux boundaries 2, 3, or 4, respectively.*

The code for the 'Position' column based on both types of data (0 and 3) used for the simulations is 1 due to the bottom boundary condition is a constant pressure head boundary.

As said, the Marquardt-Levenberg optimization algorithm was used to minimize the objective function. The objective function adopted by HYDRUS® is the sum of squared residual (SSQ), which mathematical expression is:

$$SSQ = w_i \sum_{i}^{N} (q_{p,i} - q_{o,i})^2 \tag{25}$$

where N is the number of the calibration points, $q_{p,i}$ is the i^{th} predicted value, $q_{o,i}$ is the i^{th} observed value, and w_i is the weight assigned to the i^{th} error. Note that there were two different simulations, one with the flux data and the other one with the cumulative volume data.

After all the information mentioned introduced, the simulations were run achieving, as a result, the values of the unknown parameters (residual water content, alpha, and n) that make the calculated values fit the best to the measurements obtained at the laboratory. At the end of these simulations, the soil hydraulic parameters of the developed filter materials were calculated.

WATER FLOW SIMULATION WITH THE NEW PARAMETERS

In the final step the water flow simulation is updated using the determined soil hydraulic parameters. It is also needed to run the calculations twice so that the steady-state flow is reached. In the first simulation the initial conditions were established to be hydrostatic equilibrium from the lowest nodal point which was set as -2 cm for the pressure head. In the second simulation, the initial conditions were the final configuration of the pressure heads of the first simulation. At the end of these simulations, the flow curves and the cumulative

volume for the studied loadings are obtained. These results will be compared with the measured data in the corresponding section of the results and discussion.

4.2.1.- Adsorption of Zinc study: an application of the model

With the established water flow model, simulations for the different filter materials using the solute transport model were carried out. What was simulated was the capacity that filter materials have for adsorbing heavy metals, more precisely their capacity for adsorbing zinc. What is looked for is to see if the model can differentiate between the adsorption capacities of the filter materials by having only in consideration their different soil hydraulic parameters.

It is in main processes and add-on module dialog window (figure 16), that the solute transport has to be activated to permit its simulation. HYDRUS® assumes nonequilibrium interaction between the solution (c) and adsorbed (s) concentrations, and equilibrium interaction between the solution (c) and gas (g) concentrations of the solute in the soil system. The adsorption isotherm relating s_k and c_k is described by a generalized nonlinear equation of the form:

$$s_k = \frac{k_{s,k} c_k^{\beta_k}}{1 + \eta_k c_k^{\beta_k}} \qquad k \in (1, n_s)$$

$$\frac{\partial s_k}{\partial t} = \frac{k_{s,k}\beta_k c_k^{\beta_k - 1}}{(1 + \eta_k c_k^{\beta_k})^2}\frac{\partial c_k}{\partial t} + \frac{c_k^{\beta_k}}{1 + \eta_k c_k^{\beta_k}}\frac{\partial k_{s,k}}{\partial t} - \frac{k_{s,k} c_k^{2\beta_k}}{\left(1 + \eta_k c_k^{\beta_k}\right)^2}\frac{\partial \eta_k}{\partial t} + \frac{k_{s,k} c_k^{2\beta_k} ln c_k}{\left(1 + \eta_k c_k^{\beta_k}\right)^2}\frac{\partial \beta_k}{\partial t} \quad (26)$$

where $k_{s,k}$, β_k, and η_k are empirical coefficients. The Freundlich, Langmuir, and linear adsorption equations are special cases of equation (26). When $\beta_k = 1$, equation (26) becomes the Langmuir equation, when $\eta_k = 0$, equation (26) becomes the Freundlich equation, and when both $\beta_k = 1$ and $\eta_k = 0$, equation (26) leads to a linear adsorption isotherm. Solute transport without adsorption is described with $k_{s,k} = 0$. While the coefficients $k_{s,k}$, β_k, and η_k are assumed to be independent of concentration, they are permitted to change as a function of time though their dependency on temperature (Šimůnek, et al., 2012).

The concept of two-site sorption is implemented in HYDRUS® to permit the consideration of nonequilibrium adsorption-desorption reactions. This concept assumes that the sorption sites

can be divided into two fractions: one is assumed to be instantaneous s_k^e (type-1 sites), while the other is considered to be time-dependent s_k^k (type-2).

$$s_k = s_k^e + s_k^k \tag{27}$$

At equilibrium it is haven for the type-1 (equilibrium) and type-2 (kinetic) sites, respectively:

$$s_k^e = f s_k \qquad k \in (1, n_s) \tag{28}$$

where f is the fraction of exchange sites assumed to be in equilibrium with the solution phase. Because type-1 sorption sites are always at equilibrium, differentiation of (28) gives immediately the sorption rate for the type-1 equilibrium sites:

$$s_k^k = (1 - f) s_k \qquad k \in (1, n_s) \tag{29}$$

$$\frac{\partial s_k^e}{\partial t} = f \frac{\partial s_k}{\partial t} \qquad k \in (1, n_s) \tag{30}$$

Sorption on the type-2 nonequilibrium sites is assumed to be a first-order kinetic rate process. The mass balance equation for the type-2 sites in the presence of production and degradation is given by:

$$\frac{\partial s_k^k}{\partial t} = w_k \left[(1 - f) \frac{k_{s,k} c_k^{\beta_k}}{1 + \eta_k c_k^{\beta_k}} - s_k \right] - \left(\mu_{s,k} - \mu_{s,k}{}' \right) s_k^k + (1 - f) \gamma_{s,k} \qquad k \in (1, n_s) \tag{31}$$

where w_k is the first-order rate constant for the k^{th} solute (Šimůnek, et al., 2012).

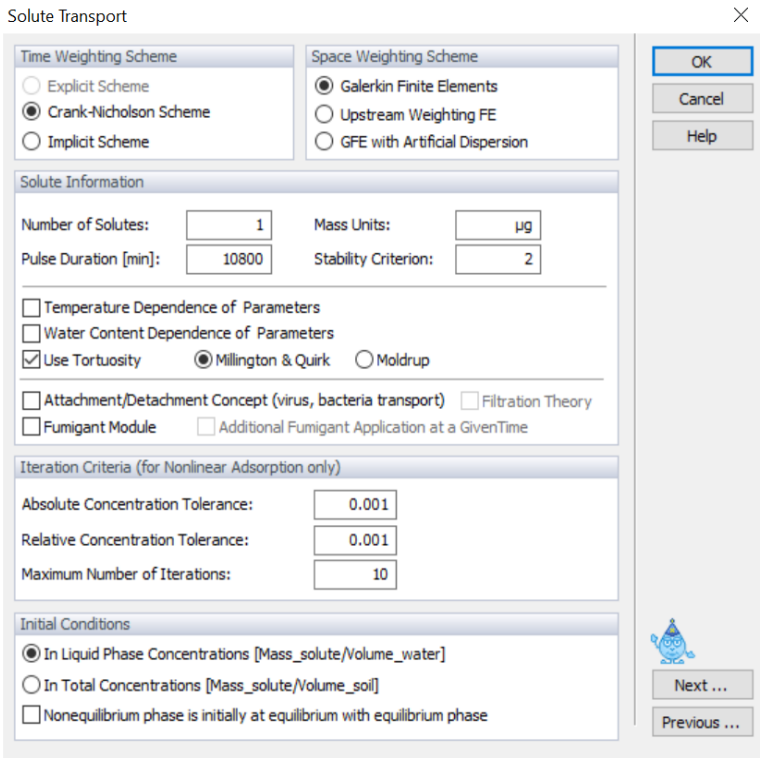

Figure 29. Solute transport dialog window.

The dialog window that appear when solute transport module is activated is shown in figure 29. The information to be introduced is the number of solutes, the mass units in which the concentration of the solute will be expressed, the absolute and relative concentration tolerances, and the maximum number of iterations. Related to the pulse duration, it is needed to be introduced the total time of the simulation.

The application consists of simulating the four loadings used for obtaining the soil hydraulic parameters of the different filter materials and with those loadings a fixed concentration of Zinc is introduced. This is why the time for all the simulations will be different from one filter material to another and it is the same that was used in the inverse solution study. In the next table the information used for the solute transport application is shown:

Table 11. Solute transport modified parameters in HYDRUS®.

Solute transport		
Number of solutes	1	
Pulse duration	Depends on the material	minutes
Mass units	µg	
Absolute concentration tolerance	0.001	
Relative concentration tolerance	0.001	
Maximum number of iterations	10	

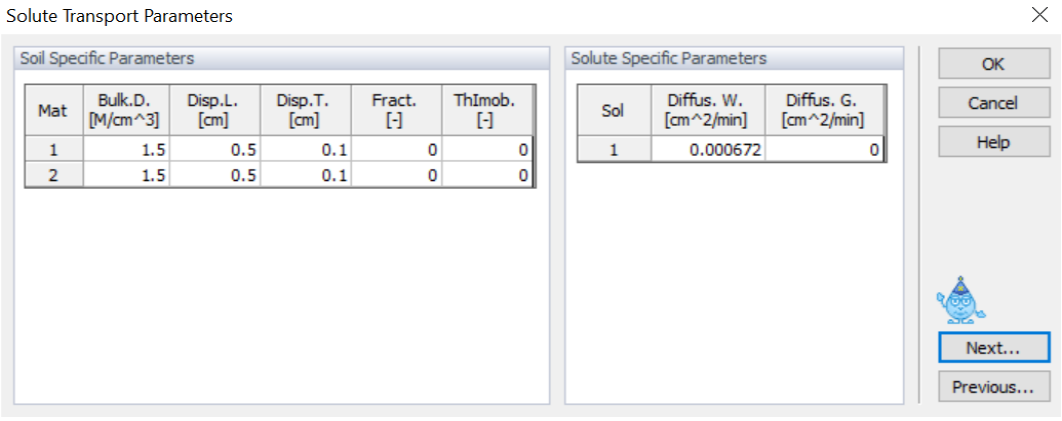

Figure 30. Soil transport parameters dialog window.

The next information about the solute transport simulation that needs to be introduced is the value of the solute transport parameters. The parameters that are needed to be modified are: the fraction of exchange sites parameter 'f' in equations (28) to (30) and the diffusion parameters in the direction of the flux (Diffus. W) and the transversal direction of the flux (Diffus. G.). The fraction of exchange sites parameter is set as 0 because it was considered that the instantaneous adsorption-desorption does not happen. Since the simulation is carried out in the columns elements, the flux is predominantly vertical so a value of 0 is considered to be the diffusion parameter in the direction transversal to the flux. The diffusion in the direction of the flux is taken from (Chalermyanont, et al., 2008) who carried out experiments in order to determine the Langmuir isotherm parameters for different heavy metals one of which was the Zinc, and also their diffusion coefficients for a sand-bentonite mixture sample. Although their values are taken for the simulations, it is recommended to do further research including some experiments for the determination of those parameters for the filter materials studied. So it is in the dialog window shown in Figure 31. Reaction parameters for solute dialog window.Figure 31 where the Langmuir isotherm parameters have to be introduced. It is in table 12 that the values of the different parameters used for the simulations can be seen.

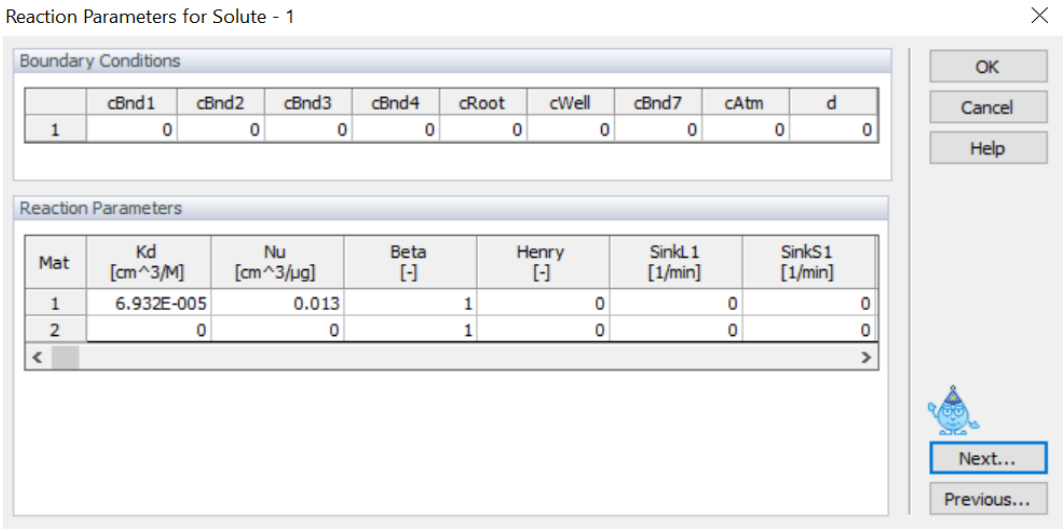

Figure 31. Reaction parameters for solute dialog window.

Table 12. Values of the solute transport parameters used for the simulation in HYDRUS®.

Solute transport parameters		
Diffusion W.	0.96768	cm^2/day
$K_d = X_m * b$	0.00030092	$cm^3/\mu g$
$N_u = b$	0.013	$cm^3/\mu g$
Zn concentration in stormwater runoff	0.4	$\mu g/cm^3$
w_k	0.000694	$minutes^{-1}$

After analysing some literature about the typical concentration of heavy metals in stormwater runoff it was decided to take 400 µg/L as the concentration of zinc which corresponds with the values studied by several authors (Davies, et al., 2000; Göbel, et al., 2007; Helmreich, et al., 2010; Scholes, et al., 1998; Taebi and Droste, 2004).

The parameter w_k is the first order rate constant which has to be set in figure 31 dialog window. It was studied by Šimůnek and van Genuchten, 2008 the influence of this parameter in the breakthrough curves by using 0.1, 0.5, and 10 $days^{-1}$. This study showed that depending on the value of this parameter the slope and the curve of the breakthrough was different which means that it has an effect on the time during which the soil can adsorb a pollutant. For the simulations this parameter is set as 0.1 day^{-1}, 0.000694 $minutes^{-1}$.

Before starting running the calculations, the initial conditions had to be established. The pressure head is established in the same way that was used for the water flow simulations, an hydrostatic equilibrium from the lowest nodal point which was set as -2 cm; the concentration of zinc in the soil was set as 0 $\mu g/cm^3$; and also this value was used for the sorbed

nonequilibrium concentration. For the boundary conditions a third type conditions was used for both the top and the bottom sections. As it was done with the water flow simulations, after finishing the first simulation, the final conditions of the pressure head were established as the initial conditions of the second simulation so that the steady-state conditions were achieved for the water flow. This procedure was not done neither with the initial concentration nor the sorbed nonequilibrium concentration as what is looked for is their change over time.

5.- RESULTS AND DISCUSSIONS

5.1.- Experimental study

5.1.1.- Water flow measurements

As described in section 4.1.3.-, the volume of the loadings was chosen based on daily precipitations in Vienna. Table 13 shows the maximum, mean, median, and standard deviation of the data. Taking the 15:1 runoff ratio (Beinlich, 2016) into account as well as the area of the column with 78.54 cm^2 a rainfall event of 77 mm equals to a feeding event on the column of 9.07 L. In table 13 the values of the statistical parameters in mm and its conversion to the feeding event in L is shown.

Table 13. Statistical parameters of the daily precipitation values between 1993 and 2015.

Parameter	Daily precipitations	Unit	Feeding event	Unit
Maximum	77.1	mm	9.07	Litres
Mean	4.37	mm	0.51	Litres
Median	1.8	mm	0.21	Litres
Standard Deviation	6.97	mm	0.82	Litres

These statistical parameters were calculated without taking into account the days with no rain. What can be seen in table 13 is that the maximum value is obtained few times during the studied period due to the difference between the maximum and the mean values.

As the data is the daily cumulative precipitation, it can be considered that the maximum precipitation does not happen instantaneously. Hence, for the feedings as they are applied instantaneously it was decided to use the mean value as one loading and use the standard deviation to determine the other loadings. As 0.82 L is in the middle of 1 L and 0.5 L, those volumes were decided to increase the 0.5 L as a result of the mean value transformation. So the three different volumes selected to carry out the experiment are shown in table 14.

Table 14. Values established for the application of the three loadings for the flow curves experiment.

Loading	Feeding event	Unit	Daily precipitation	Unit
Loading 1	1	Litre	8.49	mm
Loading 2	1.5	Litres	12.73	mm
Loading 3	0.5	Litres	4.24	mm

These selected loadings were applied one after the other when almost all the volume of the previous loading was collected.

Furthermore, in this chapter results of selected filter materials are shown in order to explain the results obtained with the experiments. Moreover, all results of the experimental work can be found in Annex 1.

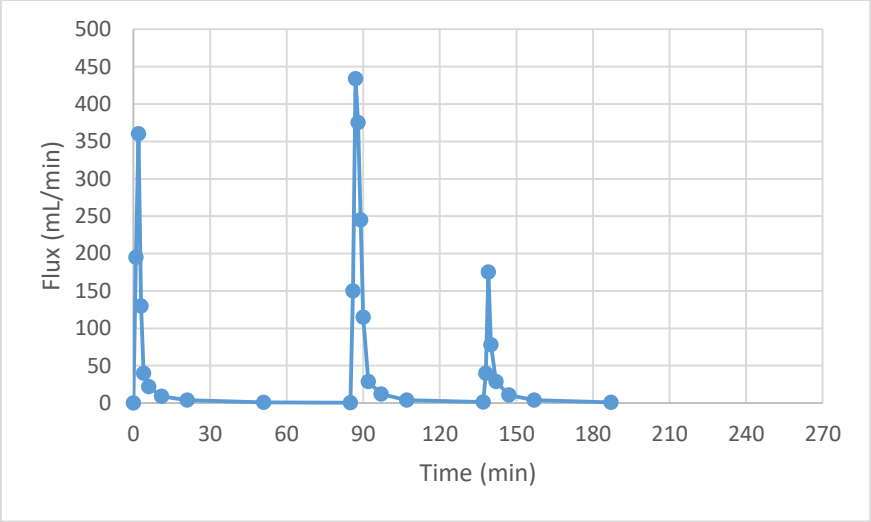

Figure 32. Flux graphic of the Plot 24.

Figure 32 shows the response of the filter material plot 24 to the three simulated rain events described in this chapter. Despite being observed in figure 32 the difference of the loaded volumes by the peaks of each of the three curves, there are other filter materials in which the difference between the 1 L and 1.5 L peaks is not significant or even the opposite. It is observable in all the materials studied that the peak of the 0.5 L is around half of the 1 L loading peak.

Furthermore, the peak value is reached between the second measurement and the third one. The fact that the water is completely or almost completely occupying the pores of the filter materials and the pressure that the water above is exerting are the reasons why it is the first minutes that the peak value is reached. Therefore, when almost all the water has come out from the column, the flux tends to be lower.

As exceptions, the peak value of the 1.5 L for Plot 30 (figure 33) and the peak values of the 1 L and 0.5 L for the Salz 2 (figure 34) are reached few minutes later. This is because these materials are finer so the infiltration takes more time and hence the generation of the peak.

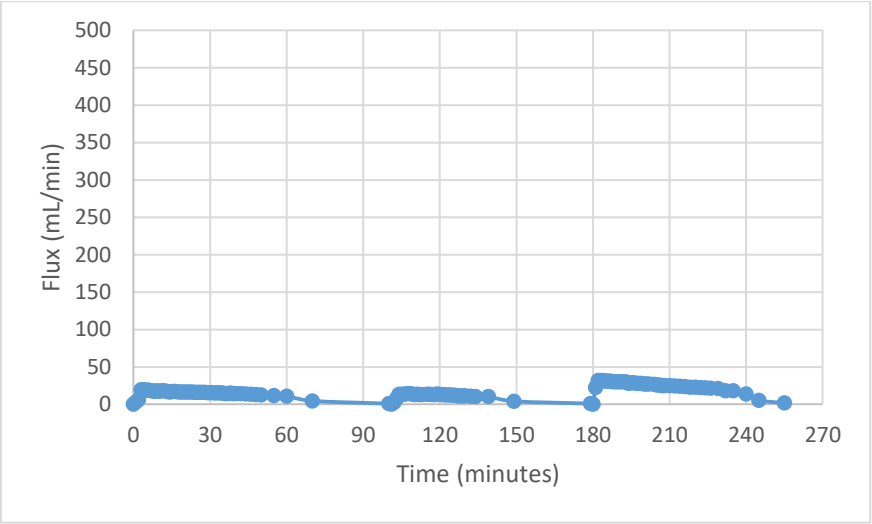

Figure 33. Flux graphic of the Plot 30.

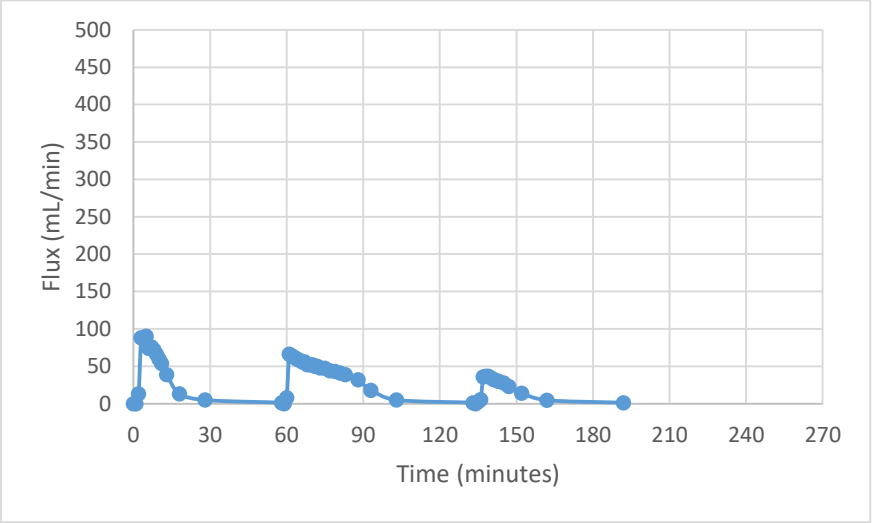

Figure 34. Flux graphic of the Salz 2.

When looking at the cumulative outflow of plot 24 it can be observed that there are some loadings in which more water than the introduced in the corresponding loading is collected. This happens in Plot 19 when the rain event of 0.5 L, in Plot 24 (figure 35) when the 1.5 L loading, and in Plot 30 (figure 36) when the 0.5 L and the 1.5 L. They all have in common that they are not the first loading (1 L). This is because not all the volume of the previous loading or loadings had been collected so that there were some water inside the pores of the material before starting with the next loadings which caused the higher cumulative effluent than expected.

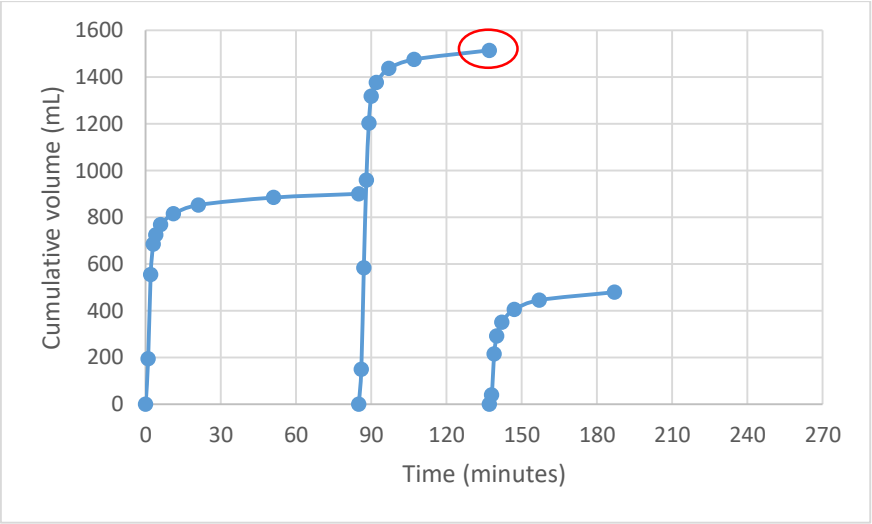

Figure 35. Cumulative volume graphic of the Plot 24.

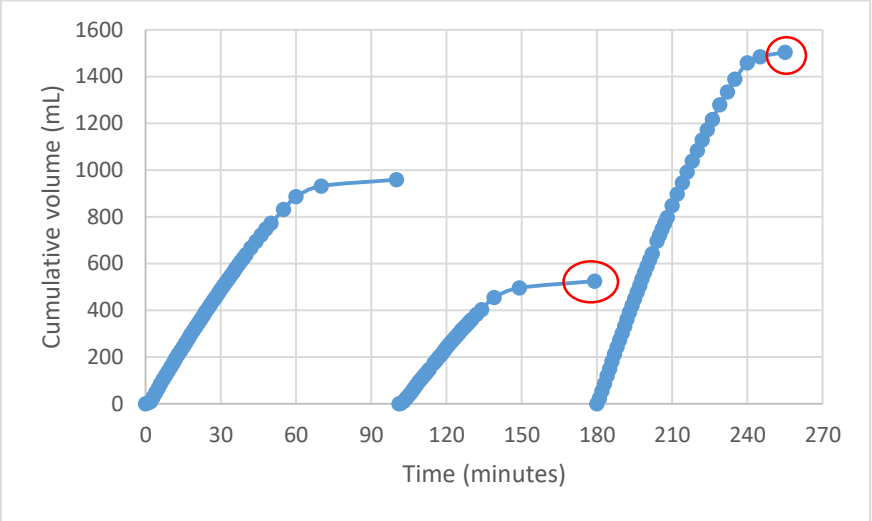

Figure 36. Cumulative volume graphic of the Plot 30.

The peak value reached in Plot 30 (figure 33) is significantly lower than the peak of the rest of the substrates and it took more time for the water to come out of the column. This is the reason why it was decided to carry out the 0.5 L rain event before the 1.5 L, just in case it was not possible to do the three loadings the same day. Moreover, as the saturated hydraulic conductivity experiment was highly likely to take several days, it was decided to not make this experiment with Plot 30 due to time issues.

Finally, it is observed that there are significant differences between two columns constructed with the same material. This is the case of Plot 3 and Plot 11. Plot 3 was repeated because when the saturated hydraulic conductivity experiment was carried out, the column was drained during the two days that took to finish the experiment, obtaining as a result different

measurements compared to the ones obtained when the material was not drained. Plot 11 was repeated twice, making Plot 11 2nd column and Plot 11 3rd column due to problems during the saturated hydraulic conductivity experiment. As there were significant differences between flow curves of Plot 11 1st column and Plot 11 3rd column it was decided to do all the experiments with another column, Plot 11 4th column. This is shown from figures 37 to 39.

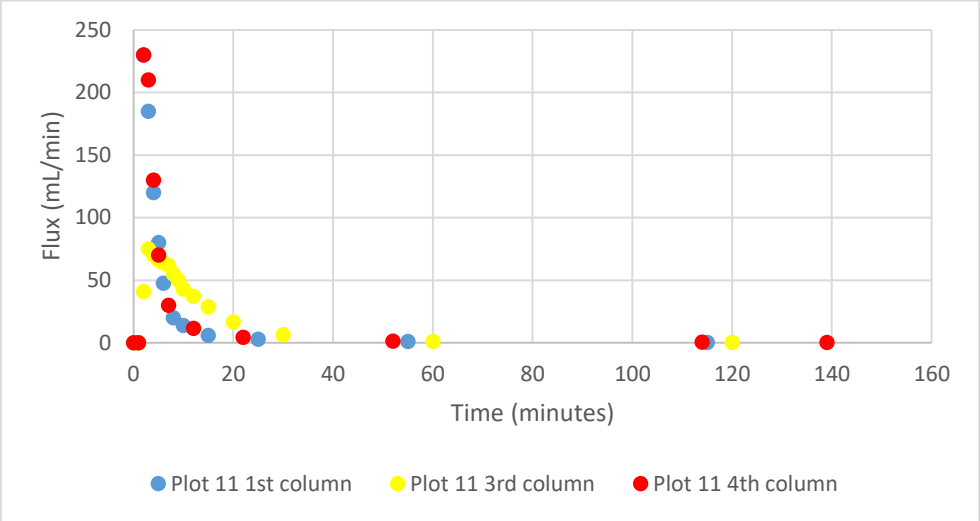

Figure 37. Comparison of the Plot 11 different columns in the 1 L loading.

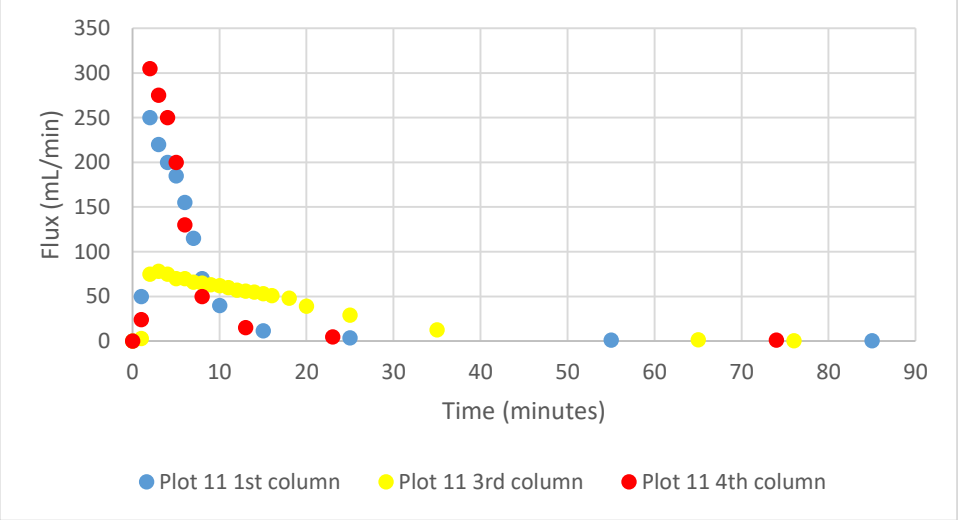

Figure 38. Comparison of the Plot 11 different columns in the 1.5 L loading.

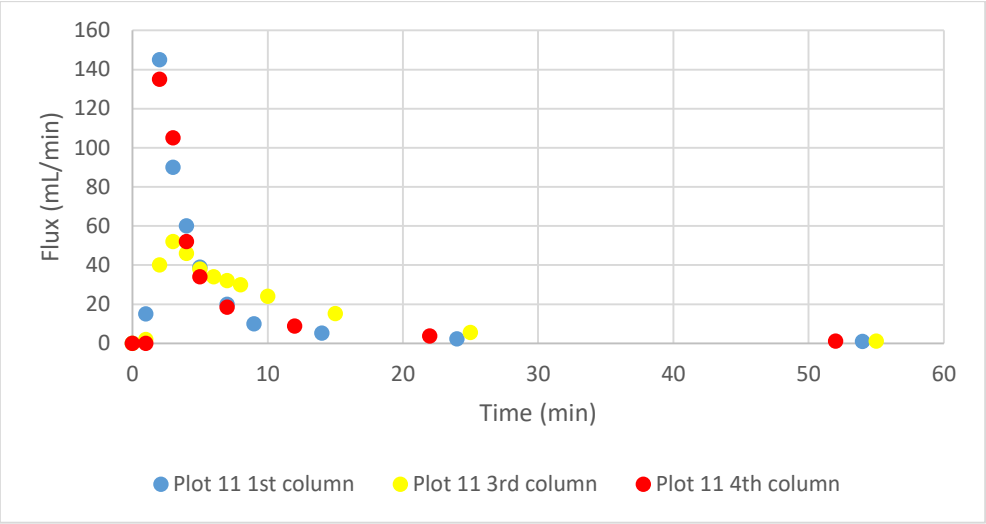

Figure 39. Comparison of the Plot 11 different columns in the 0.5 L loading.

The differences between two columns made of the same filter material have the main motive in the construction of the columns. Despite being the same materials and build up the columns the same way, the disposition of the particulates inside the column are never the same. This means that there can be preferential pathways that make the water flow faster or some compaction of a transversal section which make the water flow slower. It is very important to have this phenomenon in consideration and be aware of the different behaviours that the same soil can show on the nature field.

5.1.2.- Saturated hydraulic conductivity

The results of the saturated hydraulic conductivity are shown in this section. For the SAVE materials this parameter was determined by Beinlich (2016). After introducing the value of the different parameters described in section 4.1.4.-, the volume of water that is needed for the saturated hydraulic conductivity experiment is 84 L (*ÖNORM B2506-3, 2016)*. Figure 40 shows the container used which is calibrated for the needed volume.

Figure 40. Plastic container used for carrying out the saturated hydraulic conductivity experiment.

The saturated hydraulic conductivity of the Draingarden materials was determined at the laboratory following the procedure described in the section 4.1.4.- figure 41 shows the variation of the saturated hydraulic conductivity over time for all filter materials also including the repetition of the experiment for Plot 3 and Plot 11. It also shows the different results obtained when one material was studied more than once. What has to be highlighted is that all of them show values higher than the threshold value of 10^{-5} m/s, defined by the Austrian Standard (*ÖNORM B2506-3, 2016)* and therefore fulfil the obligated requirement.

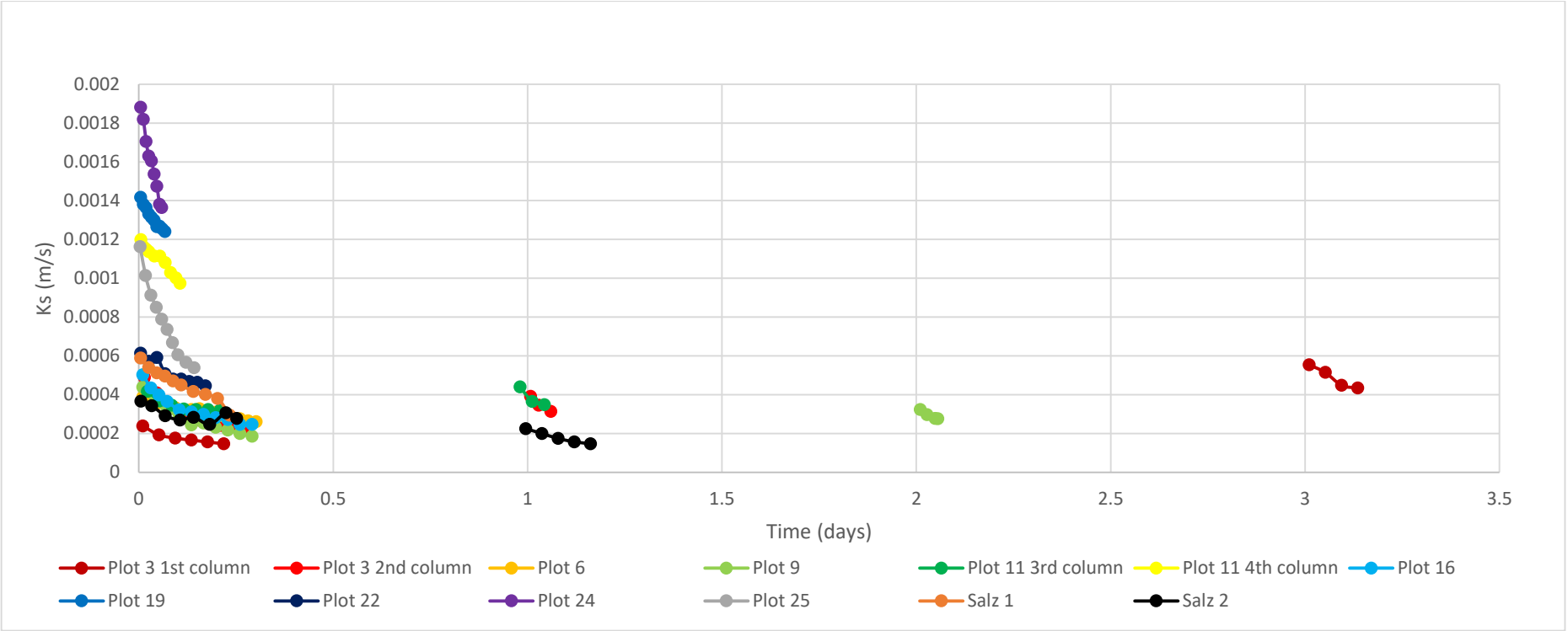

Figure 41. Measurements of the saturated hydraulic conductivity experiment for the Draingarden materials.

As it can be observed in figure 41, some materials needed more than one day for having all the 84 L passed through the column. Figures 42 to 47 provide a more detailed look on the k_{sat} determination.

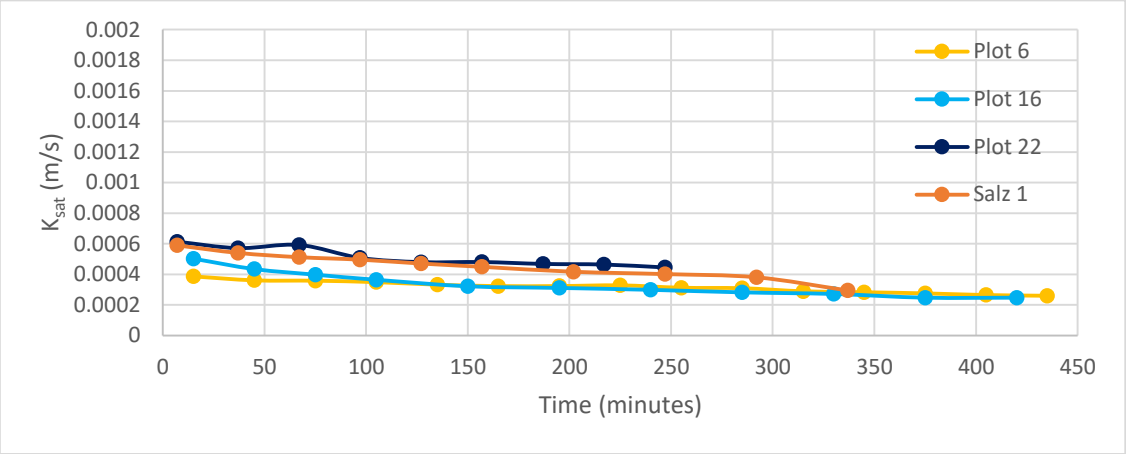

Figure 42. Saturated hydraulic conductivity experiment of the slower materials finished in one day.

figure 42 shows the materials that only took one day to have the 84 L passed through and it took more than 250 minutes for the experiment to be finished. These materials are Plot 6, Plot 16, Plot 22, and Salz 1. It can be observed that the saturated hydraulic conductivity tends to be smaller over time.

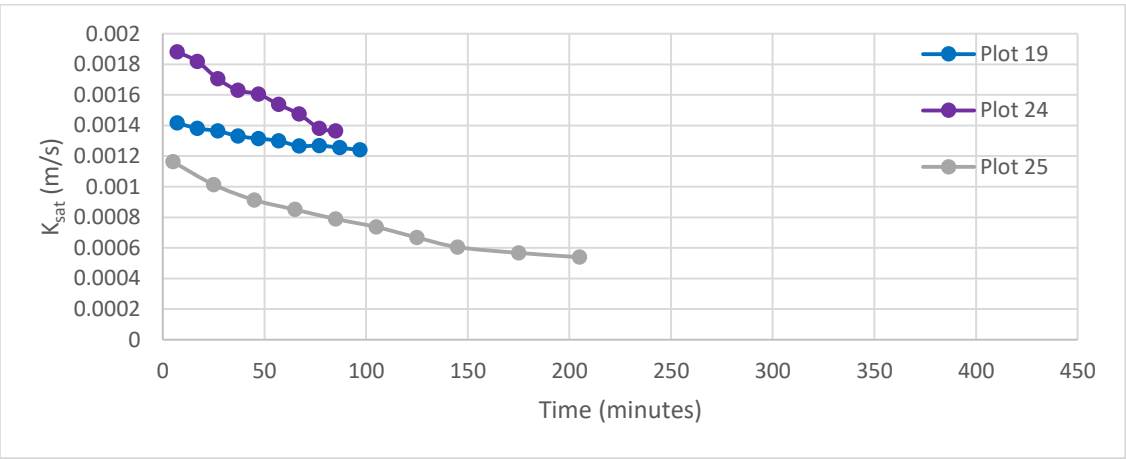

Figure 43. Saturated hydraulic conductivity experiment faster materials finished in one day.

In figure 43 the materials are shown are those which took less than 250 minutes for the experiment to be finished, which means that they were the fastest, and consequently the Draingarden materials with higher saturated hydraulic conductivity. It can also be observed that this parameter diminish over time, having the same behaviour than the slower materials.

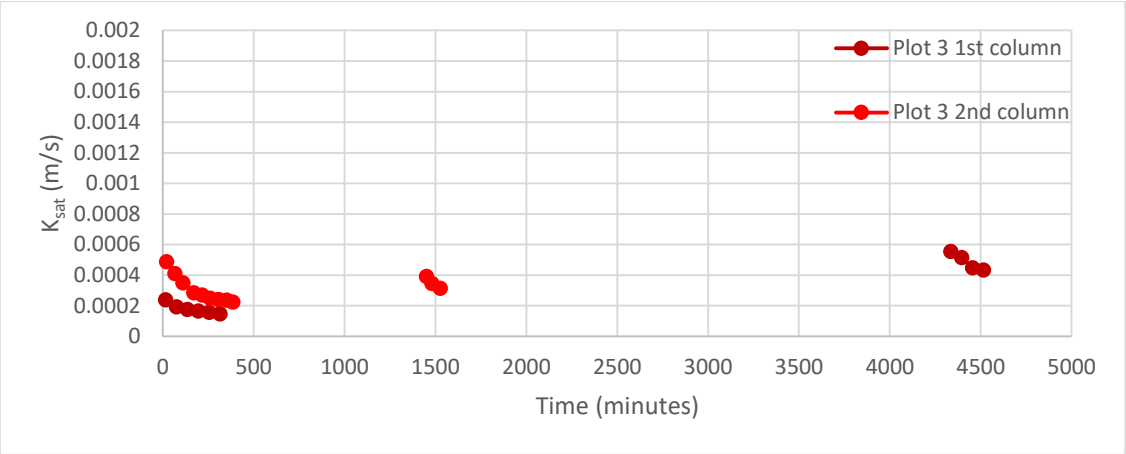

Figure 44. Saturated hydraulic conductivity experiment Plot 3.

Plot 3 was the first material to which the saturated hydraulic conductivity test was done. The first time, Plot 3 1st column, the column was drained between the two days that took the experiment to be finished. What can be observed is that this material in such conditions of drainage, was the only one that presented faster saturated hydraulic conductivity measurements the second day compared to the first day measurements. For that reason, the experiment was carried out again by building up a second column. Hence, when the rest of the materials needed more than one day, the water was left inside the column without being drained.

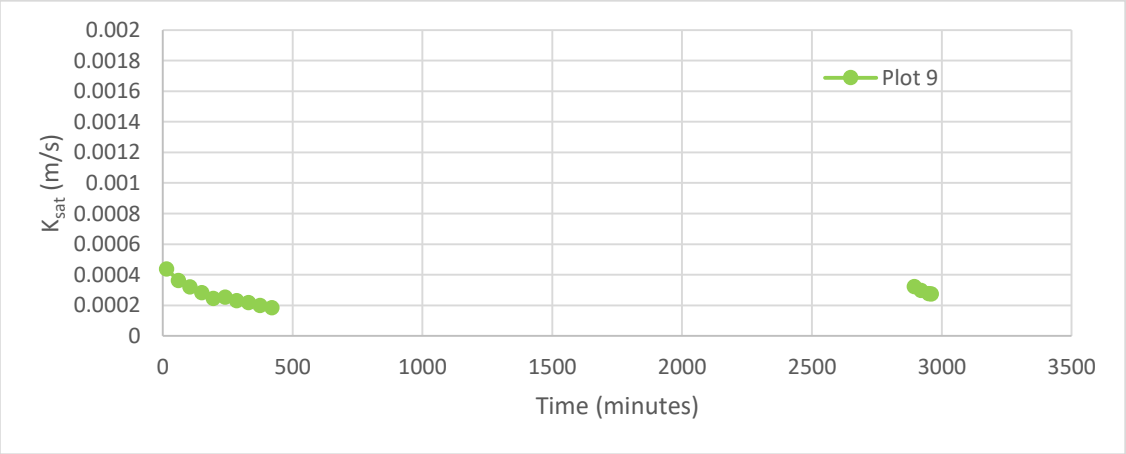

Figure 45. Saturated hydraulic conductivity experiment Plot 9.

Plot 9 (figure 45) was the first column to not be drained for the time between the two days that took the experiment to be finished. What can be observed is that in the first measure of the second day the value of the saturated hydraulic conductivity is higher than the last measure done the first day but smaller than the first one, which means that it is in the same

magnitude order as the previous measurements. This is the behaviour that was observed to be normal when the column was not drained.

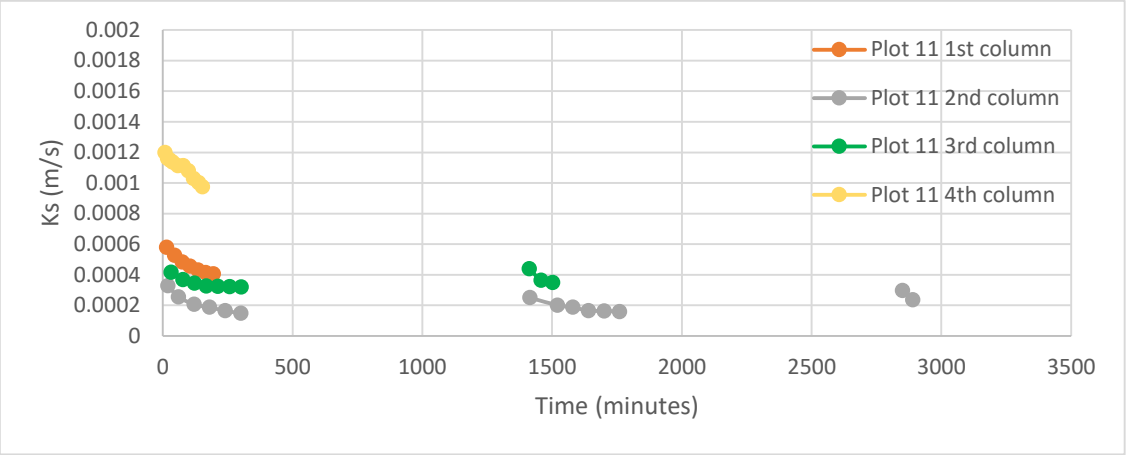

Figure 46. Saturated hydraulic conductivity experiment Plot 11.

Results for Plot 11 are shown in figure 46. The experiment had to be carried out a second time due to the entrance of air bubbles inside the column that made the water to flush out of the column so a second column was built to carry out the saturated hydraulic conductivity. The new results were different compared to the interrupted first data set. As the flow curves of the second column were not made, there was no possibility to compare that results so that it was decided to do both of them again by building up a third column.

The third column showed that the flow curves measurements were not similar to the measurements taken with the first column. So a fourth column was constructed in order to verify which behaviour was more common. This last column showed that the flow curves were quite similar to the first column but again the saturated hydraulic conductivity was bigger than the previous columns.

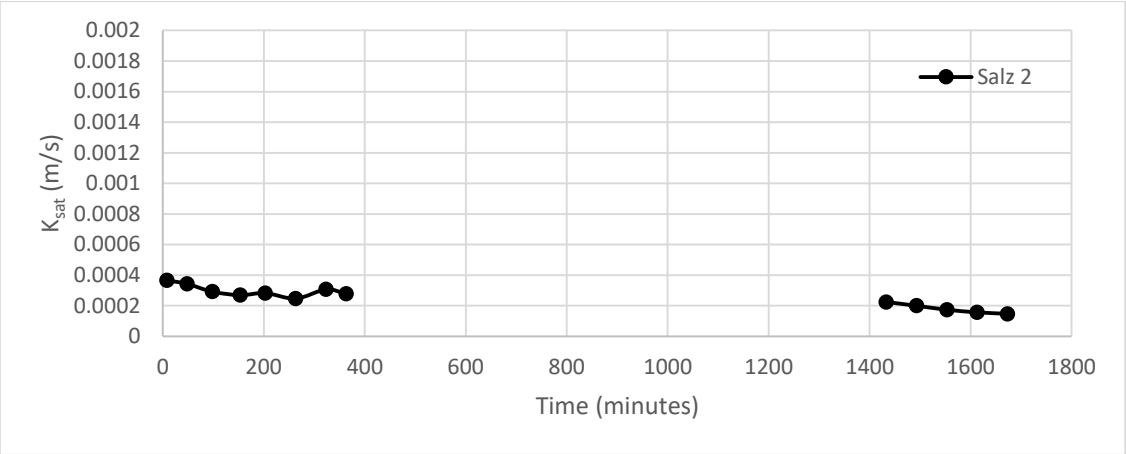

Figure 47. Saturated hydraulic conductivity experiment Salz 2.

The results of the Salz 2 (figure 47) show that the new measurements taken the second day were in the same magnitude than the previous ones.

Table 15 shows the overall results of the saturated hydraulic conductivity measurements calculated as the mean value of the measured data points.

Table 15. Saturated hydraulic conductivity of the filter materials studied.

Draingarden material	K_{sat} (m/s)	K_{sat} (cm/min)
Plot 3 1st column	3.03E-04	1.818
Plot 3 2nd column	3.17E-04	1.902
Plot 6	3.17E-04	1.902
Plot 9	2.79E-04	1.674
Plot 11 2nd column	2.10E-04	1.26
Plot 11 3rd column	3.58E-04	2.148
Plot 11 4th column	1.10E-03	6.6
Plot 16	3.35E-04	2.01
Plot 19	1.31E-03	7.86
Plot 22	5.14E-04	3.084
Plot 24	1.60E-03	9.6
Plot 25	7.84E-04	4.704
Plot 30	–	–
Salz 1	4.55E-04	2.73
Salz 2	2.53E-04	1.518
Pflanz Kalk*	2.25E-03	13.5
Granulit*	1.41E-03	8.46
Pflanz Kombi*	1.13E-03	6.78
Pflanz Zeolith*	3.53E-04	2.118
MA 42*	–	–

– Indicates that the experiment was not done for this material.
** This data was determined by Lisa Beinlich* (Beinlich, 2016).

The typical studies of the saturated hydraulic conductivity have been made to materials attending to the following classification: gravels (10^{-2} – 1); sands (10^{-3} - 10^{-1}); silty sands, and fine sands (10^{-3} - 10^{-5}); silts, sandy silts, and clayey sands (10^{-6} - 10^{-4}); and clays (10^{-6} - 10^{-9}), which values of the saturated hydraulic conductivity are expressed in cm/s. Due to the innovative purpose of this thesis there is still a lack of information related to the properties of the materials studied as a filter materials. This is the reason why this results are not compared to other studies. However, comparing the results obtained to the values of the typical materials mentioned we can situate the developed filter materials between gravels and sands.

5.1.3.- Pore volume

The pore volume was not determined within this thesis but determined within the two projects SAVE and Draingarden. The pore volume of the Draingarden filter materials (table 16) was estimated by the Institute of Sanitary Engineering at BOKU University, and the pore volume of the SAVE materials was determined by Lisa Beinlich (Beinlich, 2016) (table 17).

Table 16. Pore volume of the Draingarden materials.

Material	Pore volume %
Plot 3	46.5
Plot 6	46.5
Plot 9	44.4
Plot 11	47.75
Plot 16	46.0
Plot 19	39.7
Plot 22	43.0
Plot 24	52.7
Plot 25	47.1
Plot 30	No information
Salz 1	No information
Salz 2	No information

Table 17. Pore volume of the SAVE materials.

Material	Pore volume %
Pflanz Kalk	47
Granulit	43
Pflanz Kombi	45
Pflanz Zeolith	42
MA 42	Not measured

5.2.- Simulation Study

The inverse solution is the method used by HYDRUS® for the determination of unknown parameters from experimental data. As explained in section 4.2.5, this tool was used for the determination of the unknown soil hydraulic parameters of the studied filter materials.

It was not possible to build up a model in HYDRUS® for the determination of the other soil hydraulic parameters for the materials about which there was no information of their porosity nor their saturated hydraulic conductivity.

This software removes water that appears as runoff, for that reason it was decided to introduce the volumes for each filter material with a loading rate equal to its saturated hydraulic conductivity, calculating then the time of application of the loadings by using the equations (33) and (34) described in section 4.2.- Table 18 shows the actual loading rates used for the simulation study.

Table 18. Conversion of units for the time variable boundary conditions.

Material	Loading (L)	Loading rate (L/min)	Time (minutes)
Plot 3 1st column	1	0.1428	7.0035
	1.5	0.1428	10.5053
	0.5	0.1428	3.5018
Plot 3 2nd column	1	0.1494	6.6942
	1.5	0.1494	10.0413
	0.5	0.1494	3.3471
Plot 6	1	0.1494	6.6942
	1.5	0.1494	10.0413
	0.5	0.1494	3.3471
Plot 9	1	0.1315	7.6060
	1.5	0.1315	11.4089
	0.5	0.1315	3.8030
Plot 11 3rd column	1	0.1687	5.9275
	1.5	0.1687	8.8913
	0.5	0.1687	2.9638
Plot 11 4th column	1	05184	1.9291
	1.5	05184	2.8937
	0.5	05184	0.9646
Plot 16	1	0.1579	6.3345
	1.5	0.1579	9.5018
	0.5	0.1579	3.1673
Plot 19	1	0.6173	1.6199
	1.5	0.6173	2.4298
	0.5	0.6173	0.8099

Material	Loading (L)	Loading rate (L/min)	Time (minutes)
Plot 22	1	0.2422	4.1285
	1.5	0.2422	6.1928
	0.5	0.2422	2.0643
Plot 24	1	0.7540	1.3263
	1.5	0.7540	1.9894
	0.5	0.7540	0.6631
Plot 25	1	0.3695	2.7067
	1.5	0.3695	4.0601
	0.5	0.3695	1.3534
Pflanz Kalk	1	1.0603	0.9431
	1.5	1.0603	1.4147
	0.5	1.0603	0.4716
Granulit	1	0.6645	1.5050
	1.5	0.6645	2.2575
	0.5	0.6645	0.7525
Pflanz Kombi	1	0.5325	1.8779
	1.5	0.5325	2.8169
	0.5	0.5325	0.9390
Pflanz Zeo	1	0.1663	6.0115
	1.5	0.1663	9.0173
	0.5	0.1663	3.0058

An example of the time variable boundary conditions is shown in the next table where the values used for the Plot 3 1st column are shown.

Table 19. Time variable boundary conditions of the Plot 3 1st column.

	Time (minutes)	Precipitation (cm/min)
1	7.003517848	12.73
2	71	0.00
3	78.00351785	12.73
4	142	0.00
5	152.5052768	19.10
6	194	0.00
7	197.5017589	6.37
8	230	0.00

The unknown parameters of van Genuchten-Mualem soil hydraulic model namely alpha, n and θ_r are obtained by using the inverse solution. Thereby the simulated boundary flux (table 20) and cumulative flux (table 21) respectively are fitted to the measured outflow data.

Table 20. Inverse solution results when flux data is used.

INVERSE SOLUTION FLUX							
Material	**Q_r**	**Q_s***	**α**	**n**	**K_{sat}* (cm/min)**	**l***	**SSQ**
Plot 3 1st column	0.1023	0.465	0.1222	1.247	1.818	0.5	8.90E-01
Plot 3 2nd column	0.008251	0.465	0.07276	1.169	1.902	0.5	3.42E-01
Plot 6	0.1269	0.465	0.000587	4.947	1.902	0.5	5.35E-01
Plot 9	0.0202	0.444	0.07723	1.649	1.674	0.5	1.28E+00
Plot 11 3rd column	0.008747	0.4775	0.08589	2.104	2.148	0.5	3.58E+00
Plot 11 4th column	0.03848	0.4775	0.1822	4.8	6.600	0.5	3.43E-01
Plot 16	0.06693	0.46	0.1541	1.367	2.010	0.5	6.96E-01
Plot 19	0.002387	0.397	0.06704	2.434	7.860	0.5	5.41E-01
Plot 22	0.0171	0.397	0.2919	1.378	3.084	0.5	1.65E-01
Plot 24	0.05394	0.527	0.1347	6.015	9.600	0.5	4.66E-01
Plot 25	0.01907	0.471	0.03123	1.534	4.704	0.5	1.56E-01
Pflanz Kalk	0.0251	0.47	0.2224	5.287	13.500	0.5	2.49E-01
Granulit	0.009622	0.43	0.06547	1.997	8.460	0.5	1.58E+00
Pflanz Kombi	0.002555	0.45	0.1747	1.513	6.780	0.5	1.74E+00
Pflanz Zeo	0.09191	0.42	0.7134	1.891	2.118	0.5	1.27E+00

**Fixed values. K_{sat} and Q_s determined at the laboratory and l is the Mualem pore connectivity parameter.*

Table 21. Inverse solution results when cumulative volume data is used.

INVERSE SOLUTION CUMULATIVE VOLUME							
Material	**Q_r**	**Q_s***	**α**	**n**	**K_{sat}* (cm/min)**	**l***	**SSQ**
Plot 3 1st column	0.0651	0.465	0.1342	1.34	1.818	0.5	1.22E-01
Plot 3 2nd column	0.0124	0.465	0.0252	1.151	1.902	0.5	1.09E-02
Plot 6	0.0272	0.465	0.000201	1.663	1.902	0.5	3.17E-02
Plot 9	0.1128	0.444	0.1065	1.269	1.674	0.5	9.06E-03
Plot 11 3rd column	0.00006352	0.4775	0.1275	2.415	2.148	0.5	3.35E-02
Plot 11 4th column	0.1501	0.4775	0.1146	3.519	6.600	0.5	5.36E-03
Plot 16	0.1586	0.46	0.07475	1.244	2.010	0.5	5.64E-03
Plot 19	0.01661	0.397	0.1035	4.239	7.860	0.5	5.23E-03
Plot 22	0.1468	0.397	0.07489	1.253	3.084	0.5	5.84E-03
Plot 24	0.1655	0.527	0.1035	3.977	9.600	0.5	7.03E-03
Plot 25	0.1122	0.471	0.09145	1.321	4.704	0.5	6.70E-03
Pflanz Kalk	0.09043	0.47	0.1198	3.497	13.500	0.5	5.94E-03
Granulit	0.0003377	0.43	0.1318	3.196	8.460	0.5	2.44E-02
Pflanz Kombi	0.002279	0.45	0.1083	3.76	6.780	0.5	3.22E-02
Pflanz Zeo	0.2481	0.42	0.1093	1.198	2.118	0.5	2.20E-02

**Fixed values. K_{sat} and Q_s determined at the laboratory and l is the Mualem pore connectivity parameter.*

From the previous tables (table 20 and table 21) it can be seen that the sum of squared residual (SSQ) values for the inverse solution method carried out with the cumulative volume

data are lower than the ones obtained with the flux data for all the filter materials studied with this tool. This means that the calculated points are closer to the measurements when the cumulative data is introduced. This can be seen in the Figures 52 to 54 (flux figures) as the peak value is hardly fitted, while for the cumulative flux the total volume can be reached more easily giving a better statistically fit.

For the inverse solution there were used four loadings instead of three as the first loading (1 L) was introduced twice. This was made because the program uses the first set of data to correct the calculations during the simulation. So there were introduced four loadings (1 L, 1 L, 1.5 L, and 0.5 L). However, the data of the first artificial loading was not introduced for the fitting.

Annex 2 includes all graphics for the simulated filter materials. In all the graphics, three curves are plotted: (i) the measured data, (ii) the fitted flux data simulated, and (iii) the fitted cumulative data simulated.

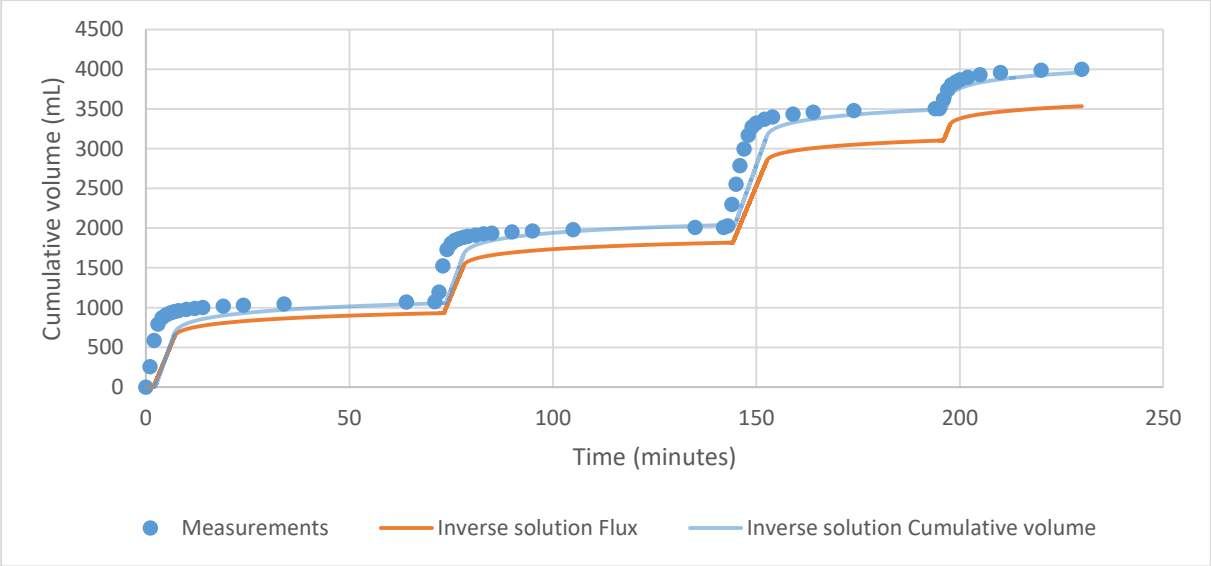

Figure 48. Inverse solution cumulative volume results of Plot 3 1st column.

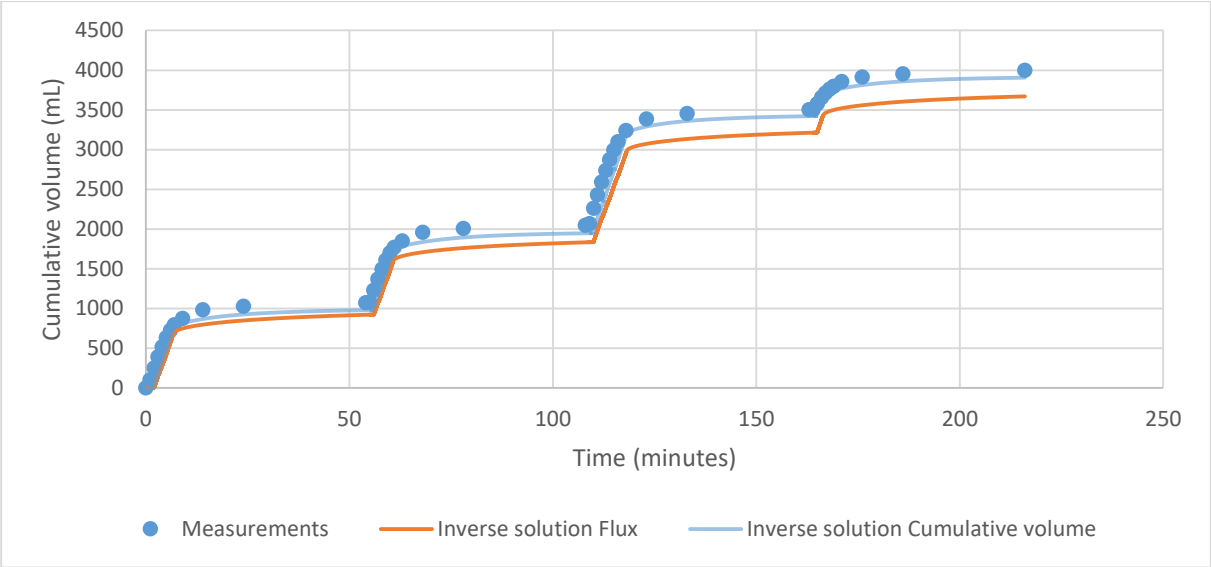

Figure 49. Inverse solution cumulative volume of Plot 3 2nd column.

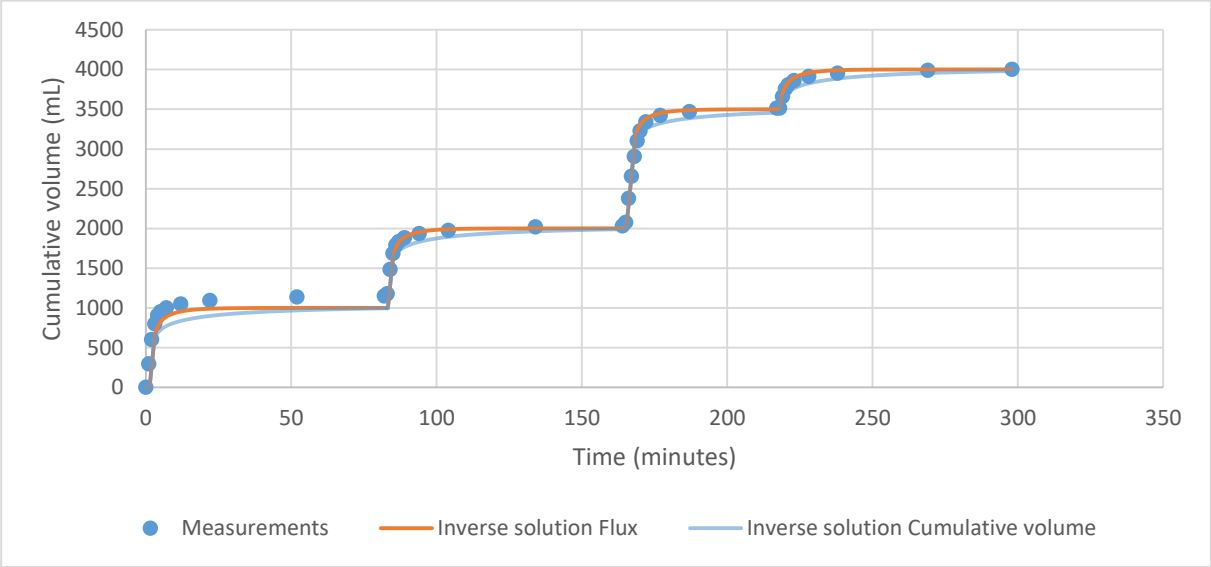

Figure 50. Inverse solution cumulative volume of Plot 25.

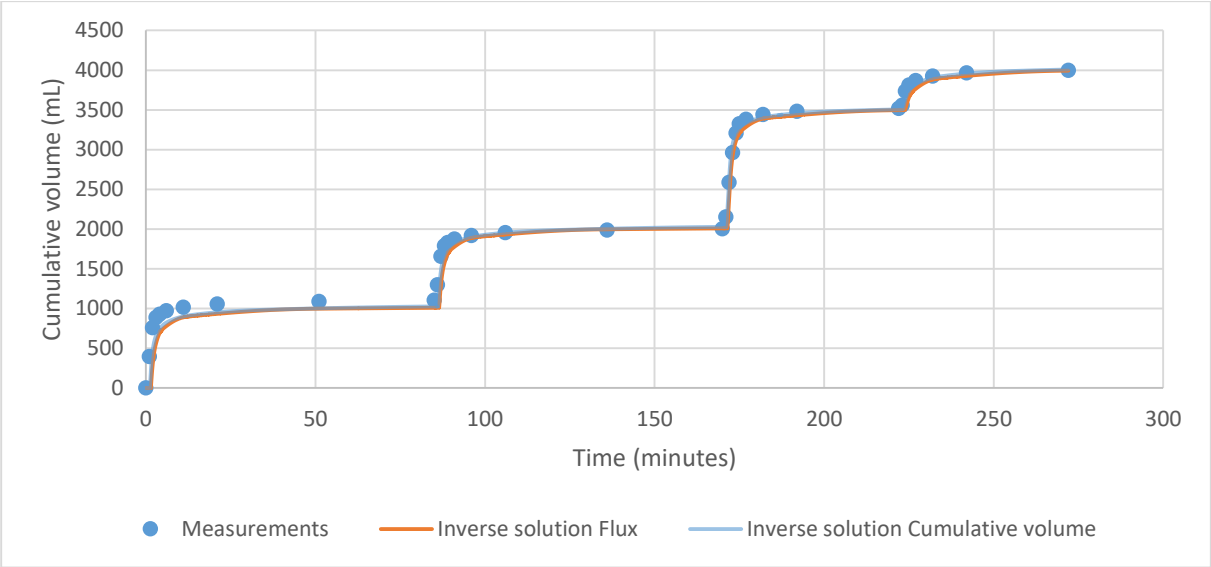

Figure 51. Inverse solution cumulative volume results of Plot 24.

From the results a good fit of the cumulative measured and simulated data can be determined. It can be observed that there are not significantly differences between the two simulations for most of the materials. In Plot 3, either the 1st column (figure 48) or the 2nd column (figure 49), the results show that the best approach is obtained when the cumulative volume data is used for the calculations. However, what can be seen in Plot 25 (figure 50) is the opposite, the inverse solution done by utilising the flux data provide the best approach. Despite generating better approach the simulations run with the cumulative volume data, the rest of the materials show that there are not significant differences between the two simulations (figure 51).

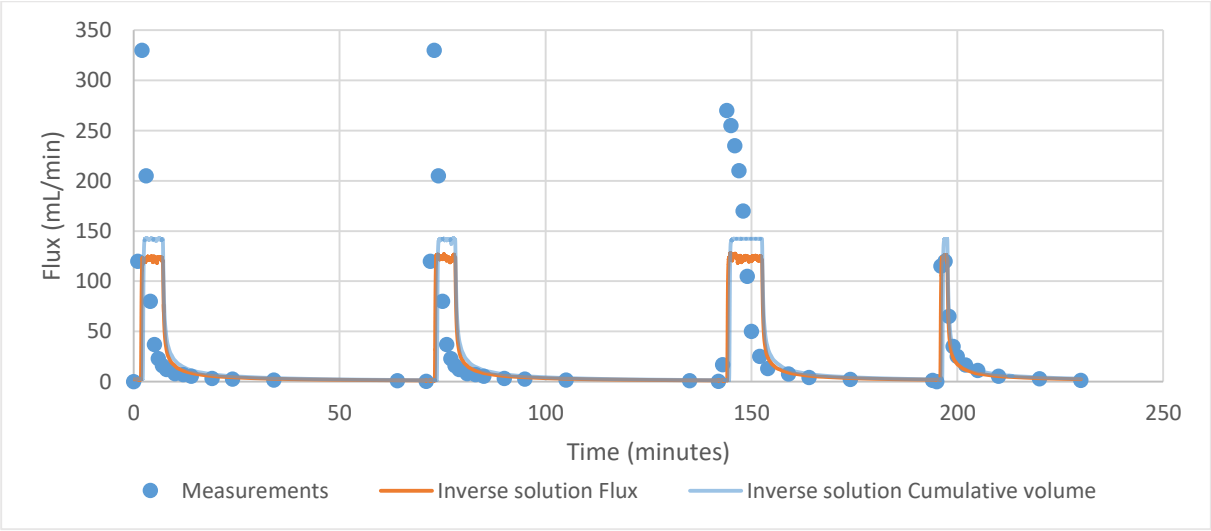

Figure 52. Inverse solution flux results of Plot 3 1st column.

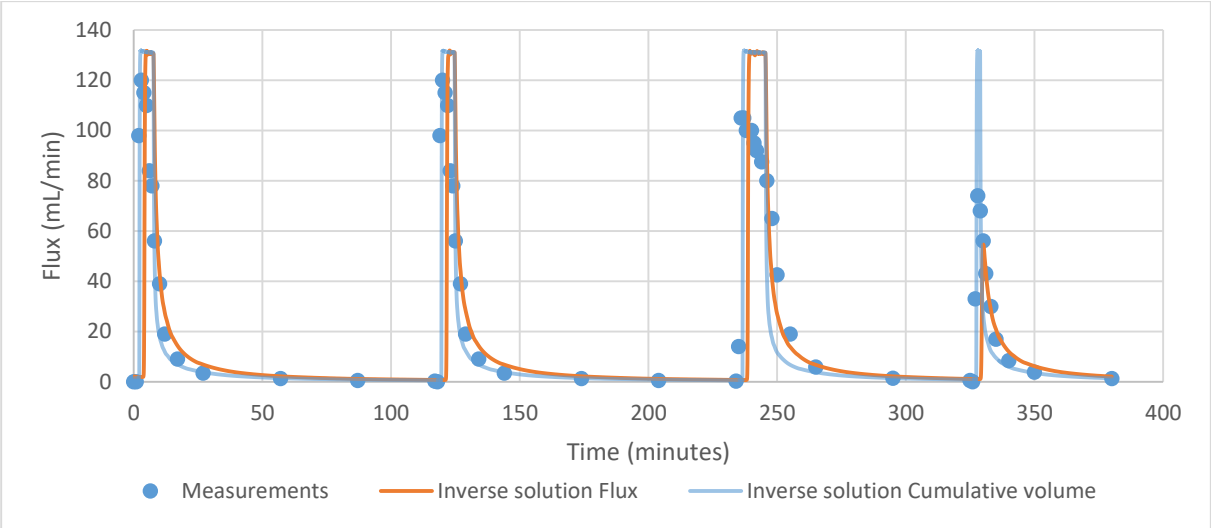

Figure 53. Inverse solution flux results of Plot 9.

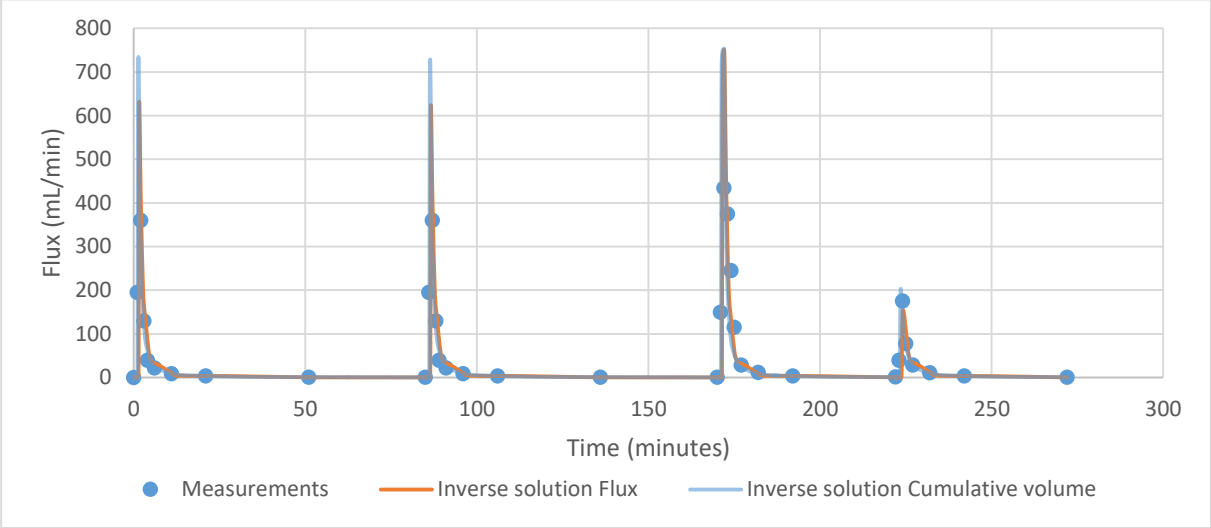

Figure 54. Inverse solution flux results of Plot 24.

Within the flux graphics two types of results can be observed. There are some materials (Plot 3 1st column (figure 52), Plot 3 2nd column, Plot 6, and Pflanz Zeolith) which simulated curves are not able to plot the peak of the curves. As can be seen in their graphics, in those cases the curves represent either a plain without arriving to the maximum measured value or an irregularity instead of the peaks. What these materials have in common is that their saturated hydraulic conductivity is small compared to the rest of the materials (1.818, 1.902, 1.902, and 2.118) except Plot 9 (1.674). This might be produced because of a numerical problem during the simulations.

There are other materials such as Plot 9 (figure 53), Plot 16 (2.01), and Plot 22 (3.084) where the 1 L and 1.5 L are quite well simulated but show a small plain instead of a peak. In these

three materials the 0.5 L simulation give a higher peak value than the measured. What happens to the 0.5 L simulation of Plot 9, Plot 16, and Plot 22 is the same that happens to the rest of the materials (Plot 11 3rd column, Plot 11 4th column, Plot 19, Plot 24 (figure 54), Plot 25, Pflanz Kalk, Granulit, and Pflanz Kombi) with all the loadings, that have higher values of saturated hydraulic conductivity, which simulated peaks are higher than the measured data. This is because the measurements were taken every minute, being possible to lose the real peak value as it is produced instantaneously.

5.2.1.- Solute transport

What it is described with the solute transport simulation is the variation over time of the relationship between the concentrations of zinc measured in the outflow (C_0) over the maximum concentration of zinc in the outflow, which is the concentration introduced in the inflow, 400 µg/L, (C). This concentration occurs when the adsorption capacity is exhausted.

As said in section 4.2.1.-, what is looked for is a comparison of the filter materials related to their different adsorption capacity. For that reason, the adsorption parameters introduced are the same for all the filter materials with the only difference of their soil hydraulic parameters.

In *Annex 3* the graphics obtained for all the filter materials can be observed. Two types of graphics can be observed: the first type is shown in figure 55, and the second type can be seen in figure 56. The first type of behaviour shows that the material adsorbs zinc until the maximum adsorption capacity is reached when the concentration of zinc in the outflow increases instantaneously. However, what can be observed in the second type of graphics is that the filter material adsorption capacity is being decreased exponentially until the time when the increase is produced instantaneously which ends with the exhaustion of their adsorption capacity.

The main difference between these two behaviours is that while the second type of filter materials is advising that the exhaustion of the adsorption capacity is being reached, the first type of filter materials does not show anything until they are completely exhausted. The filter materials that show the first type behaviour are dolomite, granulite, the mixture of granulite and perlite, and Haldit. The criteria followed was that the maximum exponential exhaustion of their adsorption capacity was less than 30%. The filter materials that follow the second type

behaviour are made of either with other materials or with some of the mentioned materials in mixtures with other materials.

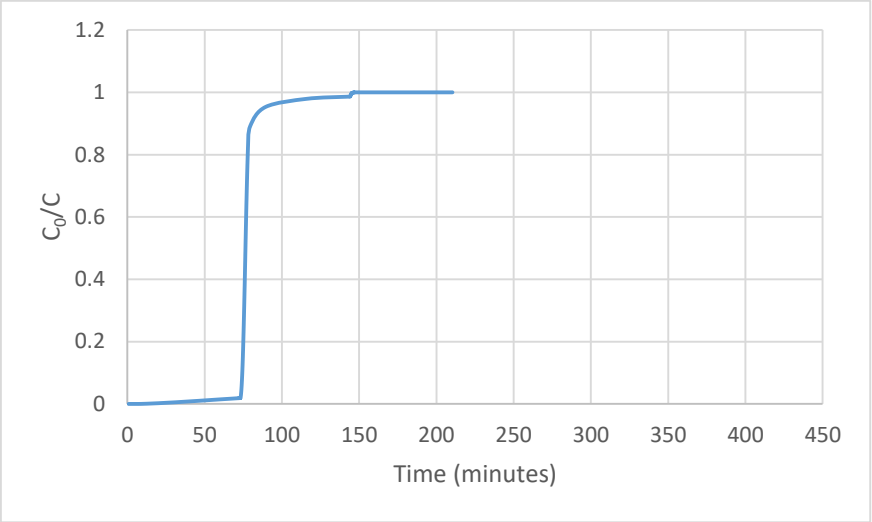

Figure 55. Breakthrough of the Plot 3 1st column.

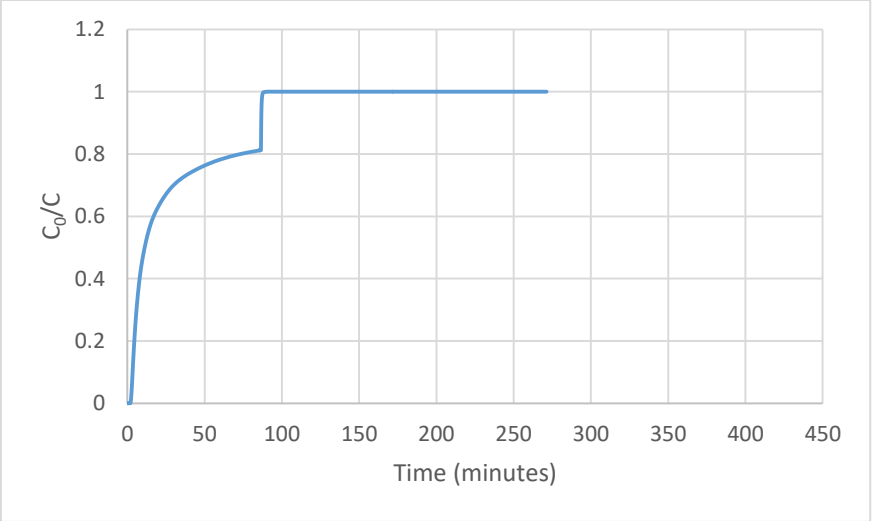

Figure 56. Breakthrough of Plot 24.

Table 22 shows the moment when 90% of the inflow concentration of zinc has reached the outflow, which is the situation considered to define their lifespan. As each of the filter materials has its own timing for the introduction of the loadings and the duration of the drainage, it has to be considered the volume of water that has been collected by the time that the breakthrough is produced.

Table 22. Time when the breakthrough is produced.

Material	Time Breakthrough (min)	Cumulative volume (mL)
Plot 3 1st column	80.75	1620
Plot 3 2nd column	74.11	1735
Plot 6	86.72	1660
Plot 9	124.31	1400
Plot 11 3rd column	124.97	1050
Plot 11 4th column	88.88	1030
Plot 16	121.33	1610
Plot 19	37.79	989
Plot 22	86.60	1380
Plot 24	86.61	1150
Plot 25	84.81	1580
Pflanz Kalk	30.07	968
Granulit	113.40	1150
Pflanz Kombi	133.88	1080
Pflanz Zeolith	120.40	1410

The results show that the material with a higher adsorption capacity is Plot 3 2nd column because the breakthrough is produced when more cumulative volume is collected out of the system for the same zinc concentration. It is shown in figure 57.

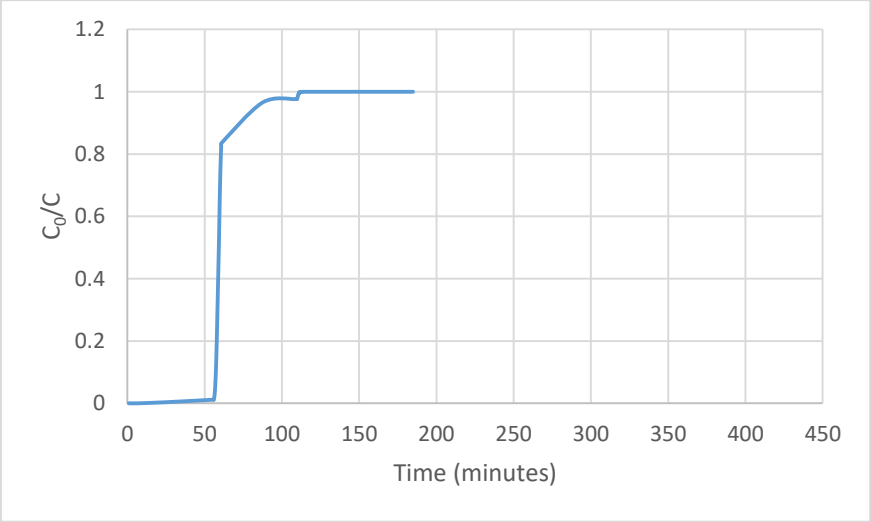

Figure 57. Breakthrough of Plot 3 2nd column.

Further studies related to the adsorption capacity and the reason why there are some filter materials that has a better response for this property have to be carried out. Not only do these studies have to obtain the real adsorption parameters for the widespread isotherm expressions but also the relationship between their adsorption capacity and composition.

6.- SUMMARY AND CONCLUSIONS

Water is the most vital resource in the world due to its importance for the human being. It is essential for human existence and human settlement and it is employed in urban areas for the disposal of wastes. With the increase of extreme events such as floods, droughts, heat islands and also water shortage, interdisciplinary solutions within the urban space are needed. Urban runoff can generate flooding, drainage, erosion and sedimentation problems which are exacerbated due to the infiltration reduction as a result of the increasing impervious areas.

The problem is not only related to stormwater runoff quantity but also its quality. In this context the green zones of the cities shall be used for the retention and treatment of street runoff and also provide a good environment for plants growth. It is not different for the city of Vienna which is working in collaboration with the Institute of Sanitary Engineering at BOKU for the development of filter materials that provide the required properties. The present work is the first approach to the filter materials developed within the SAVE and Draingarden projects.

The filter materials are tested in the laboratory of the Institute of Sanitary Engineering and Water Pollution Control at the University of Natural Resources and Life Science, Vienna (BOKU) between October and December 2016. The experiments are carried out into columns. The saturated hydraulic conductivity and the porosity experiments are done according to the requirements of the Austrian Standard *ÖNORM B2506-3 "Soakaways for rainwater from roof gutters and reinforced surfaces – Part 3: Filter materials – Requirements and tests"*. This norm is chosen as a guideline for the evaluation of these two parameters. It is also carried out an experiment that provides the flow curves for three different loadings with which an own experimental procedure is created in the frame of this work.

The information of the flow curves experiment is needed for the determination of the other soil hydraulic parameters for the van Genuchten-Mualem soil hydraulic model. With this measured data, the unknown soil hydraulic parameters are determined by using the inverse solution of the water flow model within the HYDRUS® software package. With these parameters, a water flow model based on three applied rain events can be setup and furthermore be used as basis for future modelling approaches.

Based on the results of the thesis it can be concluded that:

- The construction of the column for the experiments is extremely important due to the effect it has on the experimental results.
- In the flow curve experiment is necessary to wait until almost all the water of one loading has been collected before starting with the next loading, so that the water from one loading is not mixed with the next one.
- When the materials are fine-textured it may take more than one day to finish the saturated hydraulic conductivity experiment. Depending on how the column is left for continuing the experiment the next day, drained or saturated, it affects the result. It was decided to leave the column saturated because the conditions will be more similar to which would be if the experimental is not interrupted. Moreover, it was observed that when the column was drained the measures taken in the second day were quite different to the ones obtained the first day. It might be caused because of the redistribution of the particles.
- In the modelling part with HYDRUS®, it is not possible to obtain good results with the inverse solution for the materials which saturated hydraulic conductivity was lower than 3 cm/min. However, good results are obtained for the rest of the materials, either the inverse solution is simulated with the flux data or the cumulative volume data.
- There are not significant differences between doing the inverse solution with flux data or with cumulative volume data for most of them. Plot 3 1st column, Plot 3 2nd column and Plot 22 show that the inverse solution with cumulative volume data is better than the inverse solution with flux data for the cumulative volume results.
- Using the model created for the zinc transport simulations throughout the filter materials, the results show that the Plot 3 2nd column is the material that has more adsorption capacity.

7.- OUTLOOK

Knowing that this work is a first approach to Draingarden materials, the future steps in SAVE and Draingarden projects will reveal the properties that the developed filter materials provide. In this sense, the next lines of investigation that should be studied are:

- Research for another soil hydraulic model with HYDRUS® that makes it possible the modelling of the filter materials with lower saturated hydraulic conductivity.
- The removal capacity of the substrates for the typical pollutants that can be found in stormwater runoff.
- It has to be studied the effect of clogging in these filter materials in order to account their lifespan.
- Some pilot-scale experiments should be required so that the experimental characteristics can be verified.
- Experiments related to the adsorption of heavy metals should be carried out in order to use that measurements to calculate the real Langmuir and/or Freundlich parameters that are intrinsic of each filter material.
- Further research that relates the adsorption capacity of the filter materials with their composition should also be carried out.

8.- REFERENCES

Ashley, R., Garvin, S., Pasche, E., Vassilopoulos, A., & Zevenbergen, C. (2007). *Advances in urban flood management.* London: Taylor and Francis/Balkema.

ASI. (2016). *ÖNORM B 2506-3: Regenwasser-Sickeranlagen für Abläufe von Dachflächen und befestigten Flächen, Teil 3: Filtermaterialien: Anforderungen und Prüfmethoden.*

Assouline, S. (2001). A model for soil relative hydraulic conductivity based on the water retention characteristic curve. *Water Resources Research*, 37: 265-272.

Austria. (2011). *Climate,* Retrieved May 9, 2017, from Austria.org: http://www.austria.org/climate

Austria. (2011). *Economy,* Retrieved May 9, 2017, from Austria.org: http://www.austria.org/economy

Austria. (2011). *Environmental protection,* Retrieved May 9, 2017, from Austria.org: http://www.austria.org/environmentalprotection

Averjanov, S. F. (1950). About permeability of subsurface soils in case of incomplete saturation. *English Collection, 7*.

Ballard, B. W., Wilson, S., Udale-Clarke, H., Illman, S., Scott, T., Ashley, R., & Kellagher, R. (2015). *The SuDS Manual.* London: Ciria C753.

Beinlich, L. (2016, August 10). Evaluation of filter materials for urban stormwater management - green infraestructure in the city of Vienna. Vienna, Austria.

Boreli , M., & Vachaud, G. (1966). Note sur la determination de la teneur en eau résiduelle et sur la variation de la perméabilité relative dans les sols non saturés. *Comptes Rendus de l'Académie des Sciences*, 263: 698-701.

Brooks, R. H., & Corey, A. T. (1964, March). Hydraulic properties of porous media. *Colorado State University Hydrology paper, 27*(3).

Burdine, N. T. (1953). Relative permeability calculation size distribution data. *Transactions of the American Institute of Mining. Metallurgical and Petroleum Engineers*, 198: 71-78.

Chalermyanont, T., Arrykul, S., & Charoenthaisong, N. (2008). Transport of heavy metals and chemical compatibility of hydraulic conductivity of a compacted sand-bentonite mixture. *Songklanakarin Journal of Science and Technology*, 30 (2): 269-276.

Childs, E. C., & Collis-George, S. a. (1950). The permeability of porous materials. *Proc. Roy. Soc. Ser.*, A, 201, 392-405.

Davies, A. P., Shokouhian, M., & Ni, S. (2000). Loading stimates of lead, cooper, cadmium and zinc in urban runoff from specific sources. *Chemosphere*, 44: 997-1009.

Durner, W. (1994). Hydraulic conductivity estimation for soils with heterogeneous pore structure. *Water Resources Research*, 32(9): 211-223.

EU. (2000). *Directive 2000/60/EC of the European Parliament and of the Council establishing a framework of the Community action in the field of water policy.*

Fredlung, D. G., Xing, A., & Huang, S. (1994). Predicting the permeability function for unsaturated soils using the soil-water characteristic curve. *Canadian Geotechnical Journal*, 31(3): 521-532.

Fryd, O., Backhaus, A., Jeppesen, J., Ingvertsen, S. T., Birch, H., Bergman, M., Petersen, T. E. P., Fratini, C., & Jensen, M. B. (2009). *Connected Disconnections: conditions for landscape-based disconnections of stormwater from the Copenhaguen sewer system in the cathcment area for river Hanestrup. The 2BG Project Working Report: River Hnestrup case study.* Copenhaguen: Danish Centre for Forest, Landscape and Planning, University of Copenhagen.

Göbel, P., Dierkes, C., & Coldewey, W. G. (2007). Storm water runoff concentration matrix for urban areas. *Journal of Contaminant Hydrology*, 91: 26-42.

Good, J. F., O'Sullivan, A. D., Wicke, D., & Cochrane, T. A. (2012). Contaminant removal and hydraulic conductivity of laboratory rain garden systems for stormwater treatment. *Water Science & Technology*, 2154-2161.

Hellström, D., Jeppsson, U., & Kärrman, E. (2000). A framework for systems analysis of sustainable urban water management. *Environ, Impact Asses*, 20: 311-321.

Helmreich, B., Hilliges, R., Schriewer, A., & Horn, H. (2010). Runoff pollutants of a highly trafficked urban road - Correlation analysis and seasonal influences. *Chemosphere*, 80: 991-997.

Hopmans, J. W., Šimůnek, J., Romano, N., & Durner, W. (2002). Inverse Modelling of Transient water flow. In *Methods of Soil Analysis, Part 1, Physical Methods, Chapter 3.6.2* (pp. 963-1008). Madison, WI: J. H. Dane and G. C. Topp, Third edition, SSSA.

Horton, R. E. (1933). The role of infiltration in the hydrologic cycle. *Transactions, American Geophysical Union*, 446-460.

Hunt, A., & Watkiss, P. (2011). Climate change impacts and adaption in cities: a review of the literature. *Climatic Change*, 104: 13-49.

Iden, S. C., Peters, A., & Durner, W. (2015). Improving prediction of hydraulic conductivity by constraining capillary bundle models to a maximum pore size. *Advances in Water Resources*, 85: 86-92.

Irmay, S. (1954). On the hydraulic conductivity of unsaturated soils. *Eos Transactions American Geophysical Union*, 35: 463-467.

Kosugi, K. (1996). Lognormal distribution model for unsaturated soil hydraulic properties. *Water Reources Research*, 32(9): 2697-2703.

Kozeny, J. (1927). Über Kapillare Leitung der Wasser im Boden. *Sitzungsberichte der Kaiserlichen Akademie der Wissenschaften*, 136: 271-306.

Krishna, R. R., Xie, T., & Dastgheibi, S. (2014). Mixed-Media Filter System for Removal of Multiple Contaminants from Urban Storm Water: Large-Scale Laboratory Testing. *Journal of Hazardous, Toxic, and Radioactive Waste*.

Kunze, R. J., Uehara, G., & Graham, K. (1968). Factors important in the calculation of hydraulic conductivity. *Soil Science Society of American Proceedings*, 32: 760-765.

Langenbach, H., Eckart, J., & Schröder, G. (2008, November-December 30 - 4). Water sensitive urban design- Results and Principles. In Proceedings of the 3rd SWITCH Scientific Meeting. Belo Horizonte, Brazil.

Langergraber, G., & Šimůnek, J. (2011). *HYDRUS Wetland Module version 2.* Riverside: Department of Environmental Sciences, University of California Riverside.

Lebeau, M., & Konrad, J. M. (2010). A new capillary and thin film flow model for predicting the hydraulic conductivity of unsaturated porous media. *Water Resources Research*, 46, W12554, doi: 10.1029/2010WR009092.

Lee, J. G., & Heaney, J. P. (2003). Estimation of Urban Imperviousness and its Impacts on Storm Water Systems. *Journal of Water Resources Planning and Management 129 (5)*, 419-426.

Luckner, L., van Genuchten, M. T., & Nielsen, D. R. (1989). A consistent set of parametric models for the two-phase flow of immiscible fluids in the subsurface. *Water Resources Research*, 25(10): 2187-2193.

Malmqvist, P. (1999). A sustainable urban water management. *Vatten*, 55: 7-17.

Millington, R. J., & Quirk, J. P. (1961). Permeability of porous solids. *Transactions of the Faraday Society*, 57: 1200-1206.

Morvannou, A., Forquet, N., Vanclooster, M., & Molle, P. (2013). Characterizing hydraulic properies of filter material of a vertical flow constructed wetland. *Ecological Engineering 60*, 325-335.

Mualem, Y. (1976). A new model for predicting the hydraulic conductivity of unsaturated porous media. *Water Resources Research*, 12(3): 513-522.

NOAA. (2017). *Hydrologic cycle*. Retrieved May 29, 2017, from nwrfc.noaa.gov: https://www.nwrfc.noaa.gov/info/water_cycle/hydrology.cgi

NSWEPA. (1997, November). *Managing urban stormwater: treatment techniques*. Retrieved May 9, 2017, from http://www.environment.nsw.gov.au/resources/stormwater/usp/treattech.pdf

Peters, A., & Durner, W. (2008). A simple model for describing hydraulic conductivity in unsaturated porous media accounting for film and capillary flow. *Water Resources Research*, 44, W11417, doi: 10.1029/2008WR007136.

Rahimi, A., Rahardjo, H., & Leong, E.-C. (2015). Effects of soil-water characteristic curve and relative permeability equations on estimation of unsaturated permeability function. *Soils and Foundations*, 55(6): 1400-1411.

Rassam, D., Šimůnek, J., & van Genuchten, M. T. (2003). *Modelling variably saturated flow with Hydrus-2D.* Brisbane: ND Consult.

Richards, L. A. (1931). Capillary conduction of liquids in porous mediums. *Physics*, 1: 318-333.

Schaap, M. G., & van Genuchten, M. T. (2006). A modifies Mualem-van Genuchten formulation for improved description of the hydraulic conductivity near saturation. *Vadose Zone Journal*, 5: 27-34.

Scholes, L., Shutes, R. E., Revitt, D. M., Forshaw, M., & Purchase, D. (1998). The treatment of heavy metals in urban runoff by constructed wetlands. *The Science of the Total Environment*, 214: 211-219.

SEPA. (2016). *Diffuse polution in urban environment,* Retrieved May 9, 2017, from SEPA.org: https://www.sepa.org.uk/regulations/water/diffuse-pollution/diffuse-pollution-in-the-urban-environment

Šimůnek, J., & van Genuchten, M. T. (2008). Modeling nonequilibrium flow and transport processes using HYDRUS. *Vadose Zone Journal*, 7: 782-797.

Šimůnek, J., van Genuchten, M. T., & Sejna, M. (2012). *The HYDRUS Software Package for Simulating the Two- and Three-Dimensional Movement of Water, Heat, and Multiple Solutes in Variably-Saturated Porous Media.* Prague: Hydrus Technical Manual.

Taebi, A., & Droste, R. L. (2004). Pollution loads in urban runoff and sanitary wastewater. *Science of the Total Environment*, 327: 175-184.

Thurston, H. W., Goddard, H. C., Szlag, D., & Lemberg, B. (2003). Controlling Storm-Water Runoff with Tradable Allowances for Impervious Sufaces. *Journal of Water Resources Planning and Management 129 (5)*, 409-418.

Touma, J. (2009). Comparison of the soil hydraulic conductivity predicted from its water retention expressed by the equations of Van Genuchten and different capillary models. *European Journal of Soil Science*, 60: 671-680.

van Genuchten, M. T. (1980). A closed-form equation for predicting the hydraulic conductivity of unsaturated soils. *Soil Science Society of America Journal* , 44: 892-898.

Vienken, T., & Dietrich, P. (2011). Field evaluation of methods for determining hydraulic conductivity from grain sieze data. *J Hydrol*, 400: 58-71.

Vogel, T., & Císlerová, M. (1988). On the reliability of unsaturated hydraulic conductivity calculated from the moisture retention curve. *Transport in Porous Media*, 3: 1-15.

Vogel, T., van Genuchten, M. T., & Cislerova, M. (2000). Effect of the shape of the soil hydrualic functions near saturation on variably-saturated flow predictions. *Advances in Water Resources*, 133-144.

Wong, T. H. (2006). Water sensitive urban design- the journey thus far. *Australian Journal of Water Resources*, 10: 213-222.

Wong, T. H., & Brown, R. (2009). The water sensitive city: Principles for practise. *Water Science Technologies*, 60: 673-682.

Zhou, Q. (2014). A review of sustainable urban drainage systems considering the climate change and urbanization impacts. *Water*, 6: 976-992.

Zoppou, C. (2001). Review of urban storm water models. *Environmental Modelling & Software 16*, 195-231.

Annex 1

It is in Annex 1 that the measurements obtained in the flow curves experiment are plotted. There are two types of graphics for all the filter materials studied: one represents the flux over the time, and the other shows the cumulative volume over the time.

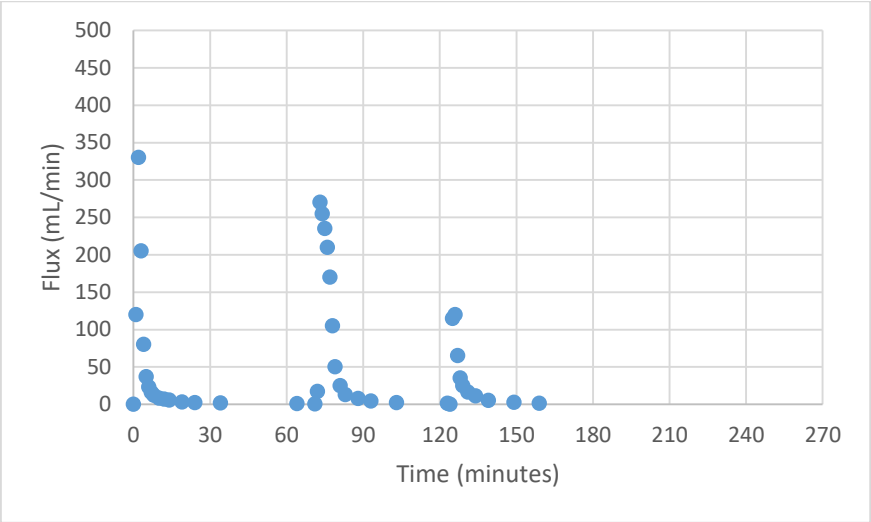

Figure A1. Flux graphic of the Plot 3 1st column.

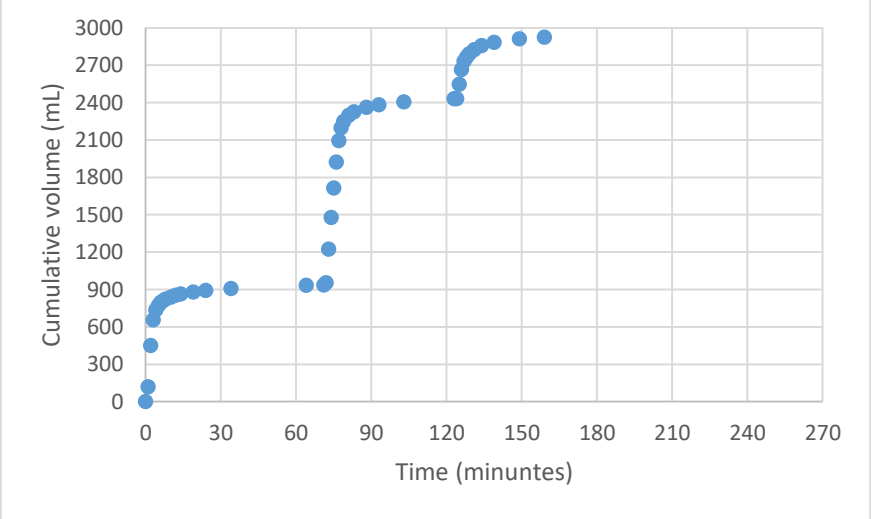

Figure A2. Cumulative volume graphic of the Plot 3 1st column.

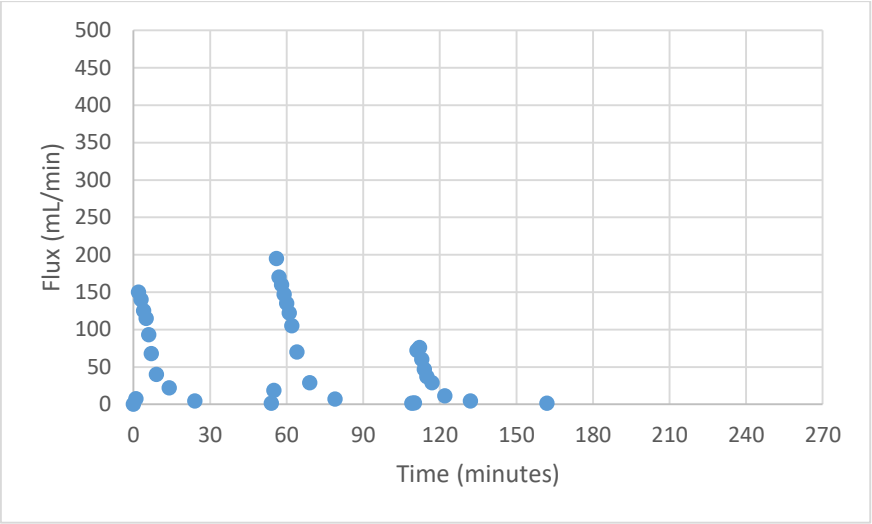

Figure A3. Flux graphic of the Plot 3 2nd column.

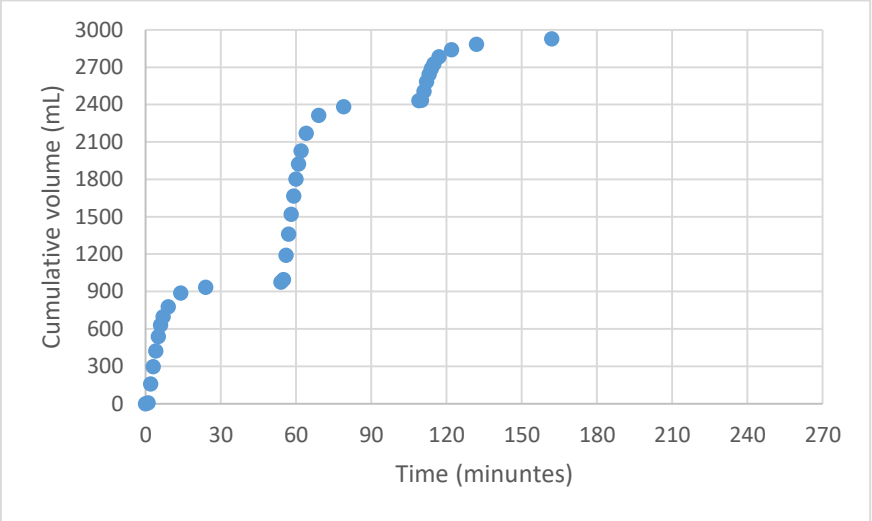

Figure A4. Cumulative volume graphic of the Plot 3 2nd column.

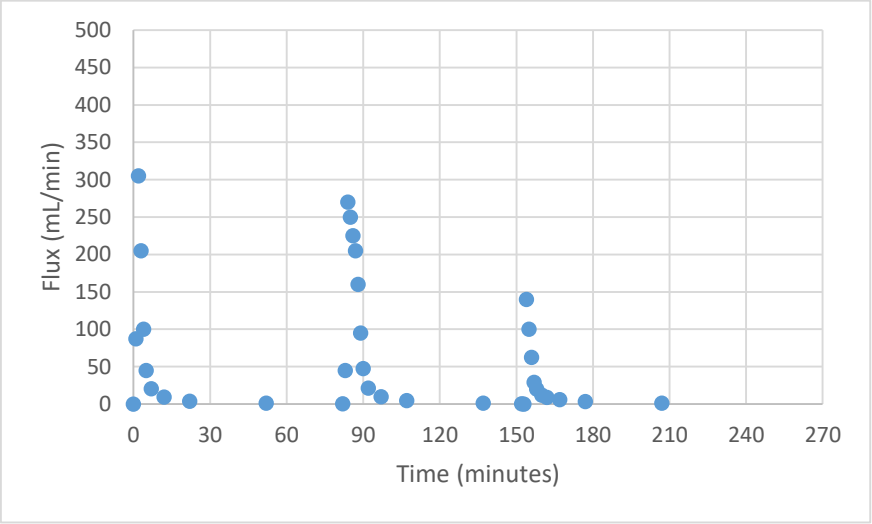

Figure A5. Flux graphic of the Plot 6.

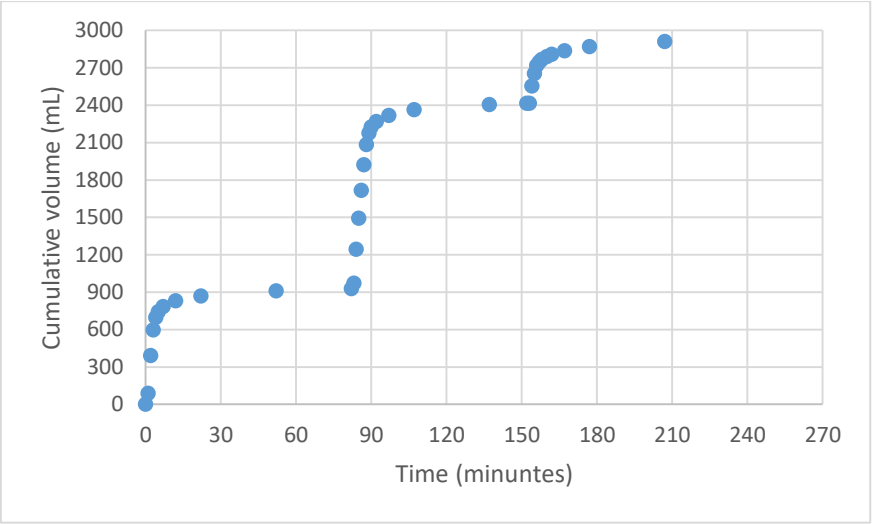

Figure A6. Cumulative volume graphic of the Plot 6.

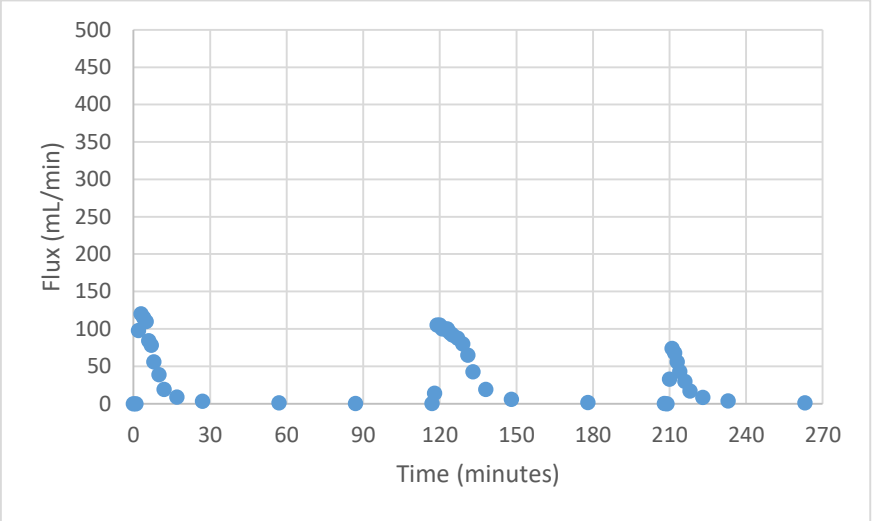

Figure A7. Flux graphic of the Plot 9.

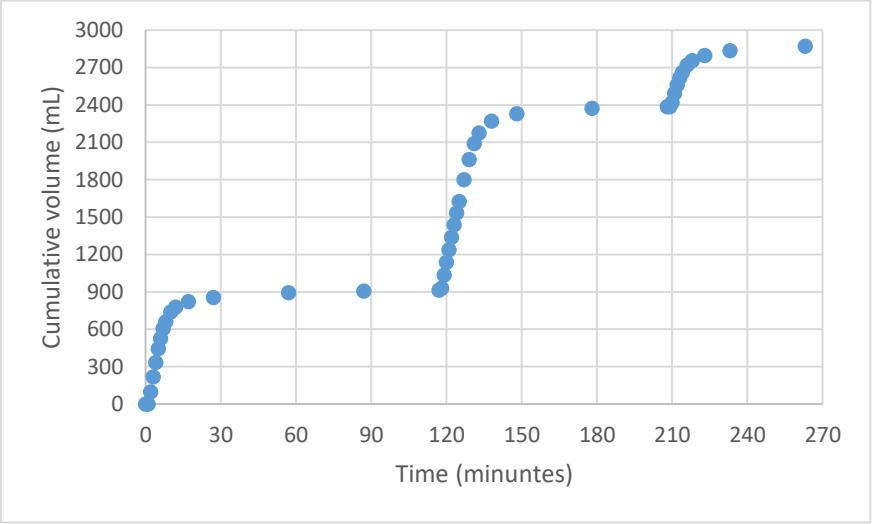

Figure A8. Cumulative volume graphic of the Plot 9.

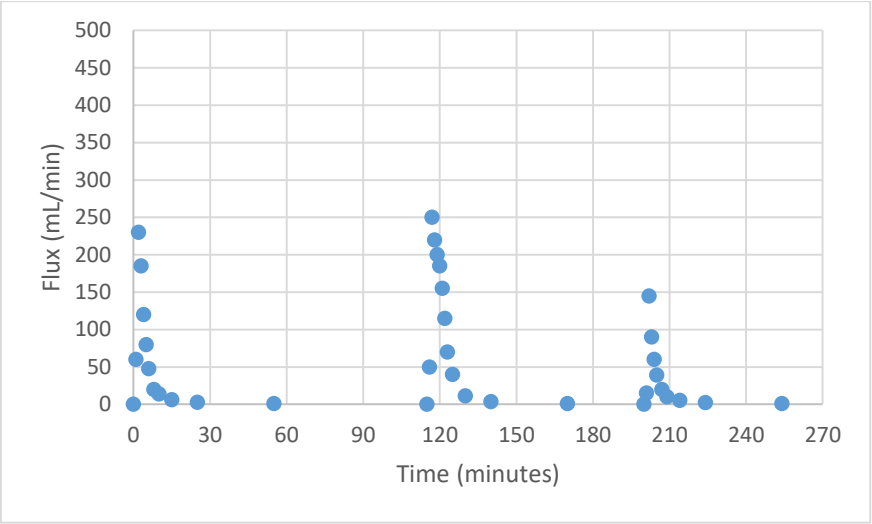

Figure A9. Flux graphic of the Plot 11 1st column.

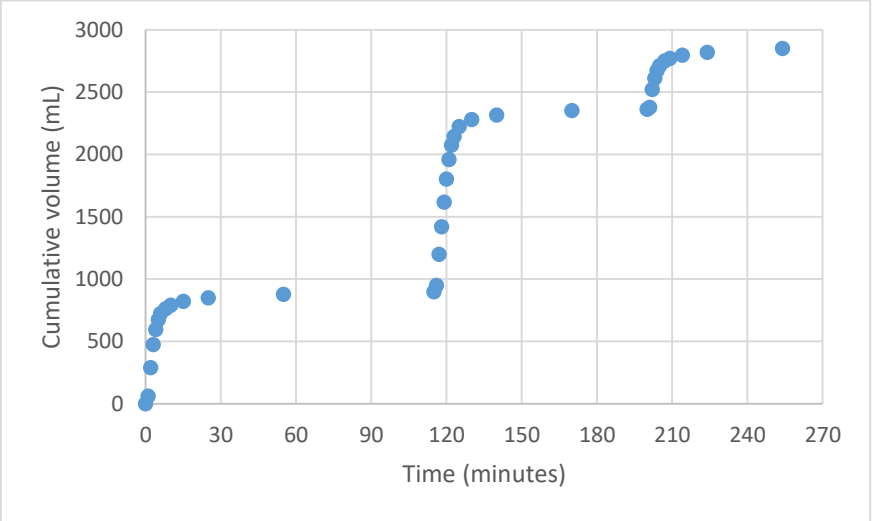

Figure A10. Cumulative volume of the Plot 11 1st column.

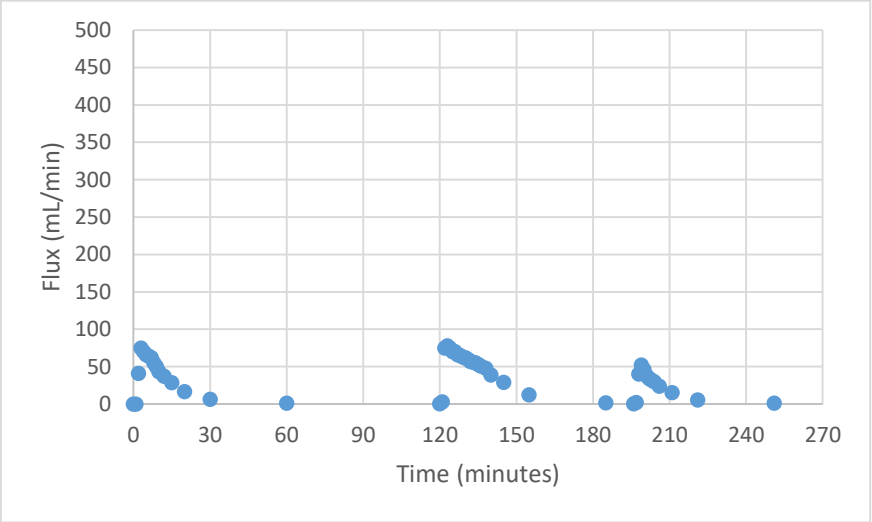

Figure A11. Flux graphic of the Plot 11 3rd column.

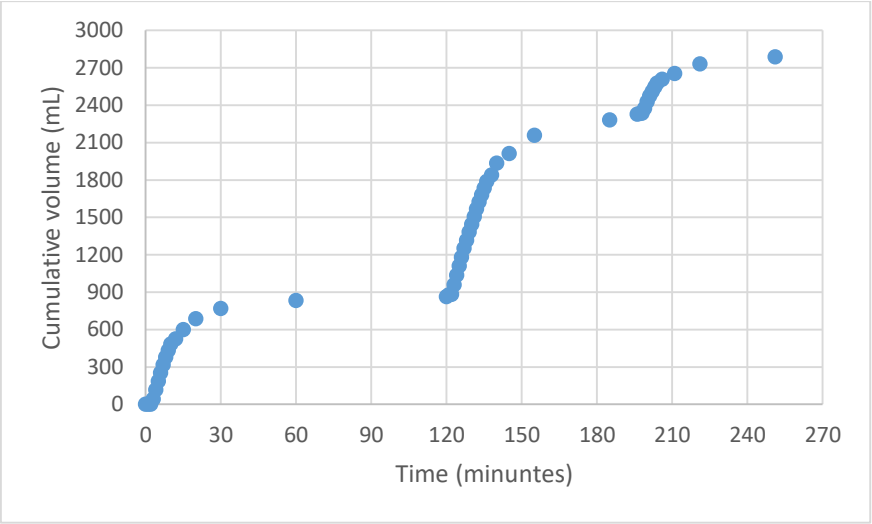

Figure A12. Cumulative volume graphic of the Plot 11 3rd column.

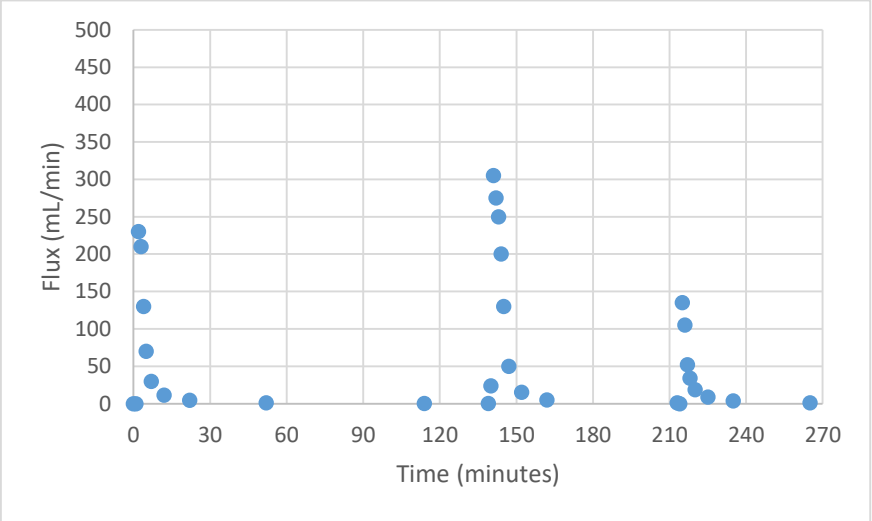

Figure A13. Flux graphic of the Plot 11 4th column.

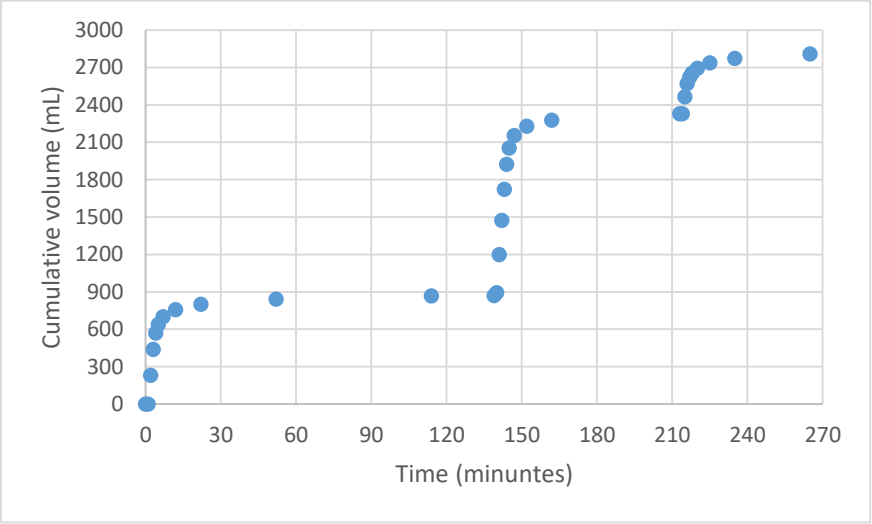

Figure A14. Cumulative volume graphic of the Plot 11 4th column.

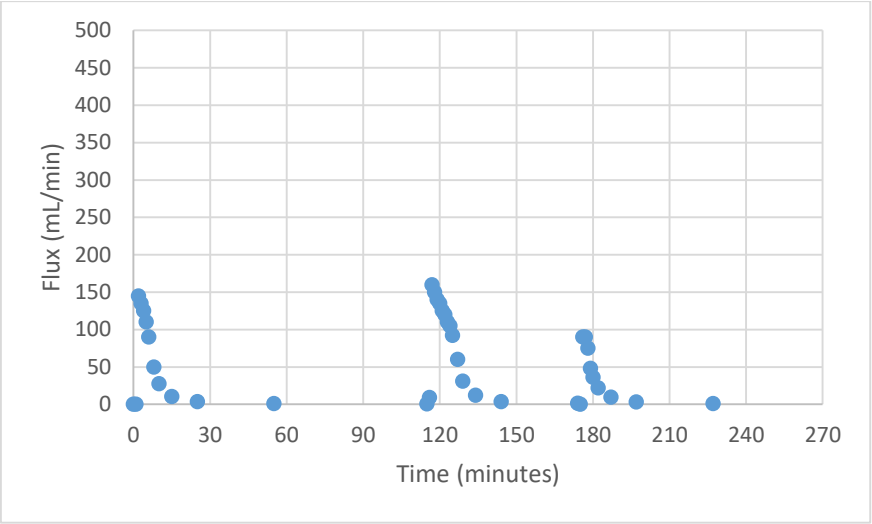

Figure A15. Flux graphic of the Plot 16.

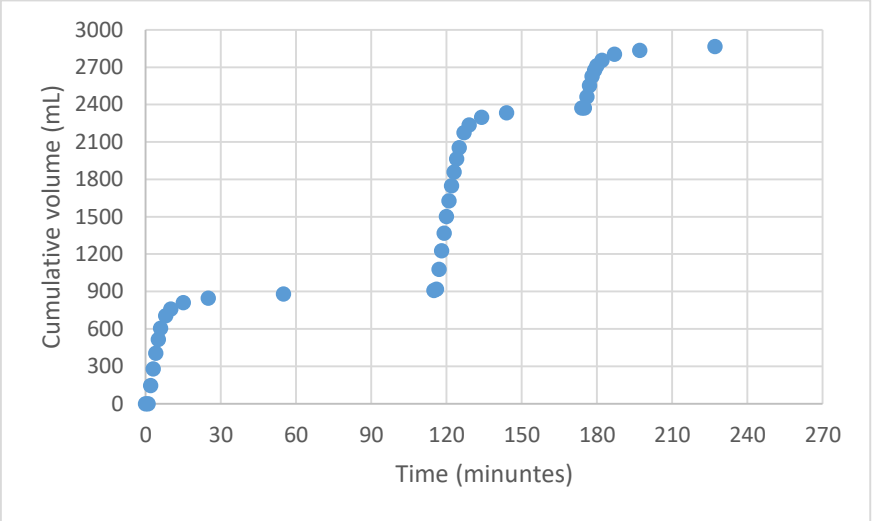

Figure A16. Cumulative volume graphic of the Plot 16.

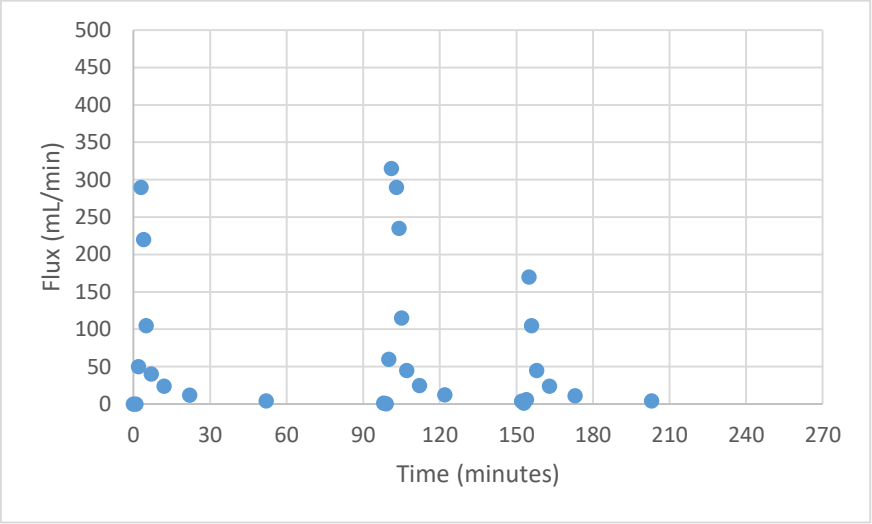

Figure A17. Flux graphic of the Plot 19.

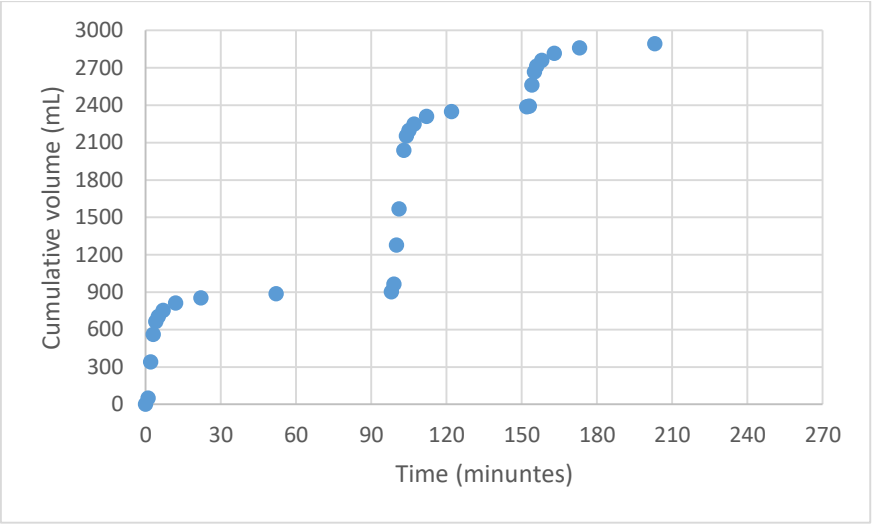

Figure A18. Cumulative volume graphic of the Plot 19.

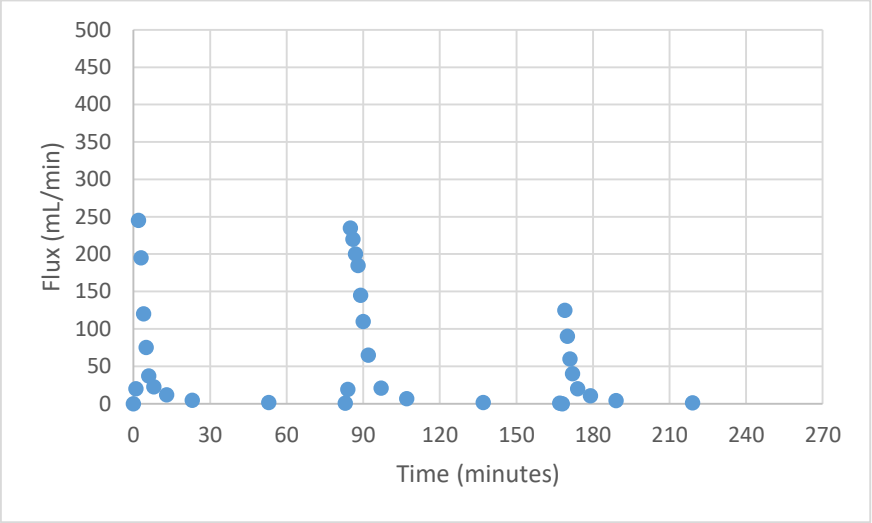

Figure A19. Flux graphic of the Plot 22.

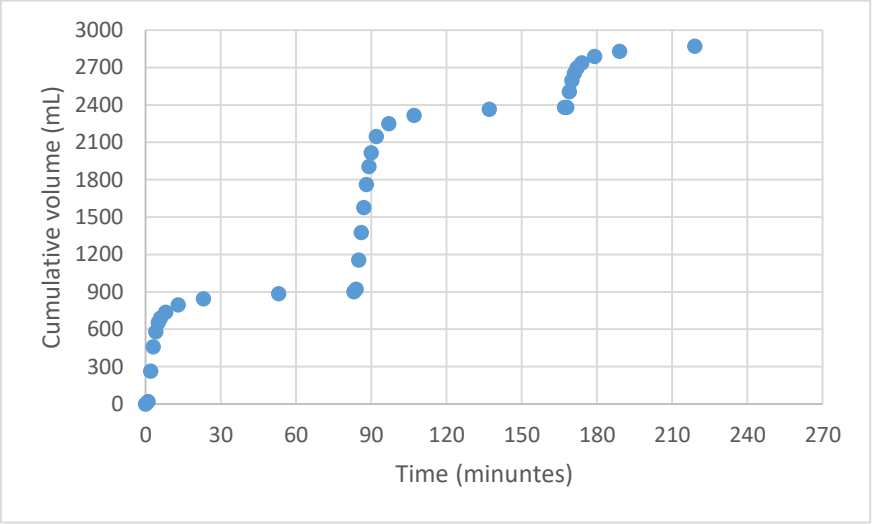

Figure A20. Cumulative volume graphic of the Plot 22.

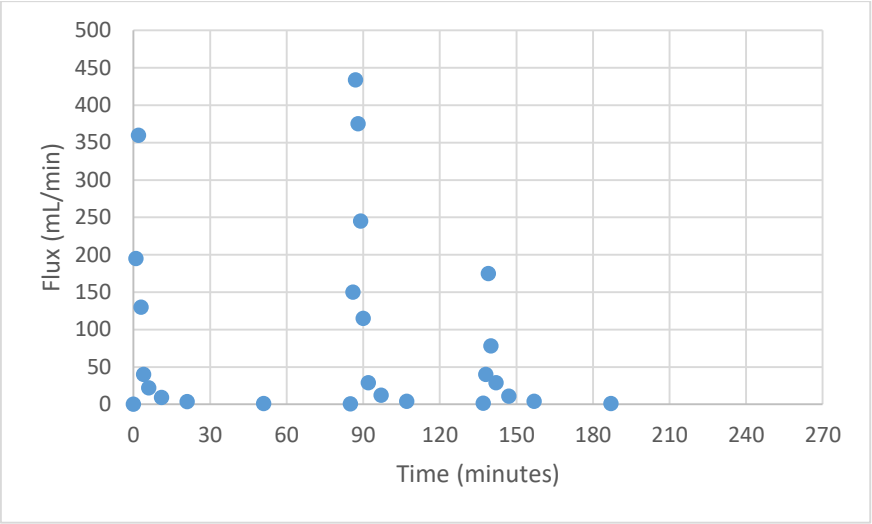

Figure A21. Flux graphic of the Plot 24.

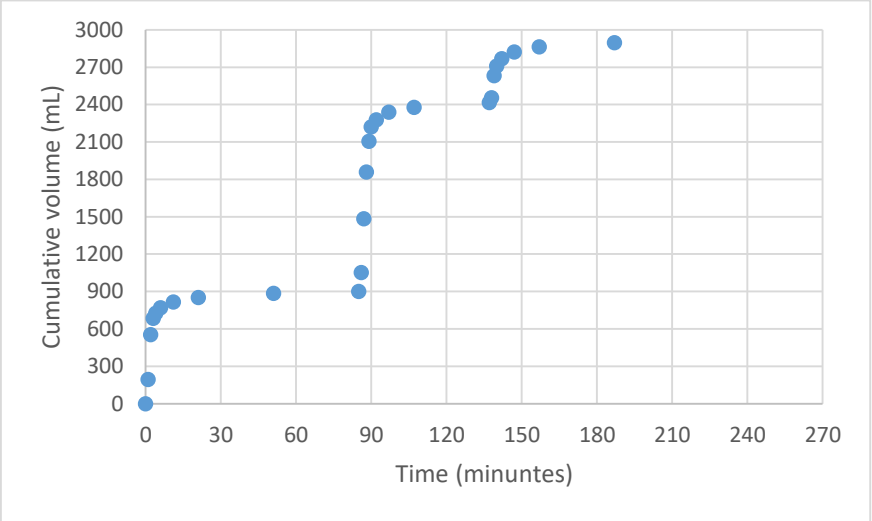

Figure A22. Cumulative volume graphic of the Plot 24.

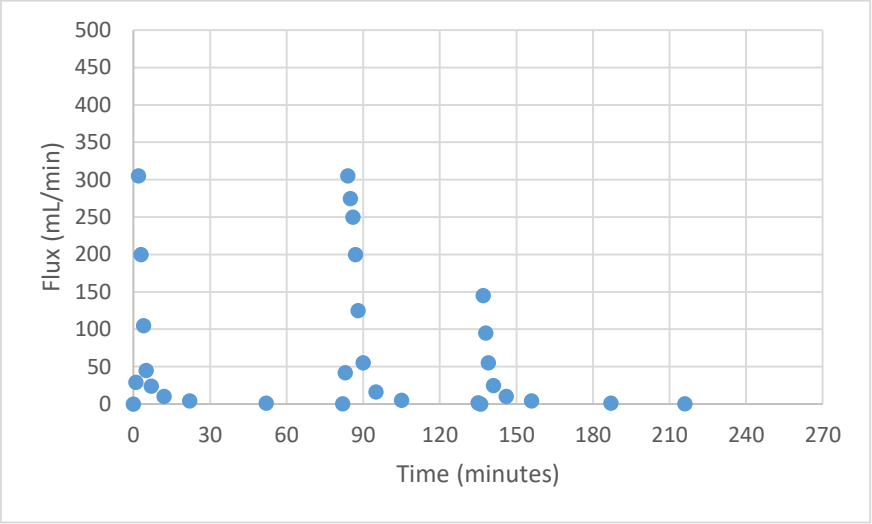

Figure A23. Flux graphic of the Plot 25.

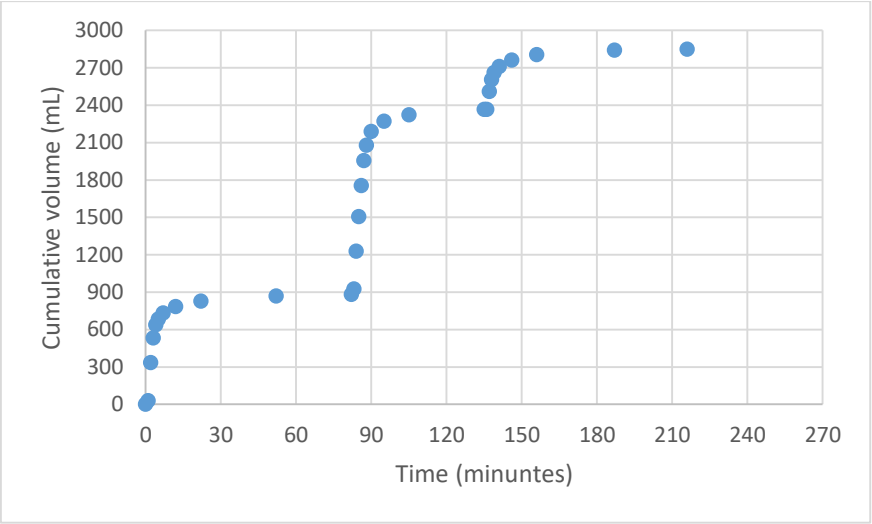

Figure A24. Cumulative volume graphic of the Plot 25.

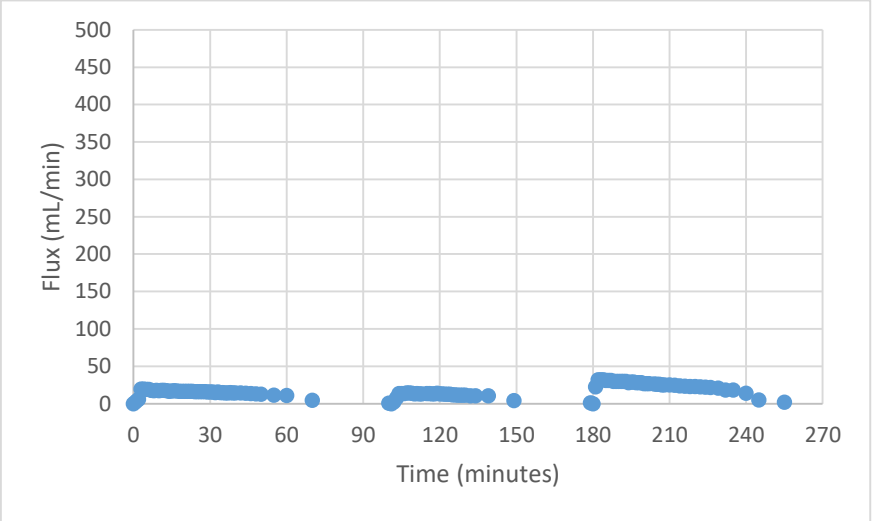

Figure A25. Flux graphic of the Plot 30.

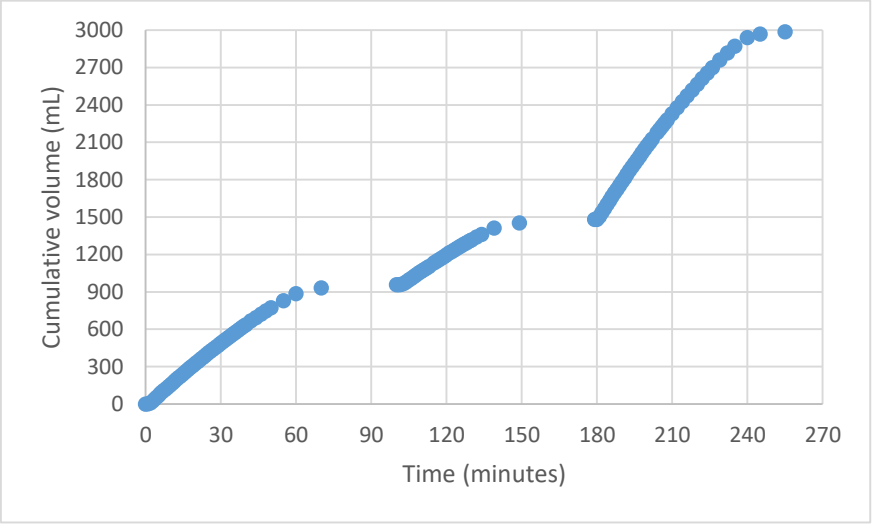

Figure A26. Cumulative volume graphic of the Plot 30.

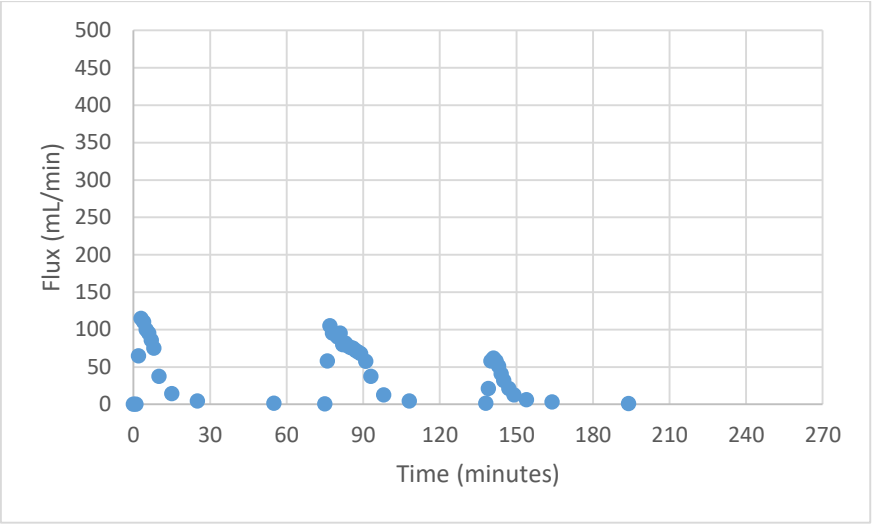

Figure A27. Flux graphic of the Salz 1.

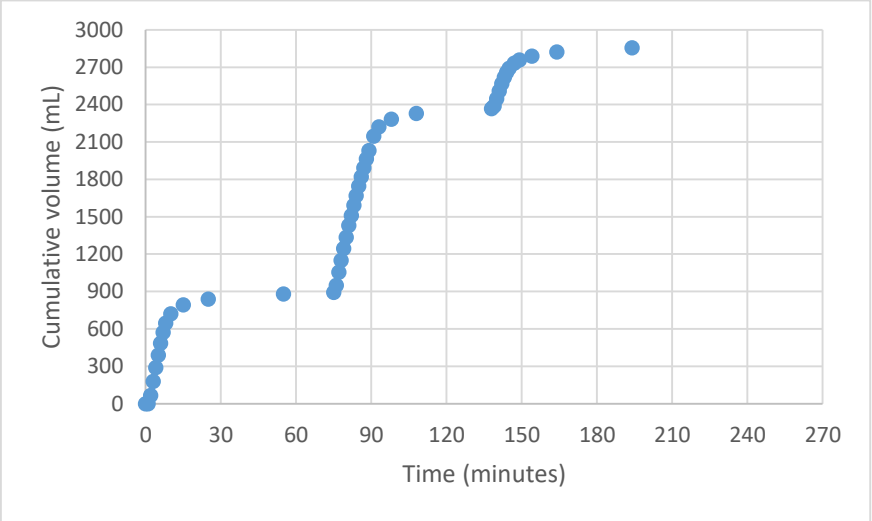

Figure A28. Cumulative volume graphic of the Salz 1.

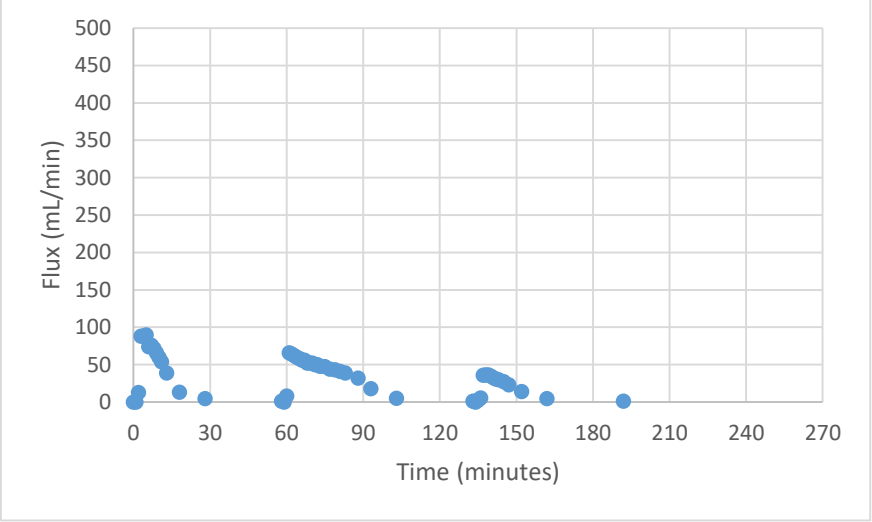

Figure A29. Flux graphic of the Salz 2.

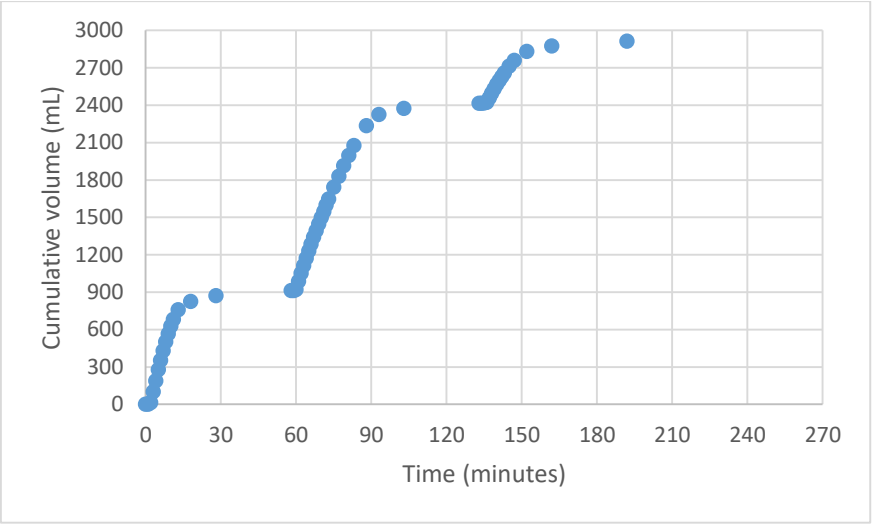

Figure A30. Cumulative volume graphic of the Salz 2.

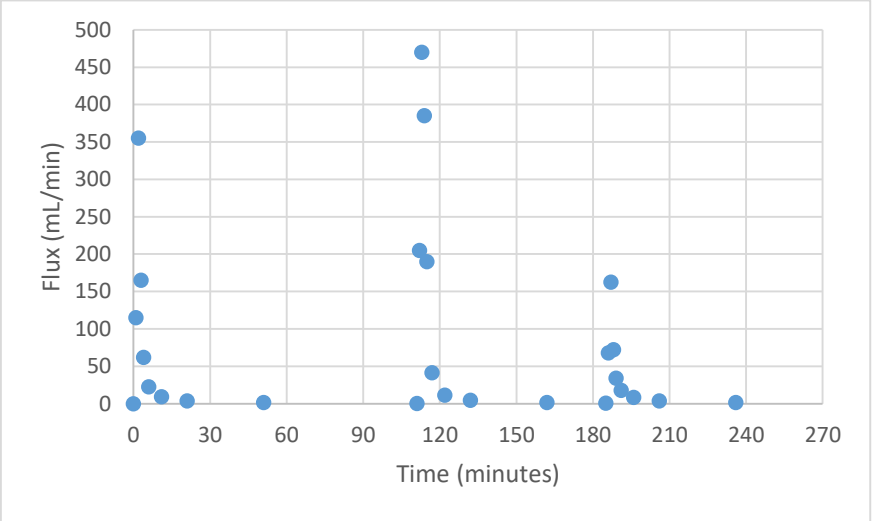

Figure A31. Flux graphic of the Pflanz Kalk.

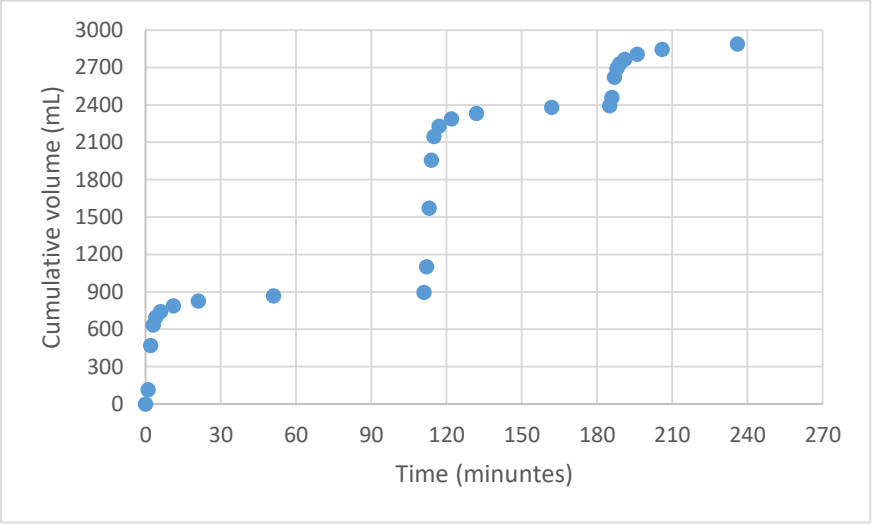

Figure A32. Cumulative volume graphic of the Pflanz Kalk.

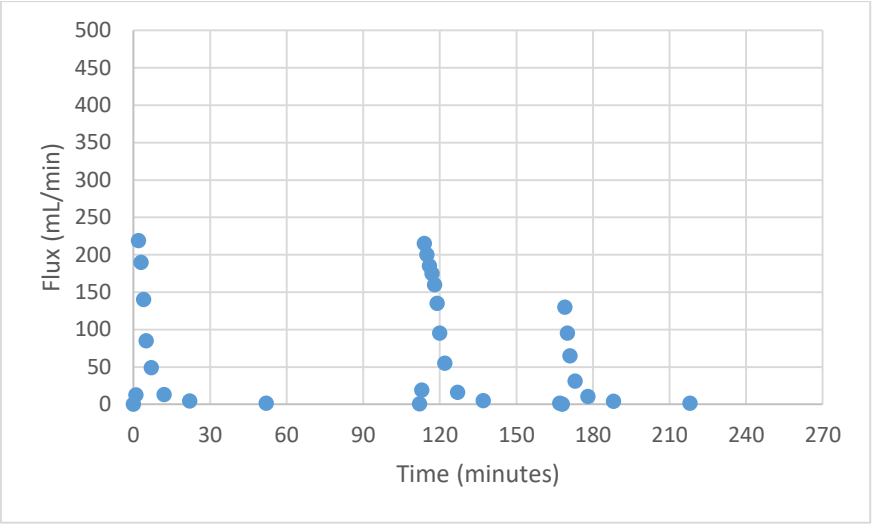

Figure A33. Flux graphic of the Granulit.

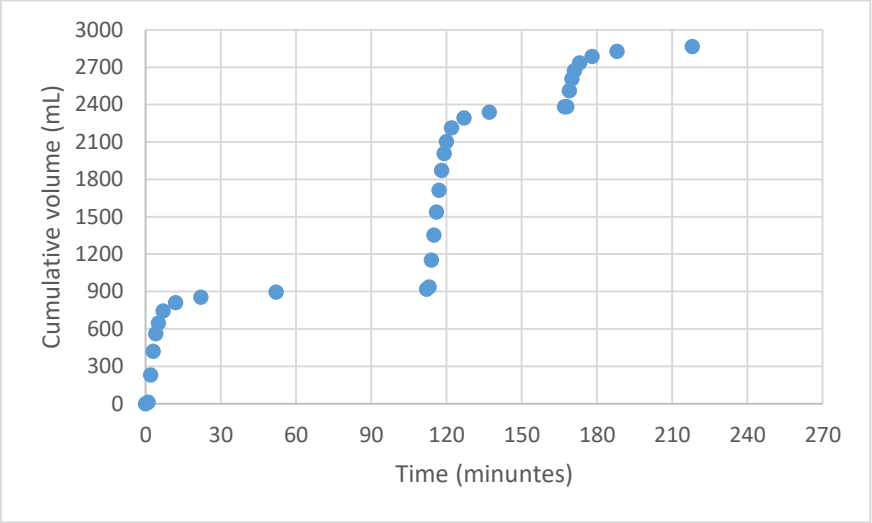

Figure A34. Cumulative volume graphic of the Granulit.

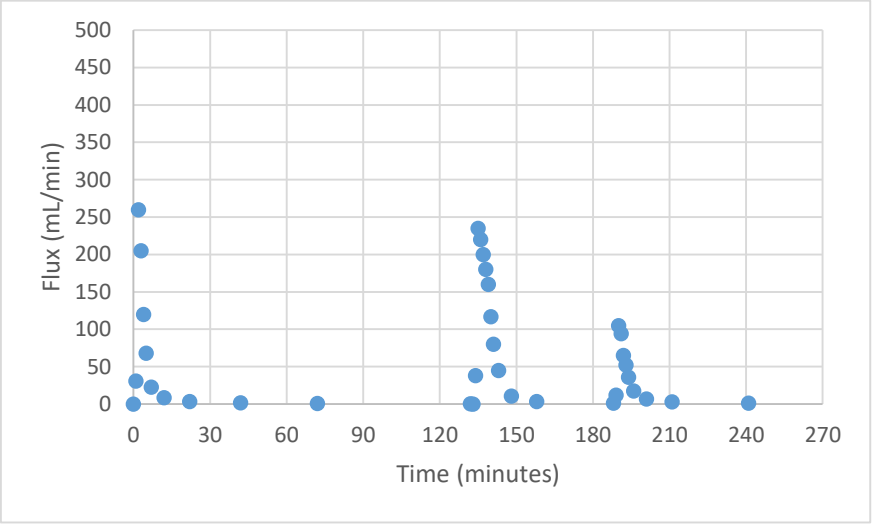

Figure A35. Flux graphic of the Pflanz Kombi.

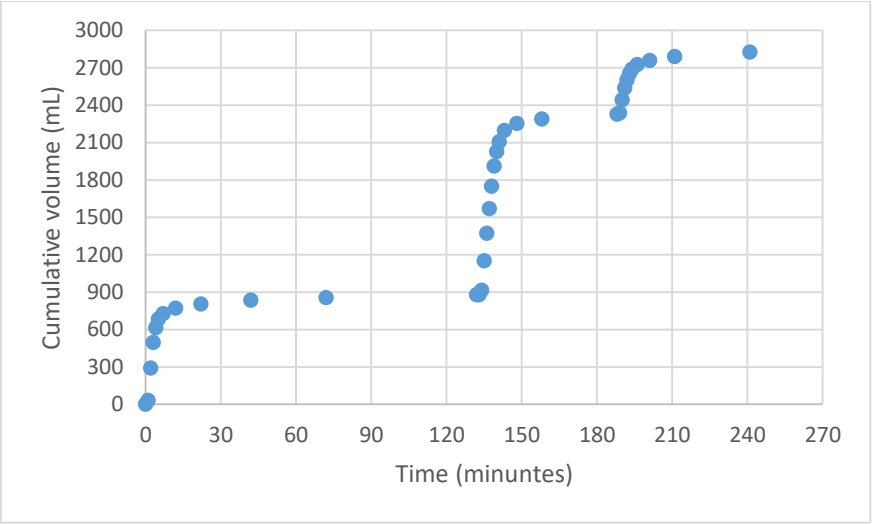

Figure A36. Cumulative volume graphic of the Pflanz Kombi.

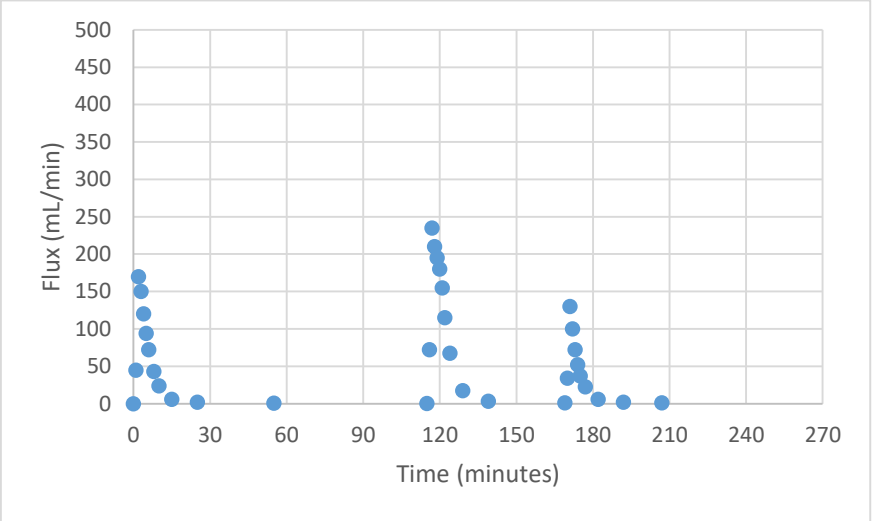

Figure A37. Flux graphic of the Pflanz Zeolith.

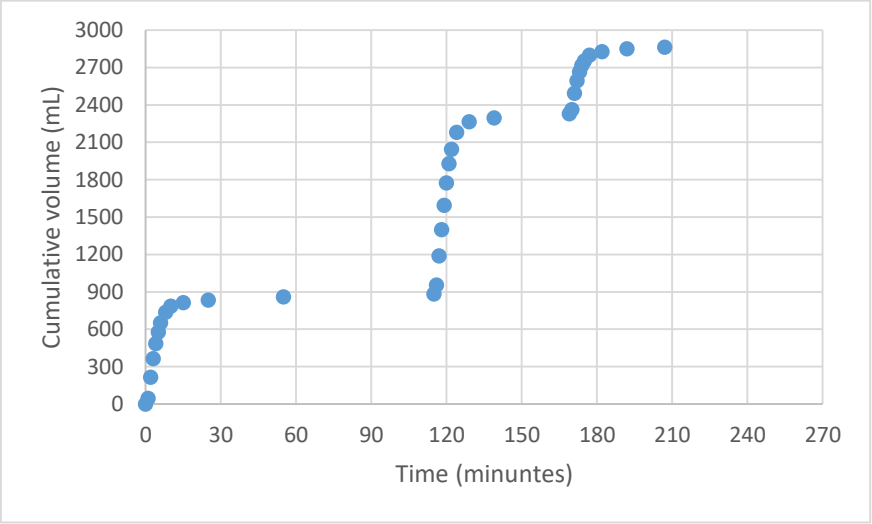

Figure A38. Cumulative volume graphic of the Pflanz Zeolith.

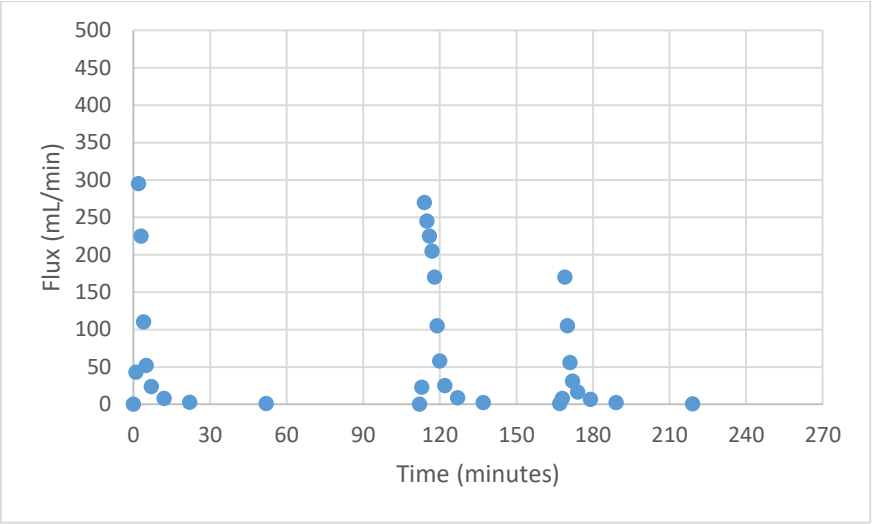

Figure A39. Flux graphic of the MA 42.

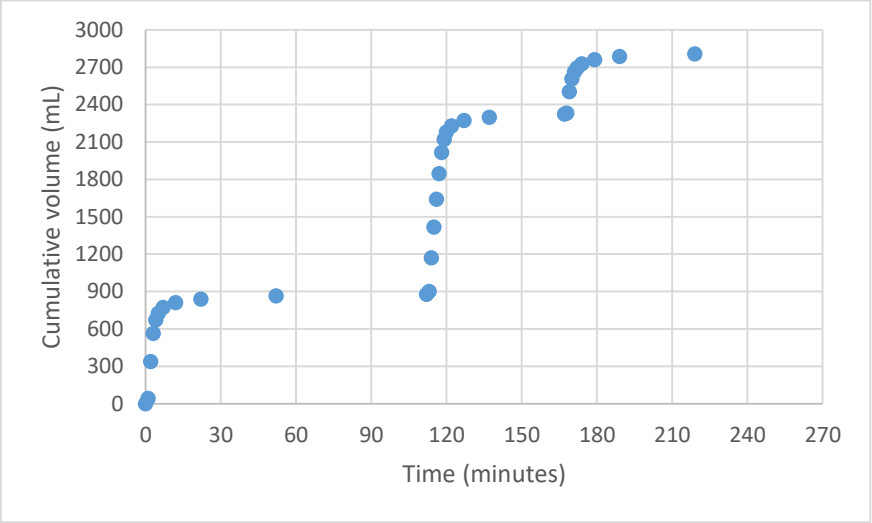

Figure A40. Cumulative volume graphic of the MA 42.

Annex 2

It is in Annex 2 that the results obtained in the inverse solution are compared to experimental data by plotting all three curves in the same graphic for each and every material modelled in HYDRUS®. There are two types of graphics for all the filter materials studied: one represents the flux over the time, and the other shows the cumulative volume over the time. All the graphics have three curves represented: the first represents the experimental data; the second one shows the curve as a result of the inverse solution using the flux data; and the last one represents the curve as a result of the inverse solution using the cumulative volume data.

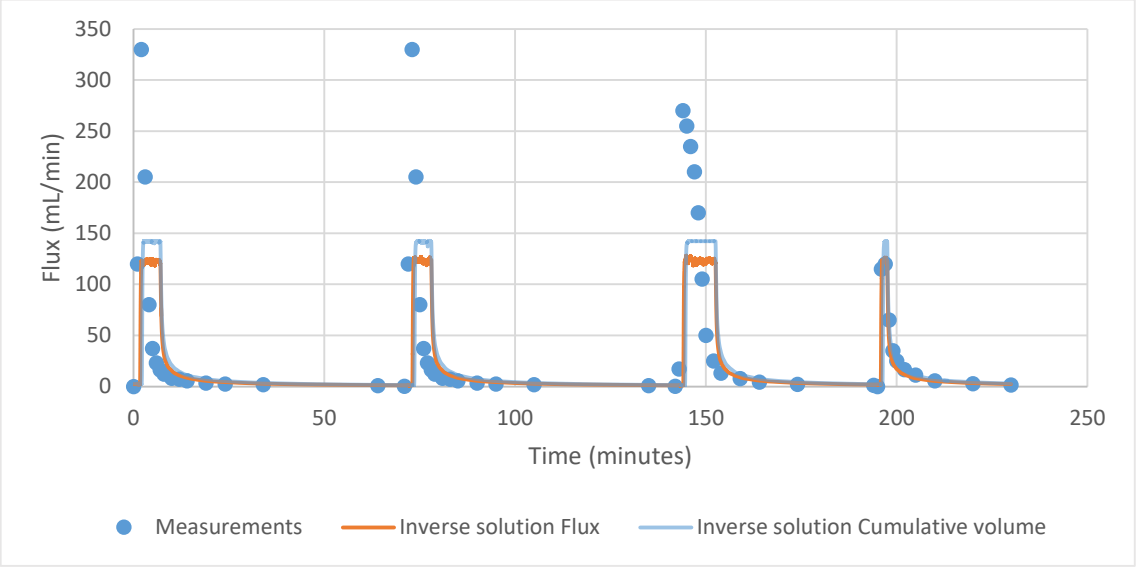

Figure A41. Inverse solution flux results of Plot 3 1st column.

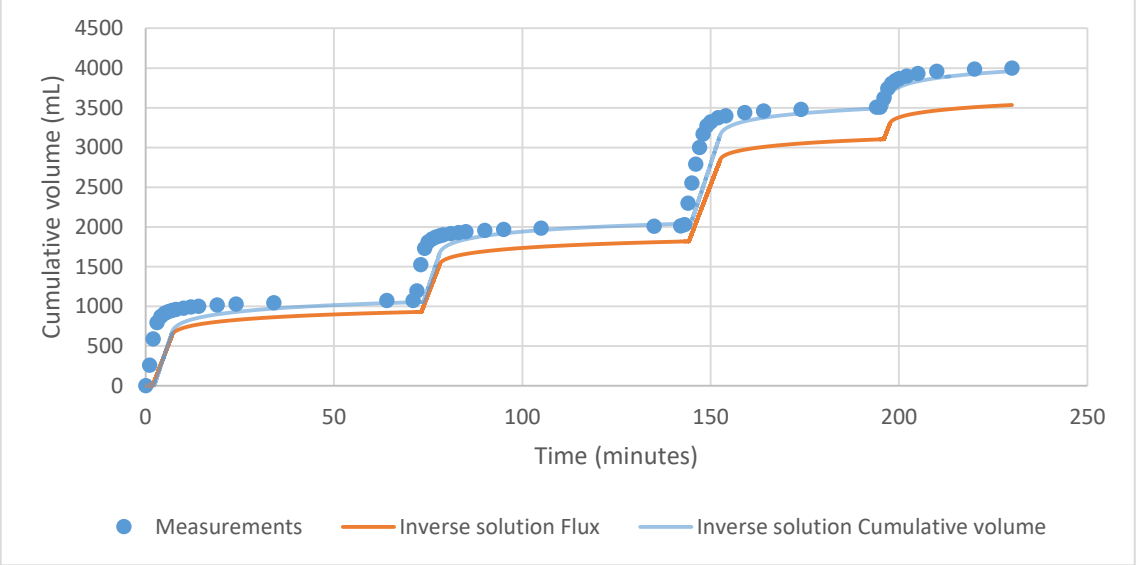

Figure A42. Inverse solution cumulative volume results of Plot 3 1st column.

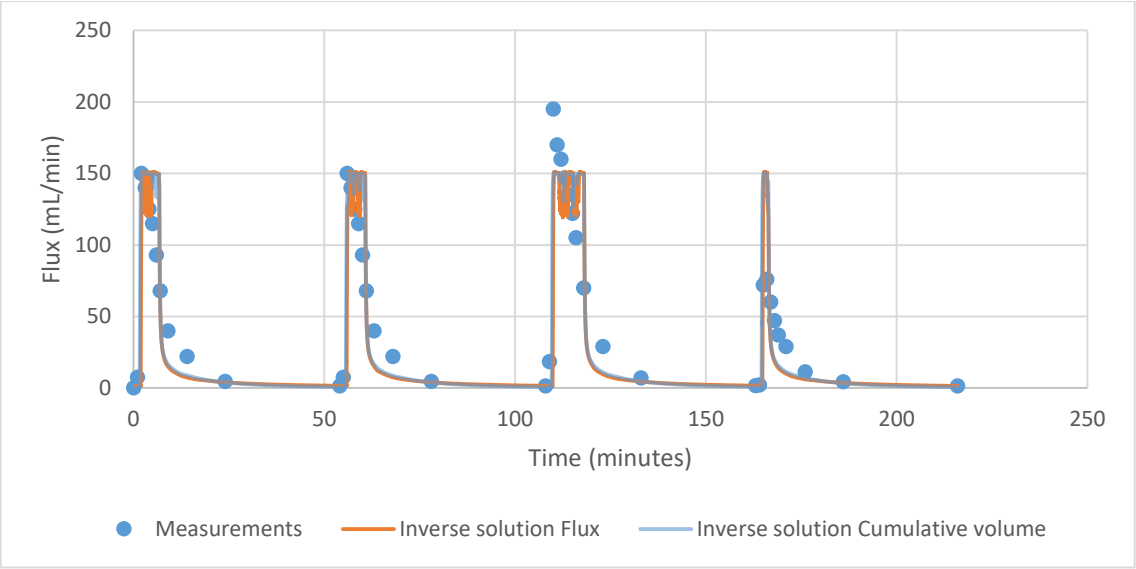

Figure A43. Inverse solution flux results of Plot 3 2nd column.

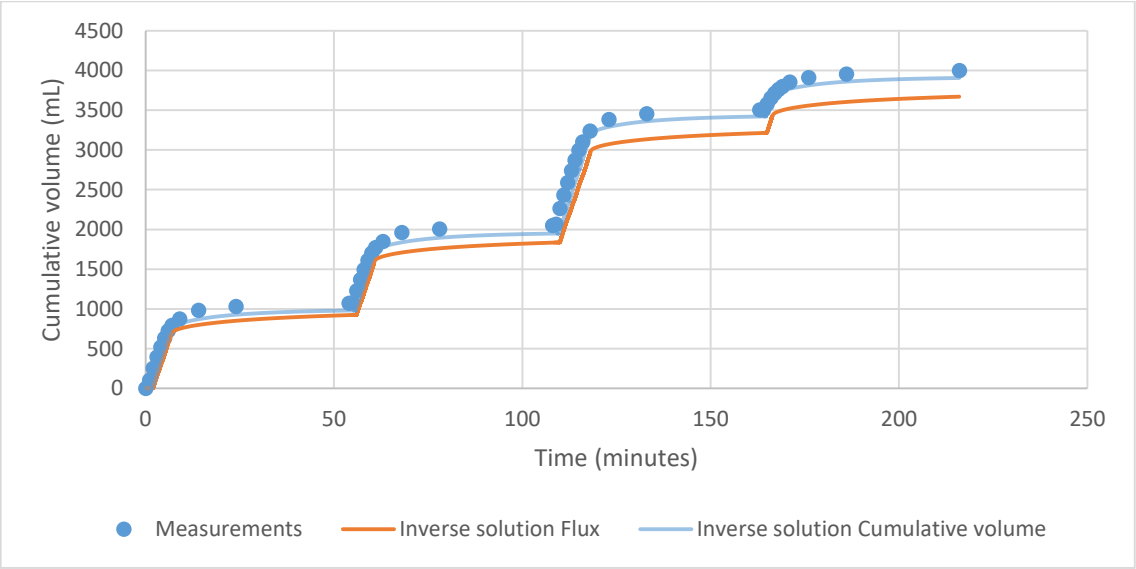

Figure A44. Inverse solution cumulative volume results of Plot 3 2nd column.

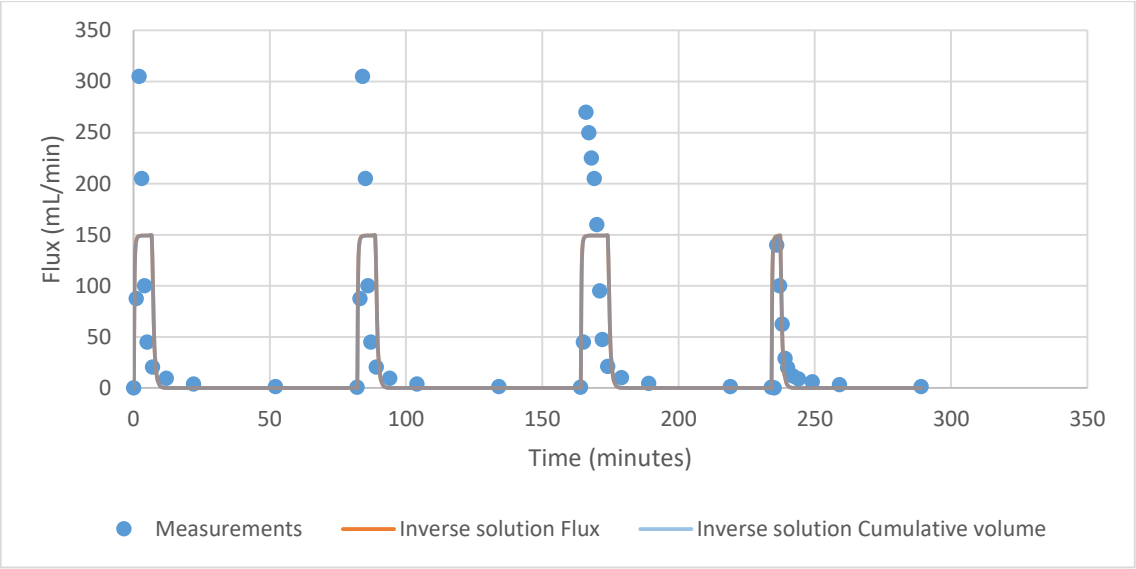

Figure A45. Inverse solution flux results of Plot 6.

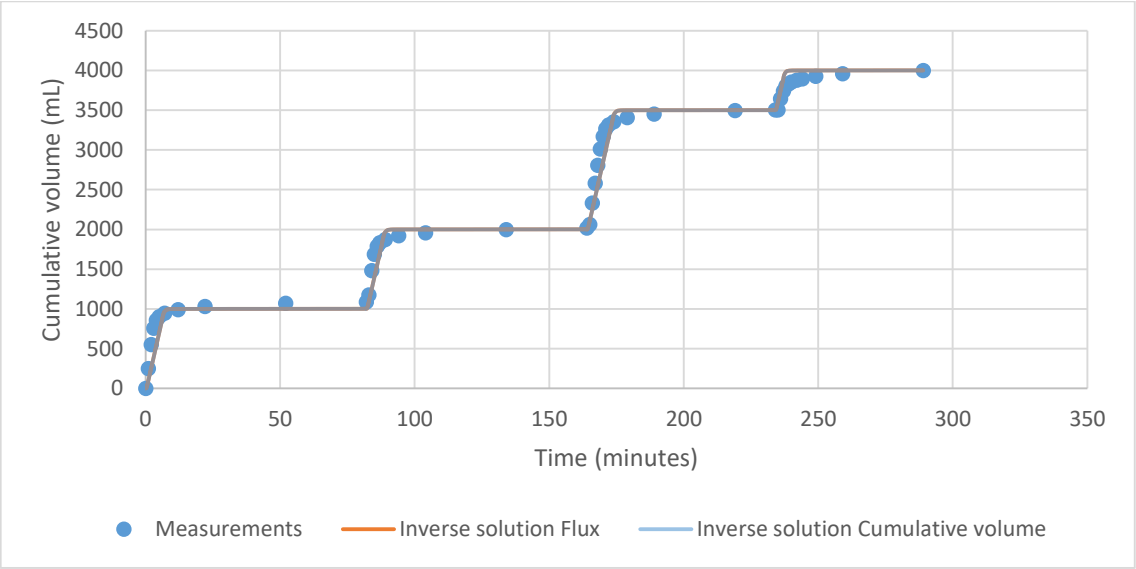

Figure A46. Inverse solution cumulative volume results of Plot 6.

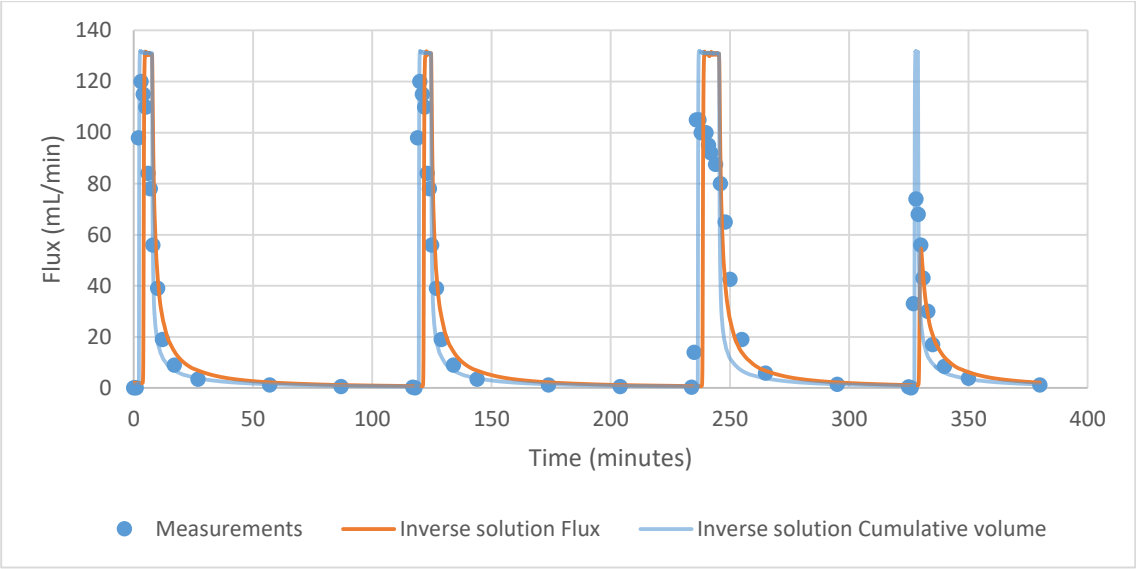

Figure A47. Inverse solution flux results of Plot 9.

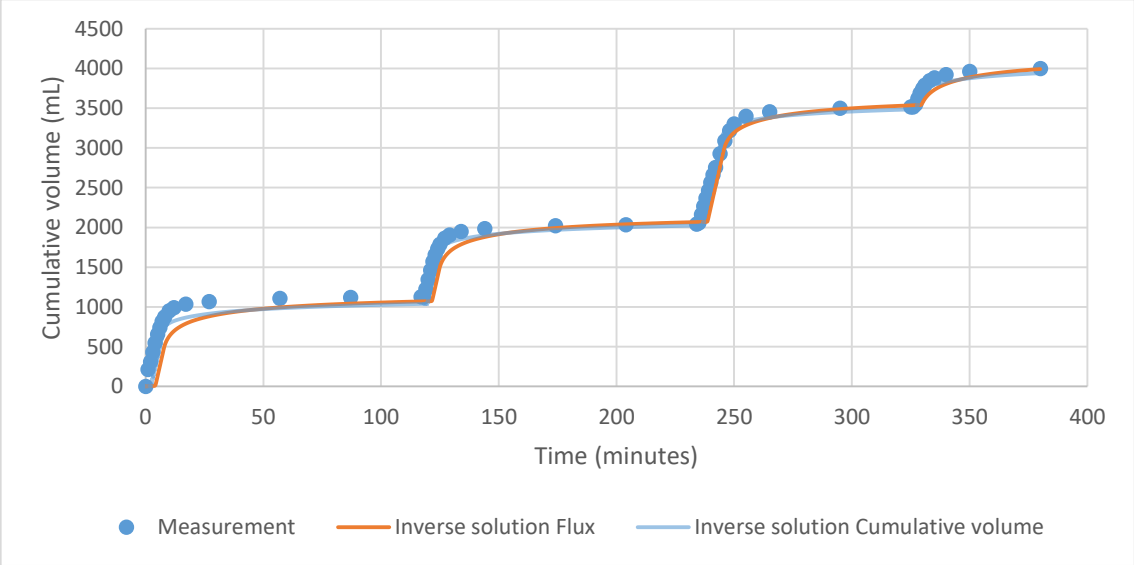

Figure A48. Inverse solution cumulative volume results of Plot 9.

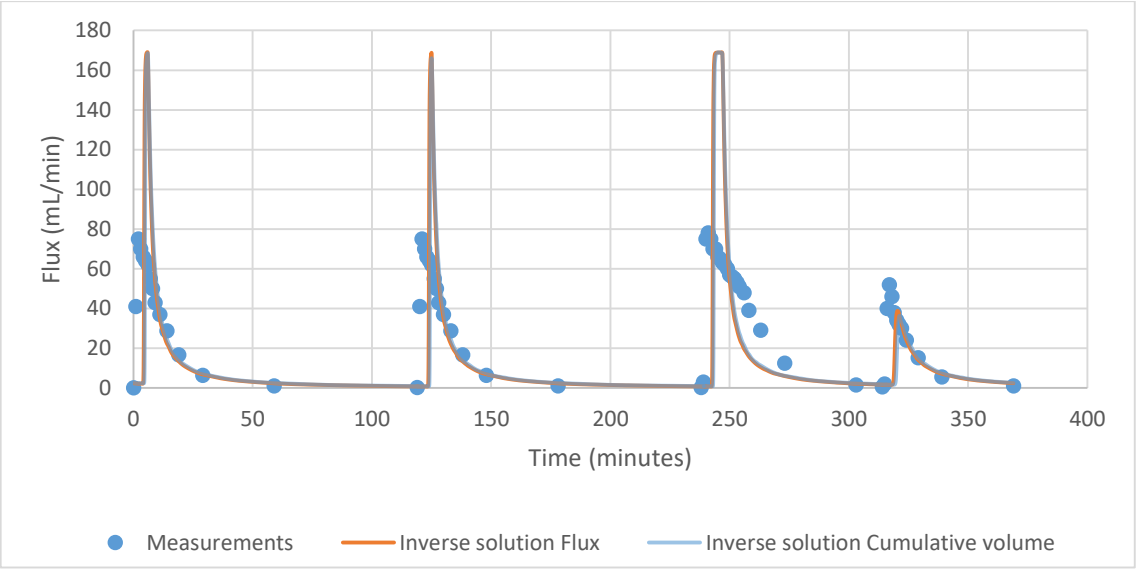

Figure A49. Inverse solution flux results of Plot 11 3rd column.

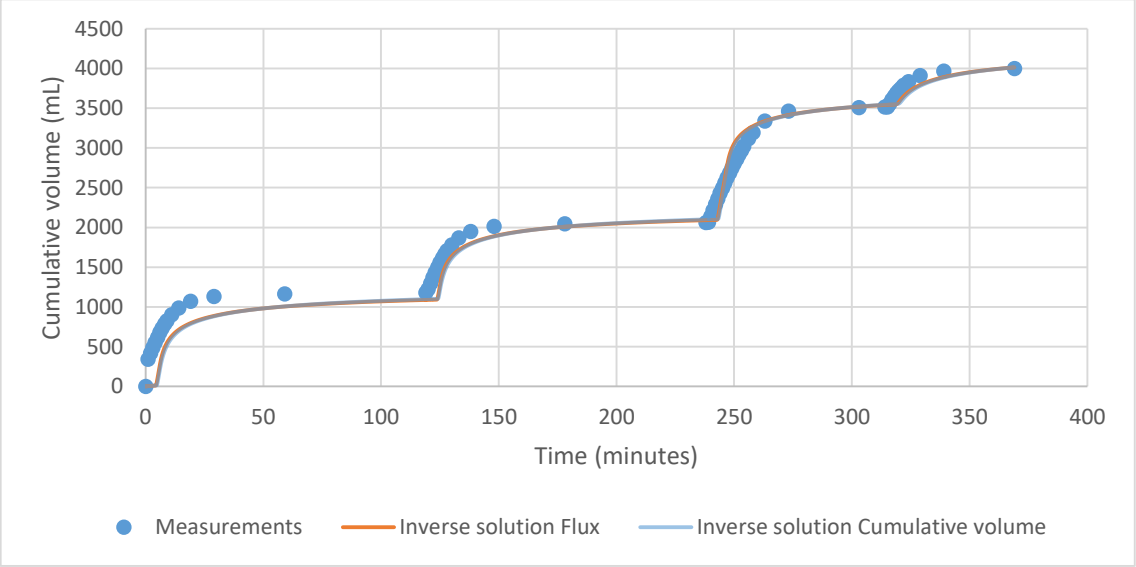

Figure A50. Inverse solution cumulative volume results of Plot 11 3rd column.

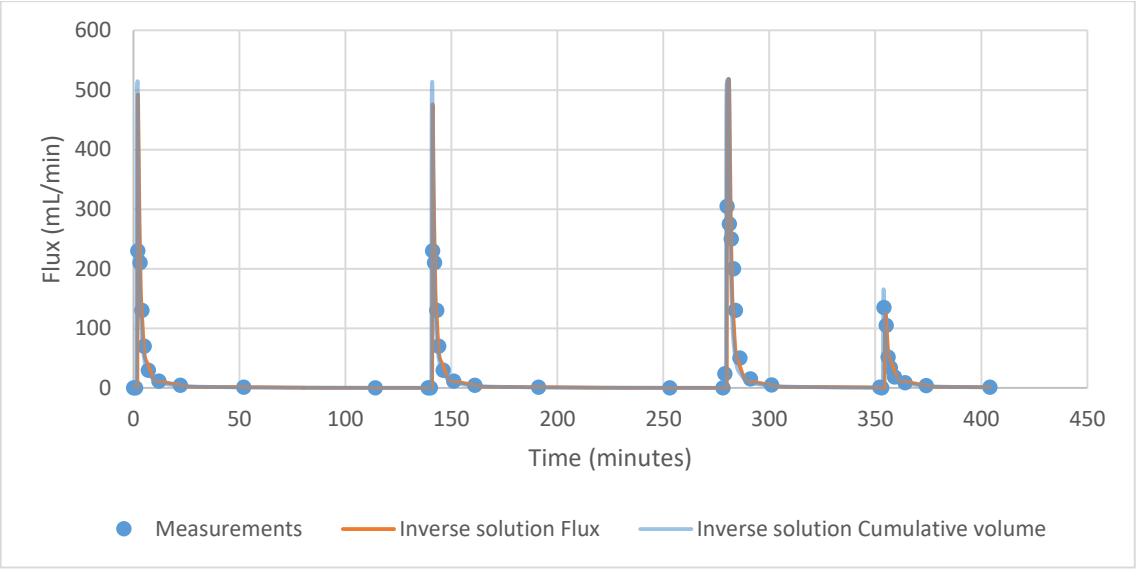

Figure A51. Inverse solution flux results of Plot 11 4th column.

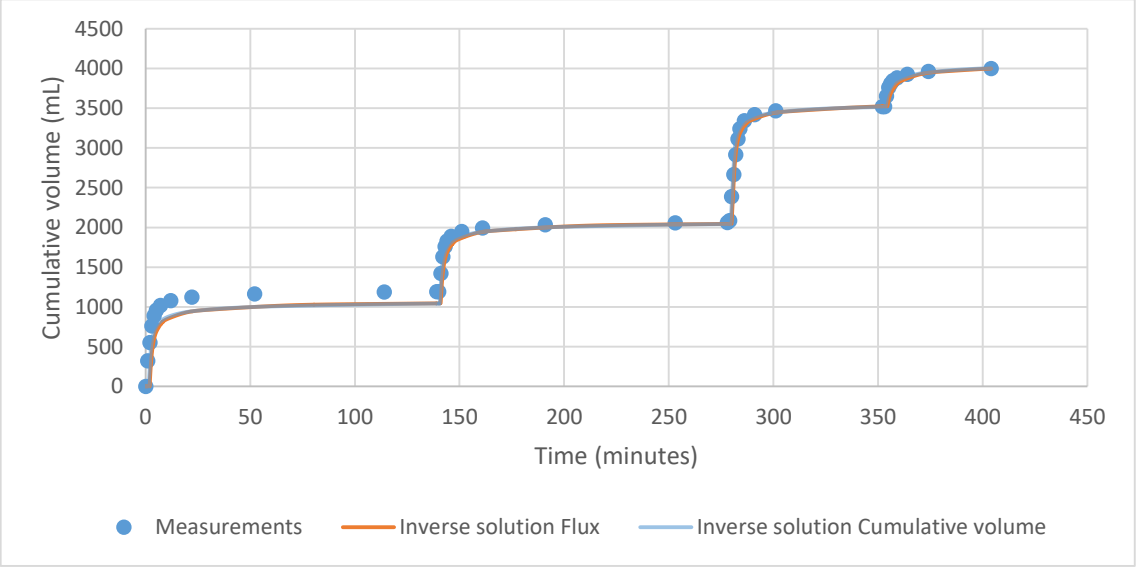

Figure A52. Inverse solution cumulative volume results of Plot 11 4th column.

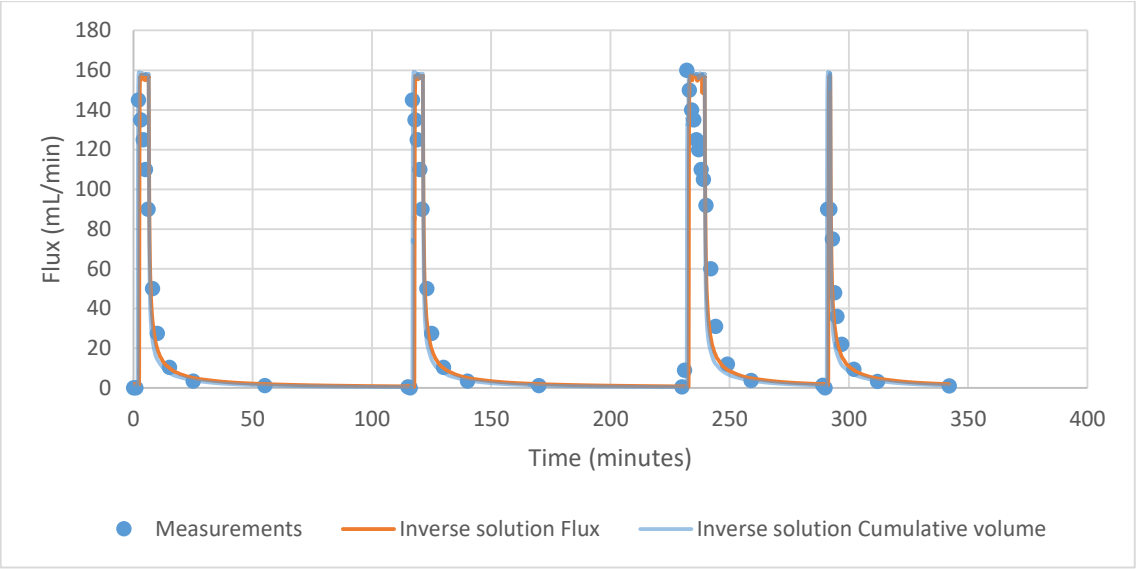

Figure A53. Inverse solution flux results of Plot 16.

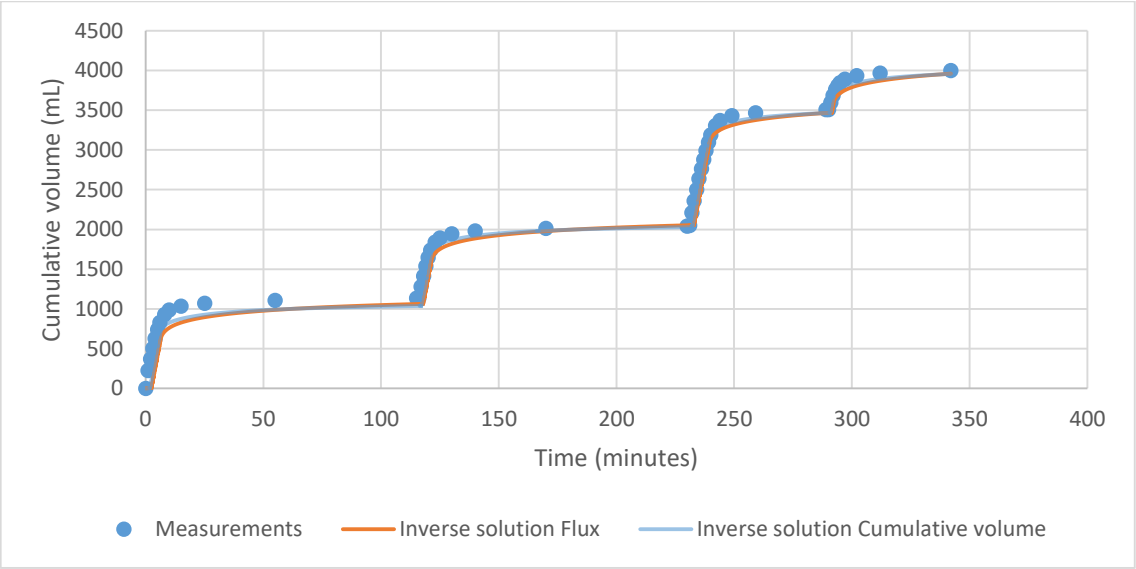

Figure A54. Inverse solution cumulative volume results of Plot 16.

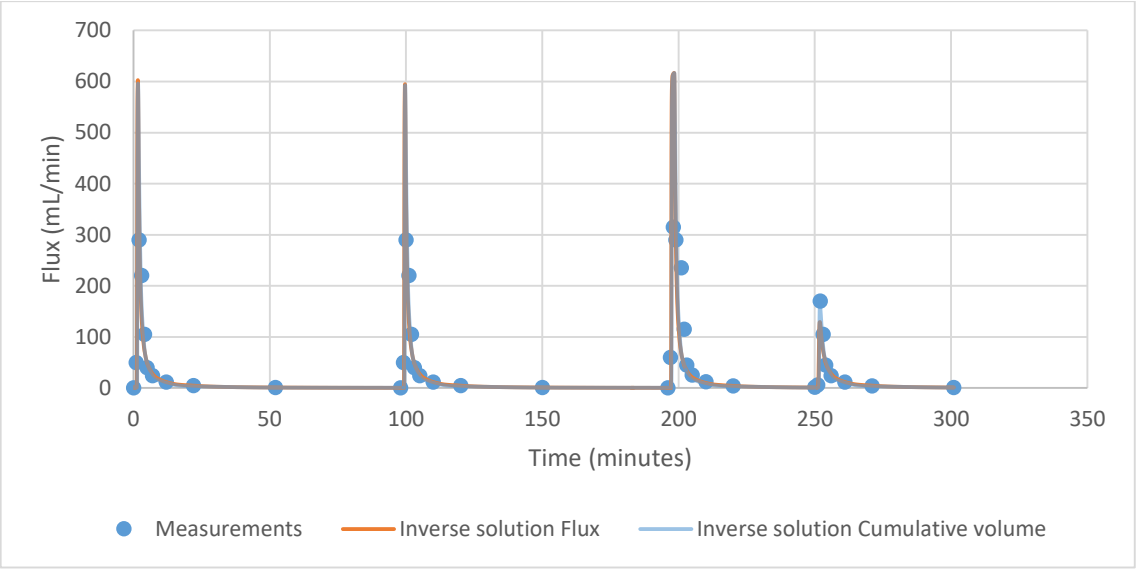

Figure A55. Inverse solution flux results of Plot 19.

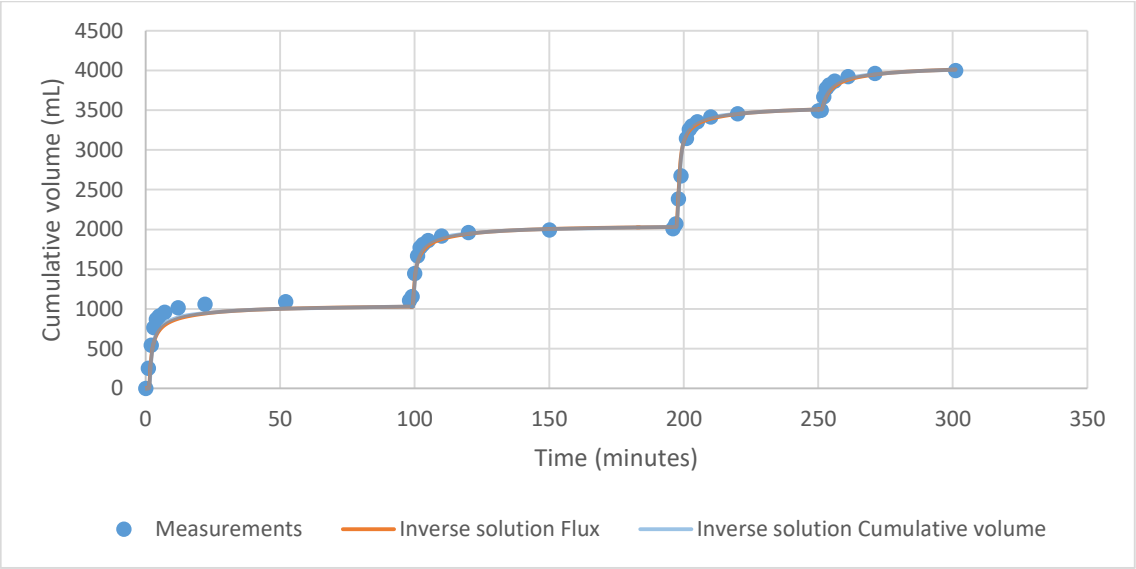

Figure A56. Inverse solution cumulative volume results of Plot 19.

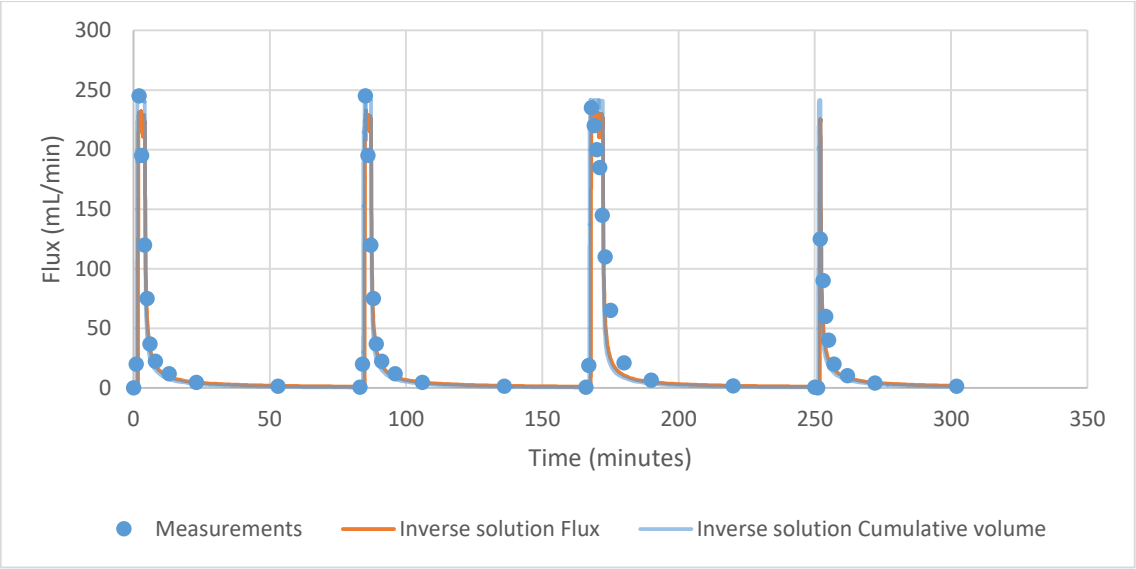

Figure A57. Inverse solution flux results of Plot 22.

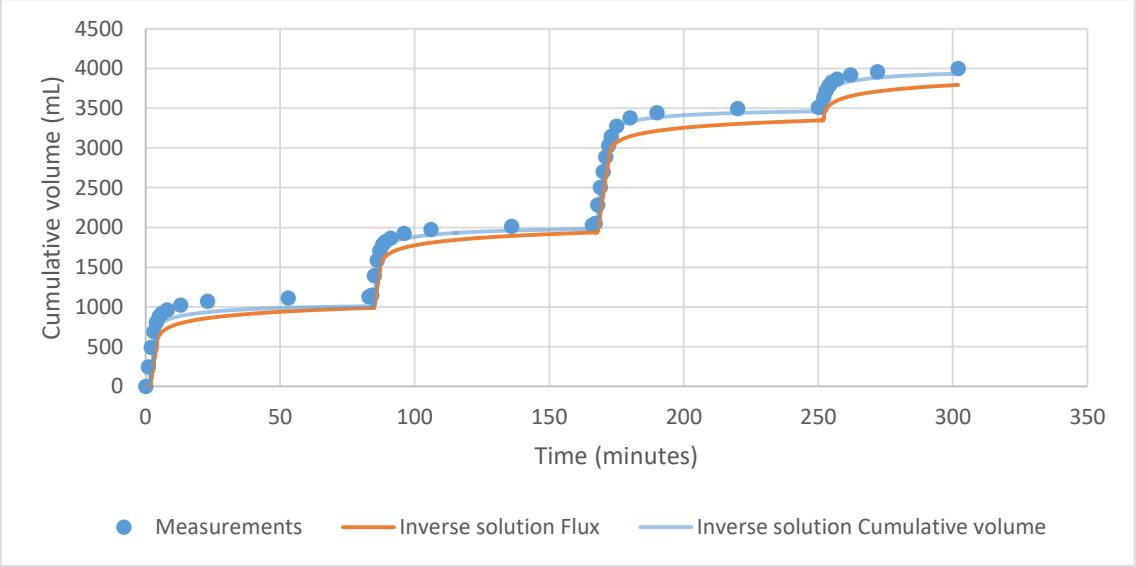

Figure A58. Inverse solution cumulative volume results of Plot 22.

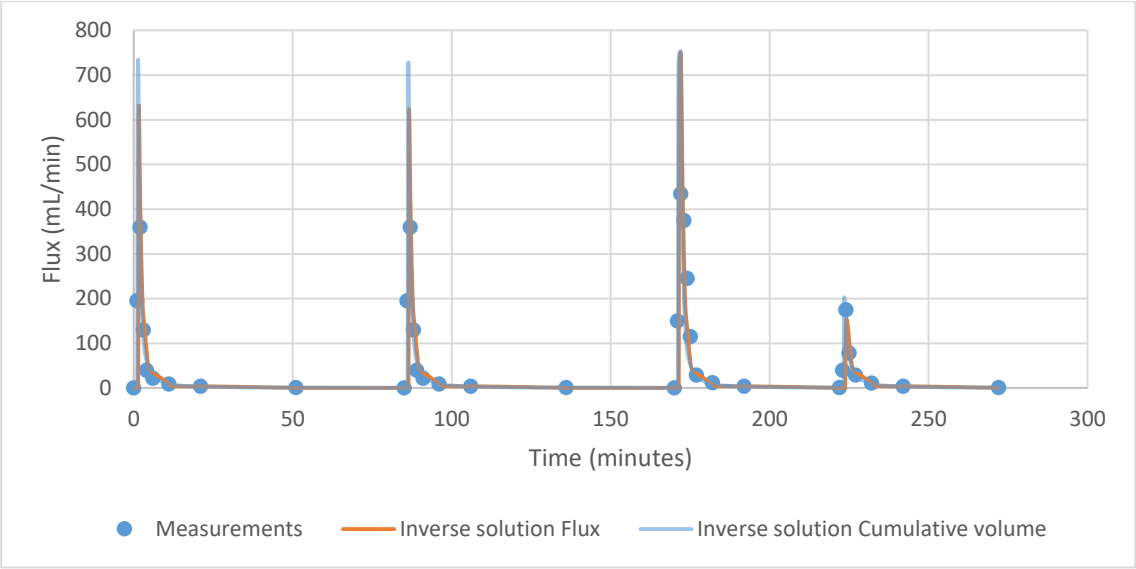

Figure A59. Inverse solution flux results of Plot 24.

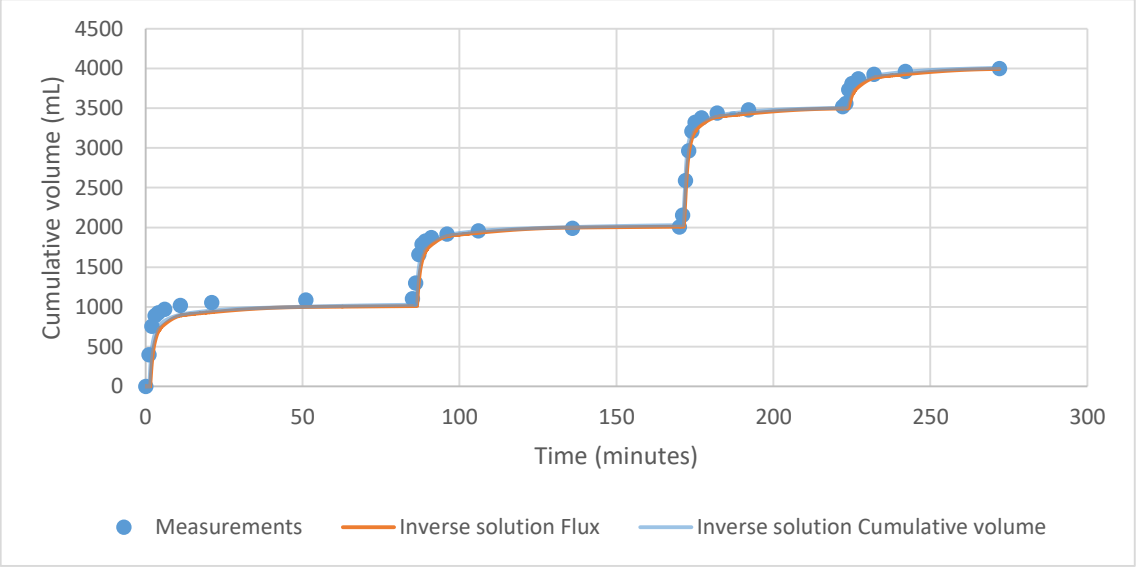

Figure A60. Inverse solution cumulative volume results of Plot 24.

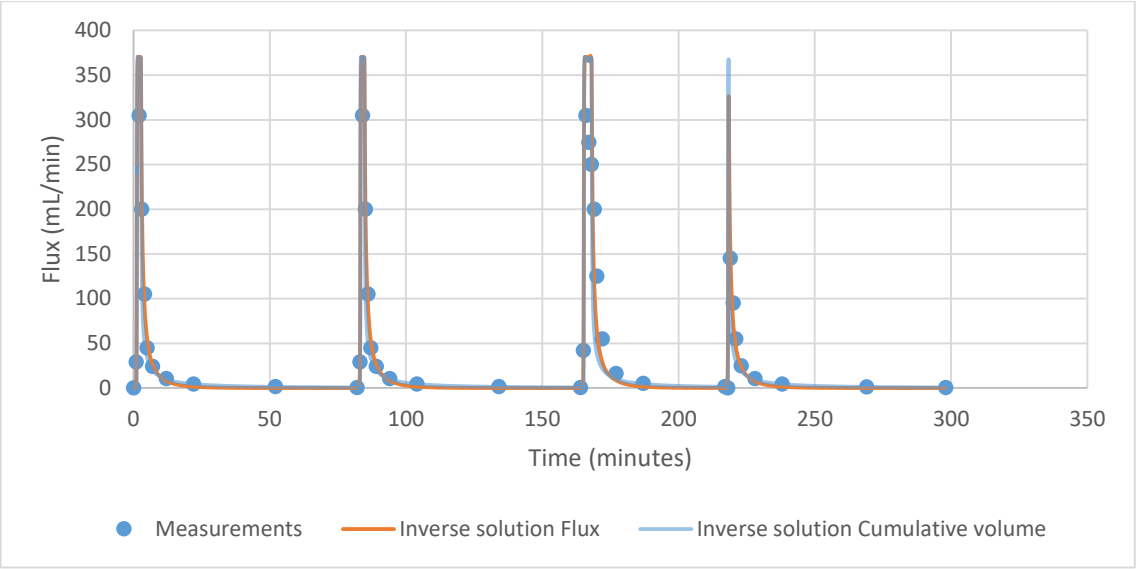

Figure A61. Inverse solution flux results of Plot 25.

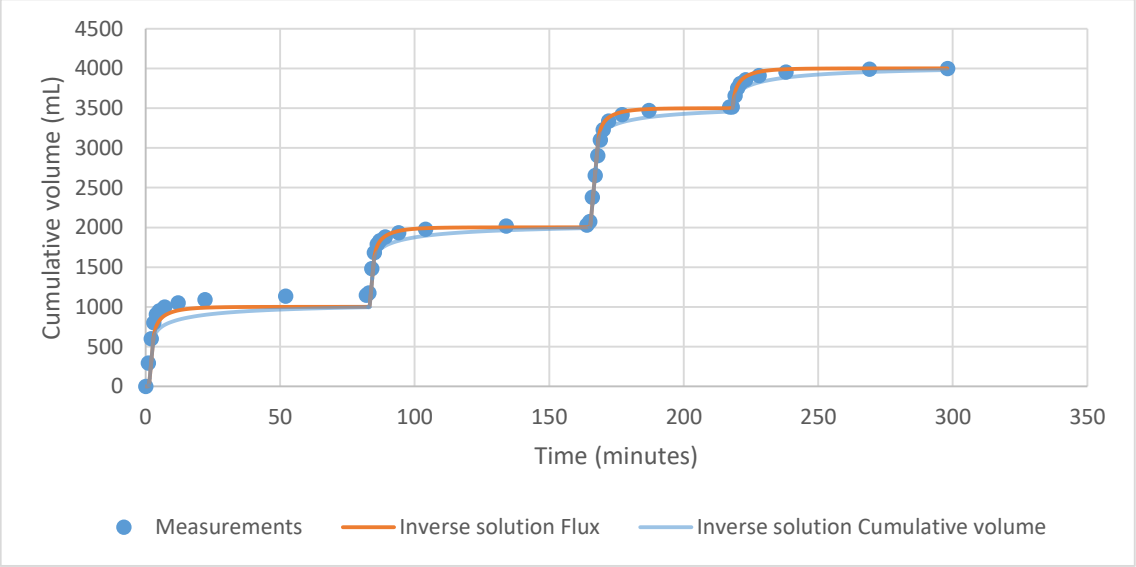

Figure A62. Inverse solution cumulative volume results of Plot 25.

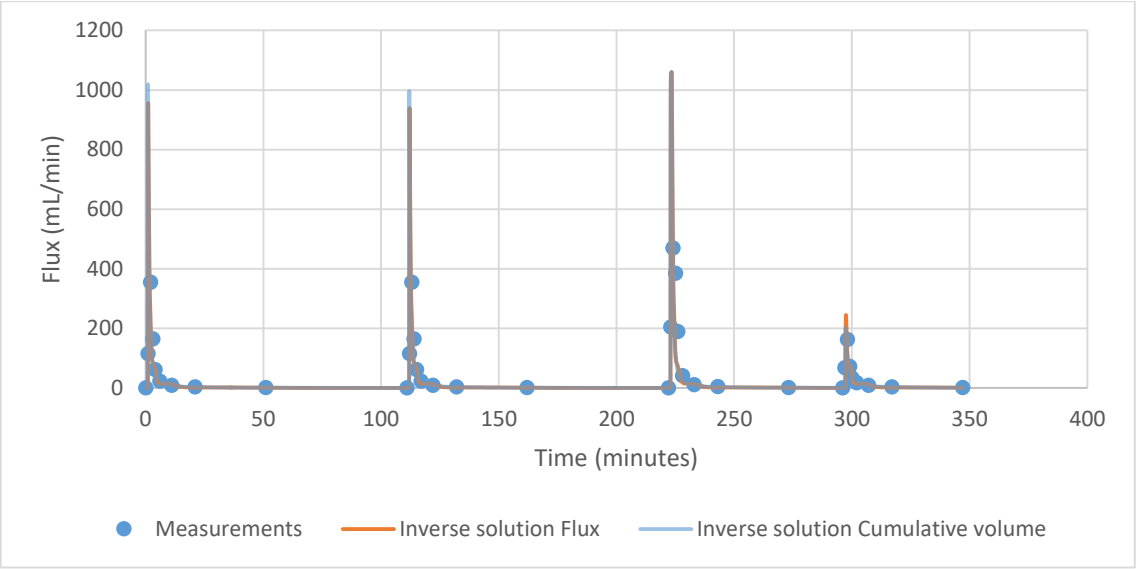

Figure A63. Inverse solution flux results of Pflanz Kalk.

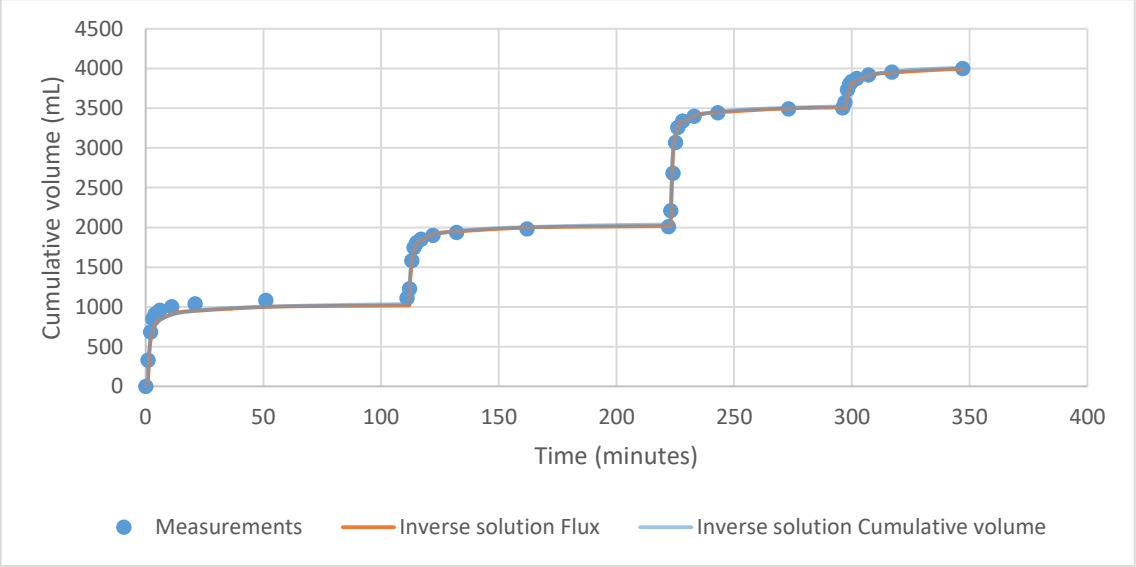

Figure A64. Inverse solution cumulative volume results of Pflanz Kalk.

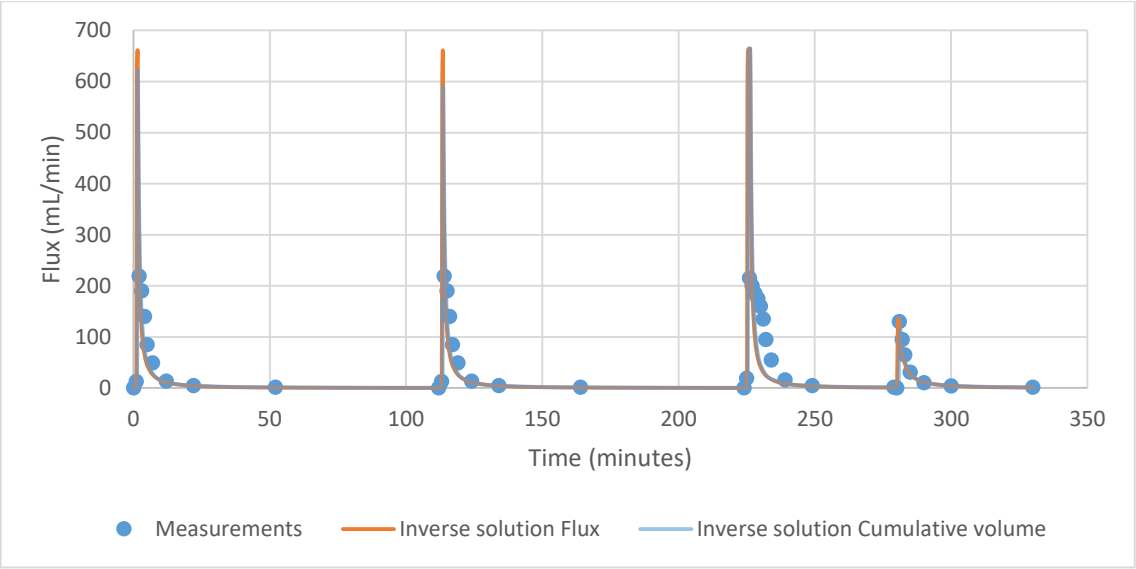

Figure A65. Inverse solution flux results of Granulit.

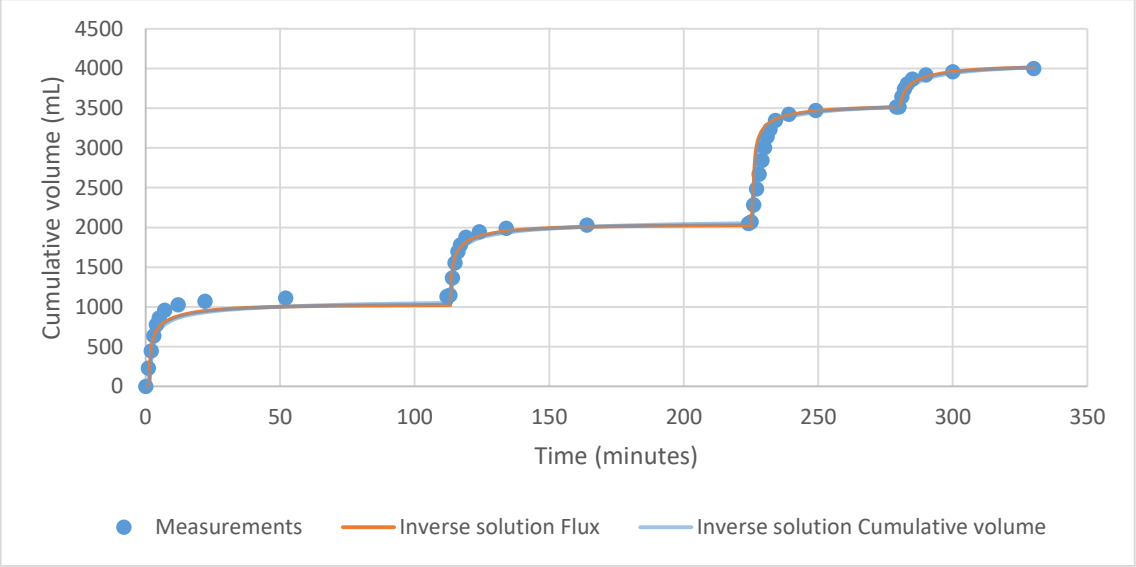

Figure A66. Inverse solution cumulative volume results of Granulit.

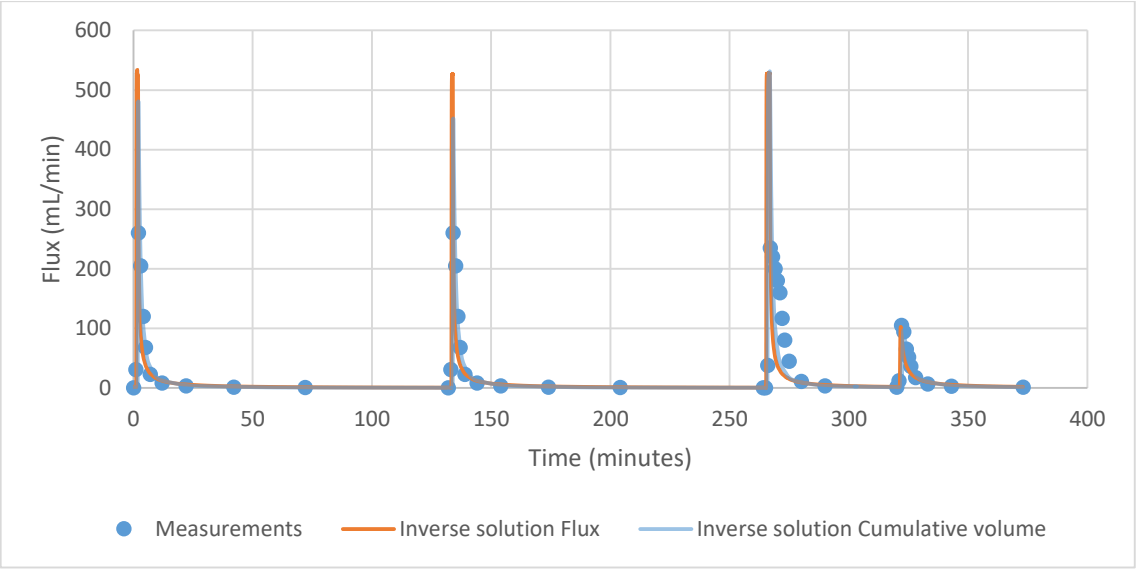

Figure A67. Inverse solution flux results of Pflanz Kombi.

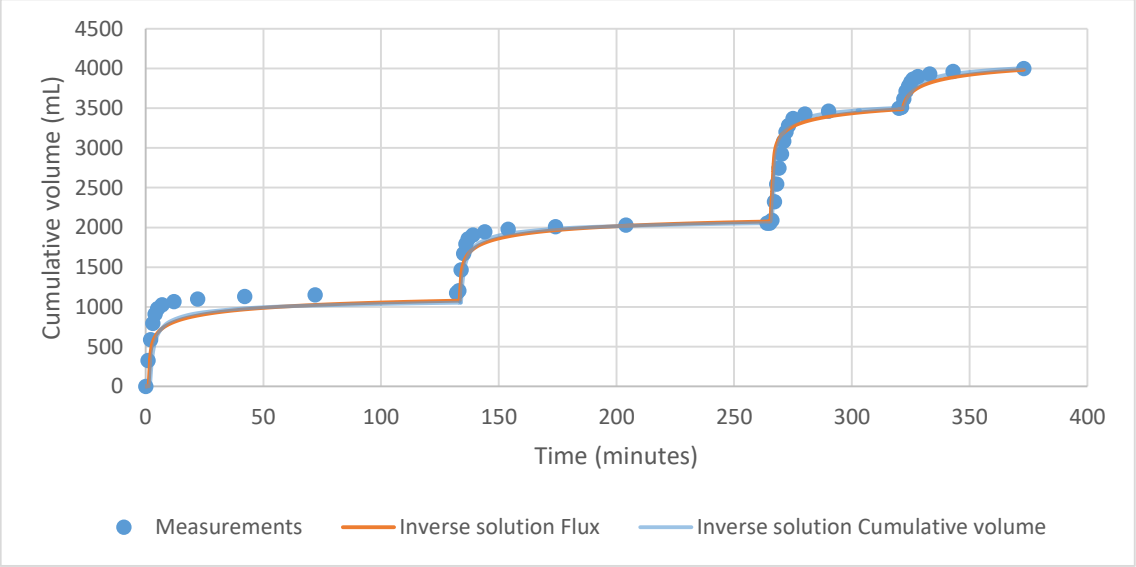

Figure A68. Inverse solution cumulative volume results of Pflanz Kombi.

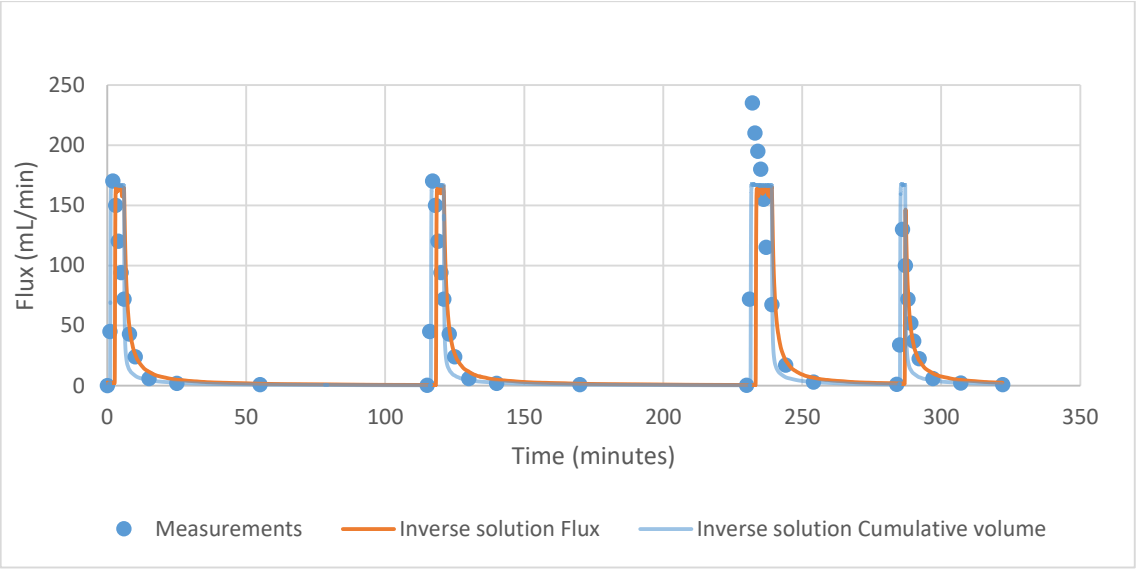

Figure A69. Inverse solution flux results of Pflanz Zeolith.

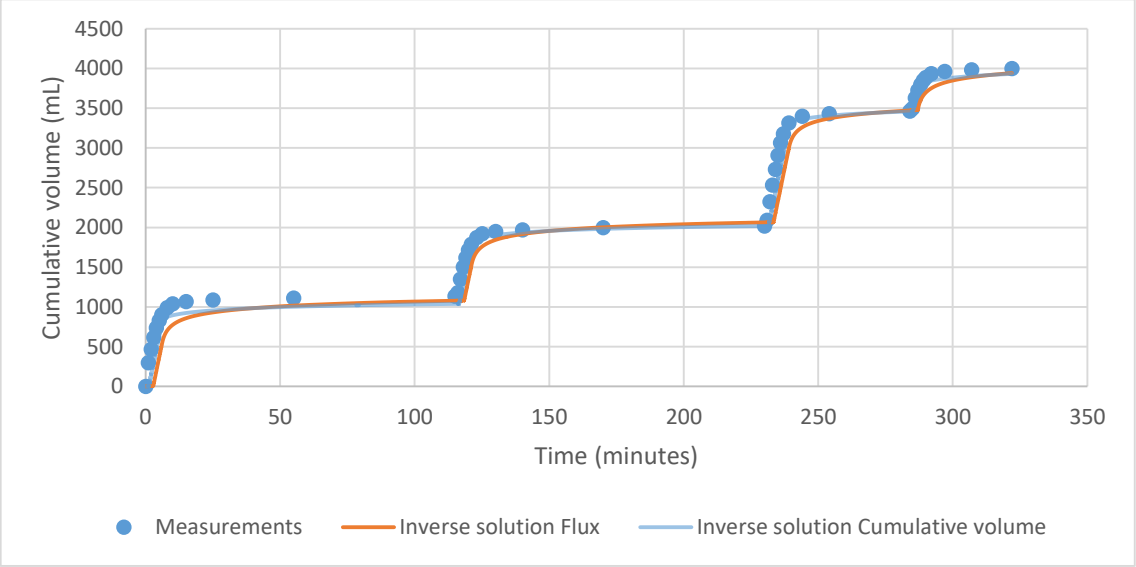

Figure A70. Inverse solution cumulative volume results of Pflanz Zeolith

Annex 3

It is in Annex 3 that the graphics obtained from the solute transport simulations are plotted. The graphics represent the relative outflow concentration, which is the outflow concentration of zinc over the inflow concentration of zinc, over time.

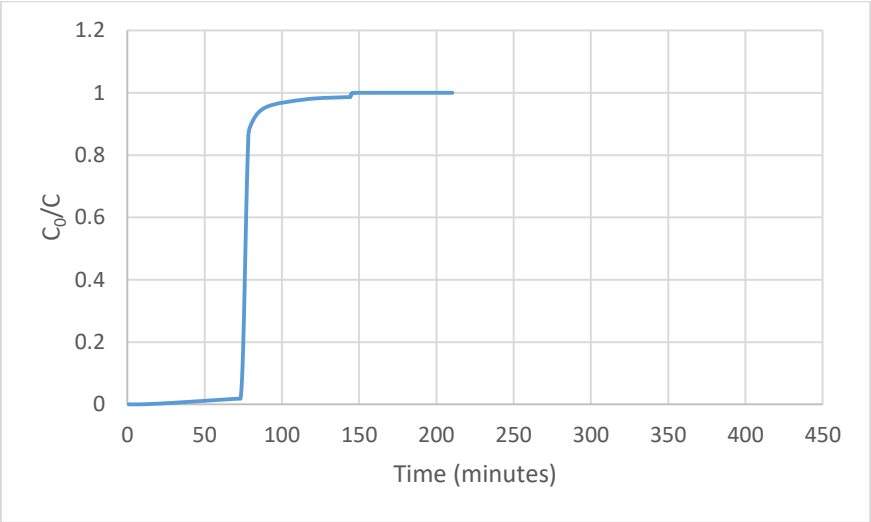

Figure A71. Breakthrough of Plot 3 1st column.

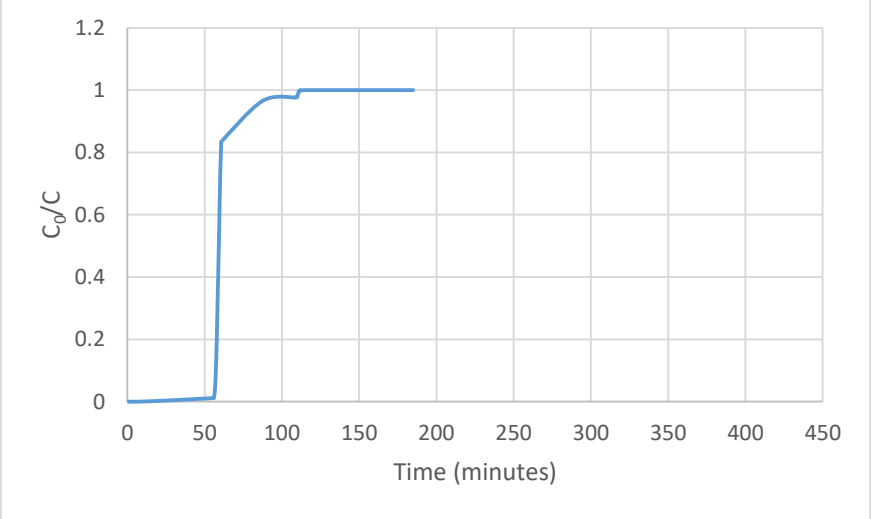

Figure A72. Breakthrough of Plot 3 2nd column.

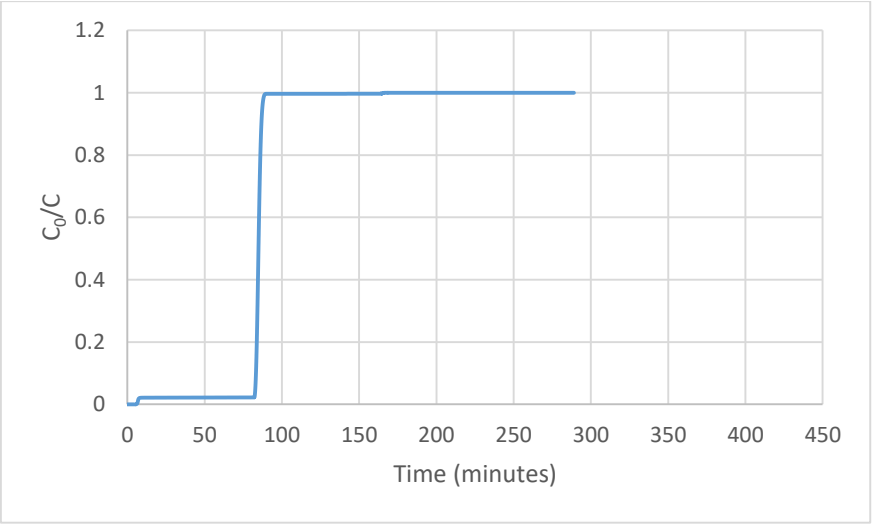

Figure A73. Breakthrough of Plot 6.

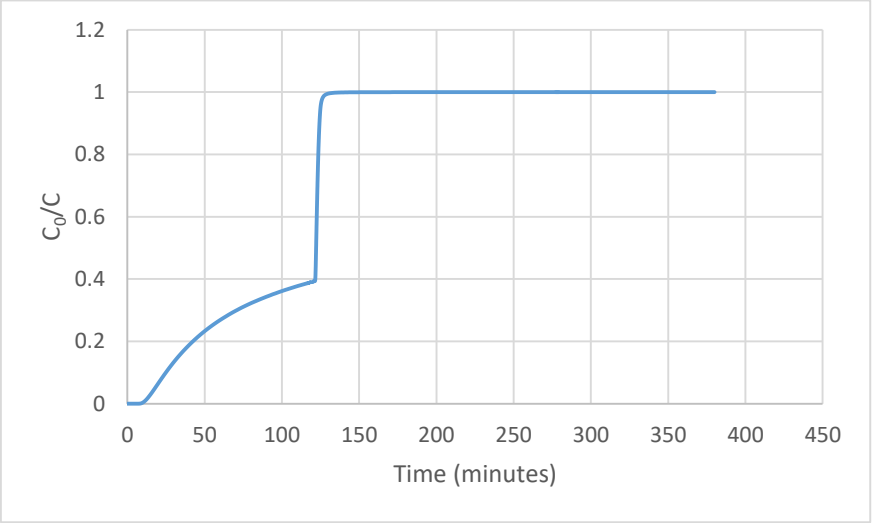

Figure A74. Breakthrough of Plot 9.

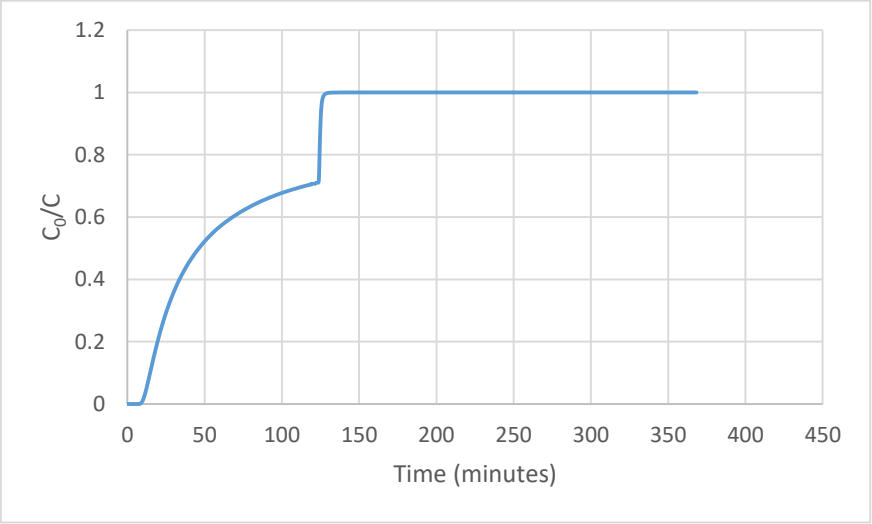

Figure A75. Breakthrough of Plot 11 3rd column.

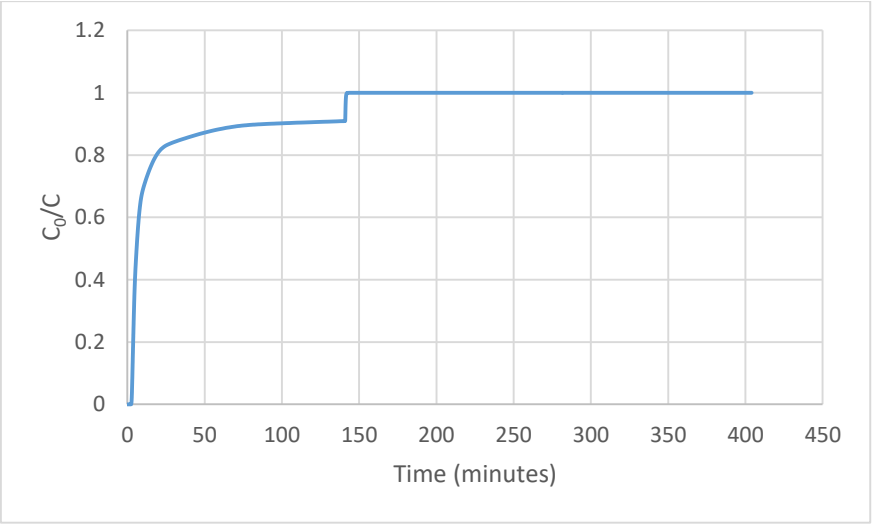

Figure A76. Breakthrough of Plot 11 4th column.

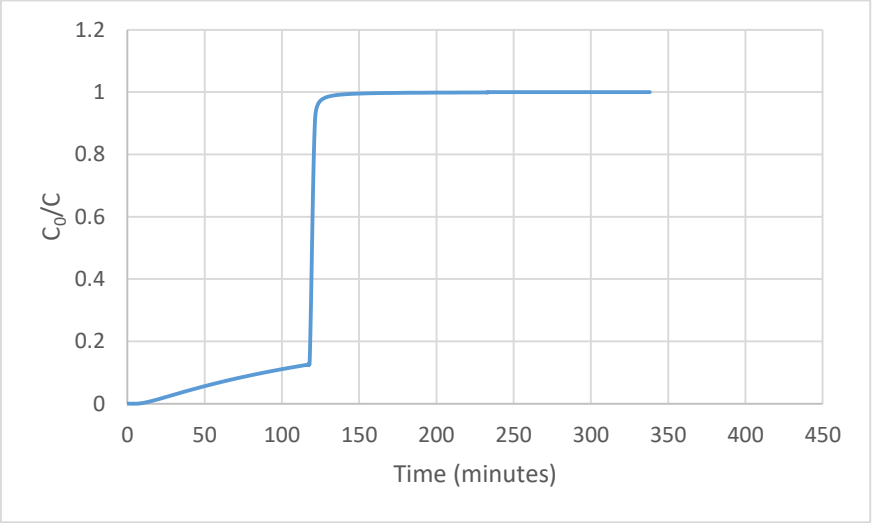

Figure A77. Breakthrough of Plot 16.

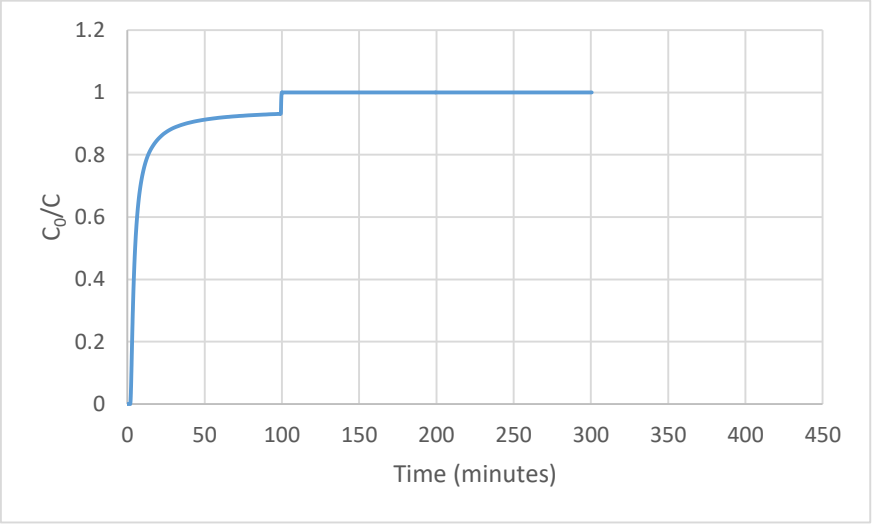

Figure A78. Breakthrough of Plot 19.

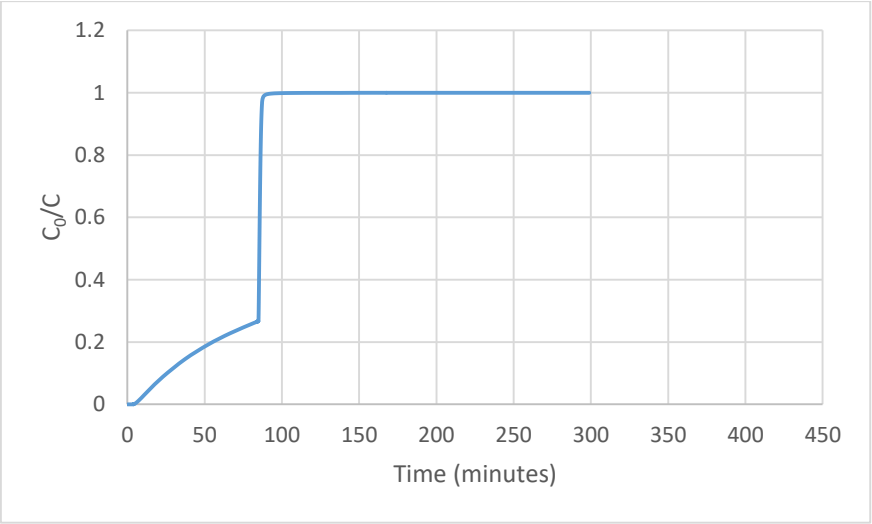

Figure A79. Breakthrough of Plot 22.

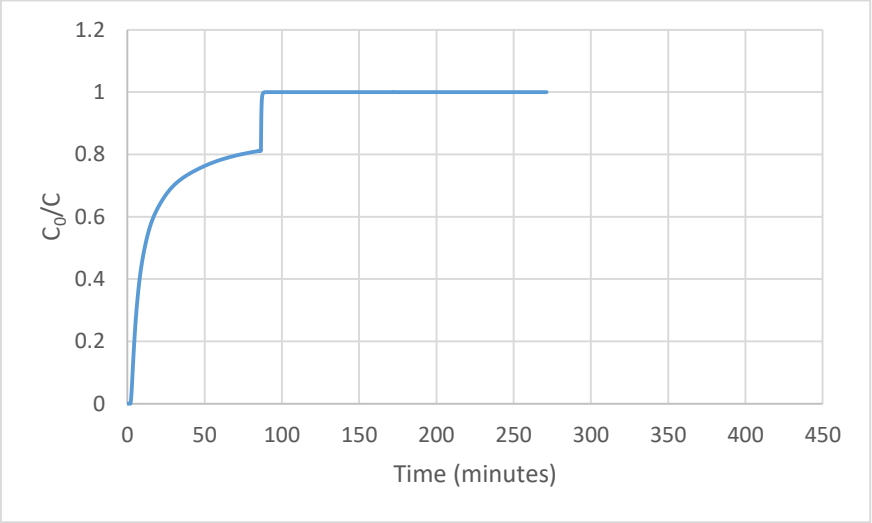

Figure A80. Breakthrough of Plot 24.

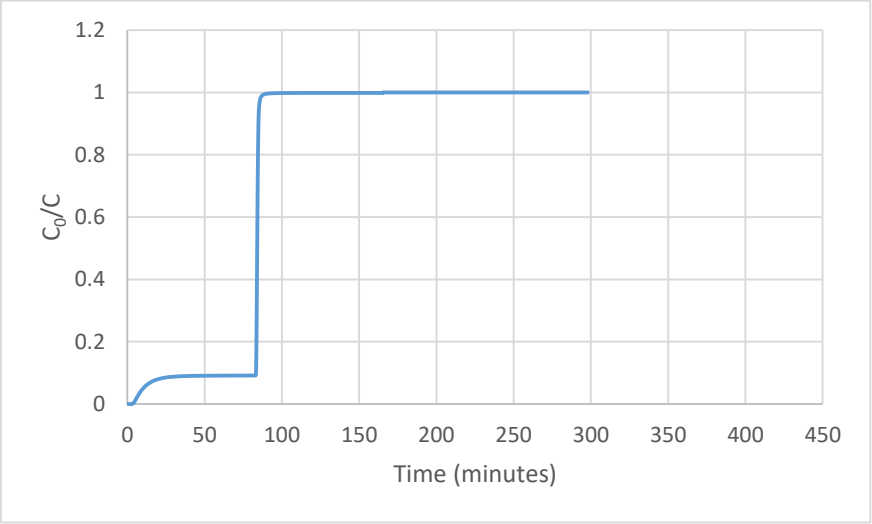

Figure A81. Breakthrough of Plot 25.

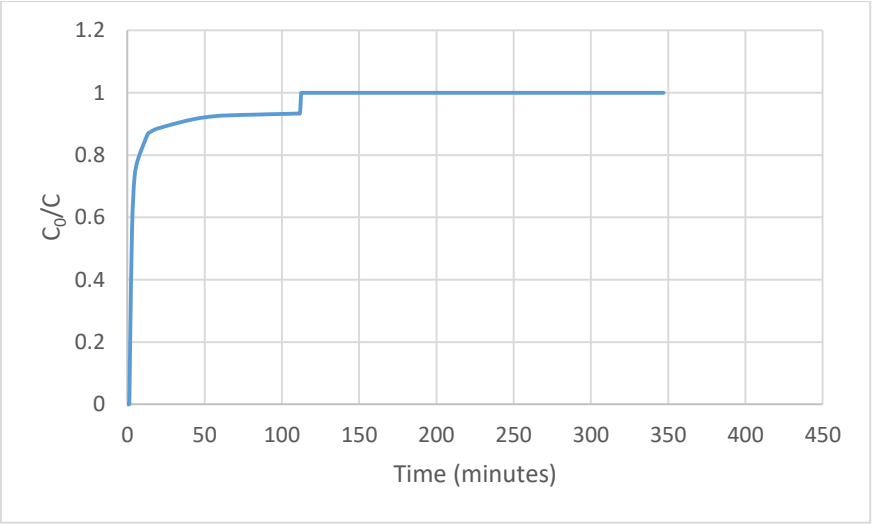

Figure A82. Breakthrough of Pflanz Kalk.

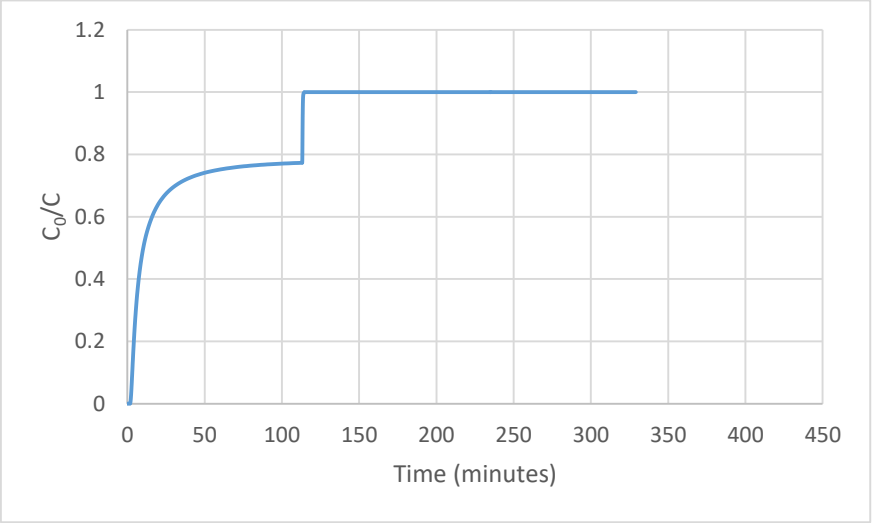

Figure A83. Breakthrough of Granulit.

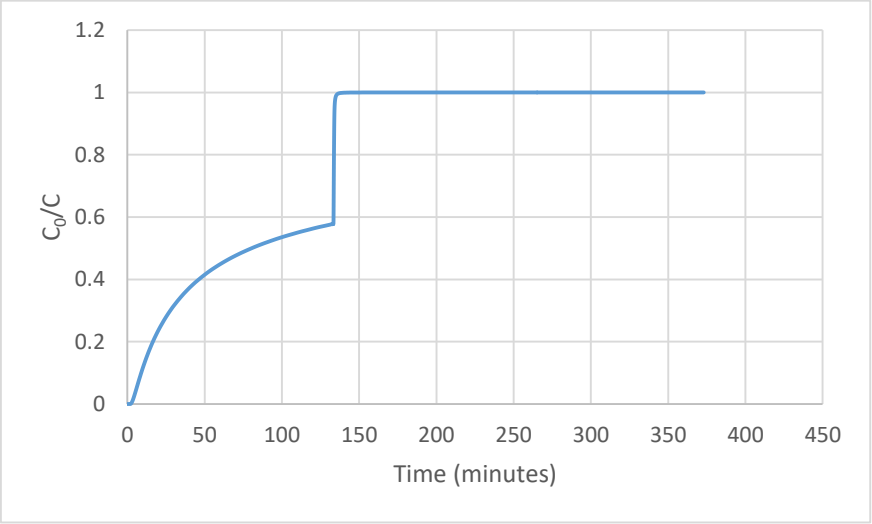

Figure A84. Breakthrough of Pflanz Kombi.

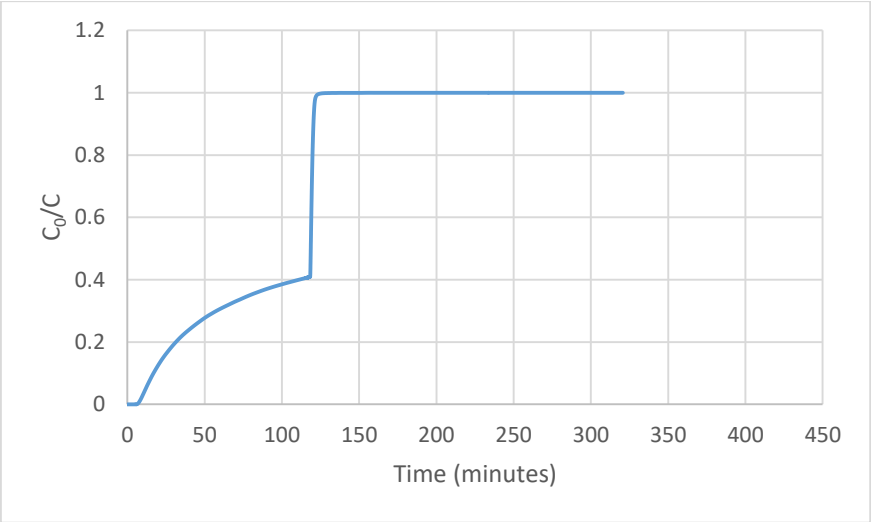

Figure A85. Breakthrough of Pflanz Zeolith.